

Catalytic Carbon Deposition on 3- Dimensional Carbon Fibre Supports

By

Matthew James Thornton, BSc (Hons)



**The University of
Nottingham**

Thesis submitted to the University of Nottingham for the degree of
Doctor of Philosophy, November 2005.

Abstract

Catalytic carbon deposition reactions, using methane, ethane or synthetic natural gas (1.8 vol. % propane, 6.7 vol. % ethane and balance methane) as the carbon-containing gas feedstock with or without the addition of hydrogen, have been investigated over nickel, cobalt and iron catalysts supported on 3-dimensional carbon fibre supports, using both a horizontal tube furnace and an isothermal, isobaric induction furnace. The transition metal catalysts were prepared by impregnating 3-dimensional carbon fibre supports with a methanolic solution of the metal nitrate, using a wet impregnation technique, and the effects of temperature, gas composition and deposition time on their catalytic behaviour was studied. Samples were characterised using a number of complementary techniques, including X-ray diffraction, scanning electron microscopy, polarised light microscopy, transmission electron microscopy, thermogravimetric analysis, digital photography and weight change measurements. The findings from these techniques were used to explain the observed type and amount of carbon deposited.

Nickel was found to be the most active catalyst and methane was found to be a poor carbon precursor for the catalytic deposition of carbon, from these findings nickel was chosen as the catalyst and ethane and synthetic natural gas were used as the carbon precursors, with and without the addition of hydrogen

The activity of the nickel catalyst was found to be dependant on a number of factors; weight percent used, temperature, gas feedstock used and deposition time. It was found, in all cases, that

increasing the deposition temperature resulted in higher deposition rates, ethane was found to yield higher deposition rates than synthetic natural gas and the effect of hydrogen addition had a negligible effect upon the rate of carbon deposition for the reactions carried out in ethane whereas it was significant for the reactions carried out in synthetic natural gas. The majority of the carbon deposition took place in the first three hours of deposition, with extended deposition times only yielding small increases in the overall rate of carbon deposition.

The type of carbon deposited varied from filamentous carbon i.e. carbon nanotubes, nanofibres and microcoils, to encapsulation. The factors affecting the type of carbon deposited were, the temperature of carbon deposition, with higher temperatures (800°C) yielding encapsulation and lower temperatures (650°C) yielding filamentous carbon, and the addition of hydrogen, with higher hydrogen concentrations favouring the formation of filamentous carbon over encapsulation. It was also found that the addition of hydrogen did not extend the lifetime of the catalysts.

It was found that nickel catalysts could be used within larger carbon fibre preforms to catalytically deposit carbon at lower temperatures than those used in industry for the manufacture of carbon-carbon composites (> 1000°C).

Abstract	i
Contents	iii
Acknowledgements	viii
List of abbreviations	ix
1 Introduction	1
1.1 The Aim of the Project	1
1.2 Carbon-Carbon Composites	1
1.3 Catalytic Carbon Deposition	6
1.4 Project Summary	8
1.5 Structure of Thesis	9
2 Literature Review	11
2.1 Introduction	11
2.2 Carbon	11
2.3 Nickel	14
2.4 Catalytic Carbon Deposition	14
2.4.1 Introduction	14
2.4.2 Carbon Structures	15
2.4.2.1 Carbon Nanofibres	16
2.4.2.2 Carbon Nanotubes	20
2.4.3 Preparation Methods	23
2.4.3.1 Catalysts and Catalyst Supports Used	25
2.4.3.2 Nickel and Nickel-Containing Catalysts	25
2.4.3.3 Nickel-Free Catalytic Carbon Deposition	37
2.4.4 Growth Mechanisms	51

2.4.5 Applications of Catalytically Deposited Carbon	60
2.5 Carbon-Carbon Composites	62
2.5.1 Introduction	62
2.5.2 Chemical Vapour Infiltration (CVI) Process	63
2.5.3 Carbon Deposited & Effect of Processing Parameters	64
2.5.4 Types of Furnaces Used	69
2.5.4.1 Isothermal, Inductively Heated, Isobaric CVI	72
2.5.4.2 Thermal Gradient, Inductively Heated, Isobaric CVI	73
2.5.4.3 Catalyst Enhanced CVI	75
2.6 Summary	77
3 Experimental	80
3.1 Introduction	80
3.2 Materials Used	80
3.3 Catalyst Impregnation	82
3.3.1 Carbon Fibre Mats	82
3.3.2 Carbon Fibre Preforms	84
3.4 Carbon Deposition	86
3.4.1 Carbon Fibre Mats	86
3.4.2 Carbon Fibre Preforms	89
3.5 Characterisation	93
3.5.1 TGA-MS	93
3.5.2 XRD	95
3.5.3 SEM	96
3.5.4 TEM	97

4.2.6	TEM	142
4.2.6.1	Ethane Gas Feedstock	142
4.2.6.2	Ethane plus Hydrogen Gas Feedstock	145
4.3	Discussion	149
4.3.1	Original Screening	149
4.3.2	Catalyst Formation	153
4.3.3	Carbon Deposition	155
4.3.3.1	Effect of Deposition Gas Mixture and Temperature	155
4.3.3.2	Effect of Hydrogen Addition	164
4.3.3.3	Effect of Deposition Time	167
4.4	Summary	172
5	Carbon Deposition on Carbon Fibre Preforms	174
5.1	Introduction	174
5.2	Results	174
5.2.1	Non-Catalytic Carbon Deposition	174
5.2.1.1	Temperature Profile	174
5.2.1.2	XRD	175
5.2.1.3	Effects of Densification Time, Temperature and Gas Feedstock	175
5.2.1.4	PLM	177
5.2.1.5	Digital Photography	178
5.2.2	Catalytic Carbon Deposition	179
5.2.2.1	Effects of Densification Temperature and Gas Flow Rate	179

5.2.2.2	SEM	180
5.3	Discussion	183
5.3.1	Non-Catalytic Carbon Deposition	183
5.3.1.1	Effects of Densification Time, Temperature and Gas Feedstock	183
5.3.1.2	PLM	186
5.3.1.3	Digital Photography	187
5.3.2	Catalytic Carbon Deposition	188
5.3.2.1	Effects of Densification Temperature and Gas Flow Rate	188
5.4	Summary	192
6	Conclusions	194
7	Future Work	196
8	References	198
	Appendices	205

Acknowledgements

I would like to take this opportunity to thank Dr Gavin Walker, under whose supervision this work has been carried out, along with Dr Toby Hutton and Dr Ron Fisher from Dunlop Aerospace. Their continued support, guidance and encouragement throughout the project has been much appreciated. I would also like to thank the EPSRC and Dunlop Aerospace for funding this work.

I wish to thank members of the research and technical staff from the School of Mechanical, Materials and Manufacturing Engineering who have given invaluable assistance. In particular, thanks are given to Mr Rory Screatton for his help in construction and maintenance of the always temperamental induction furnace, Mr Keith Dinsdale for his expertise in TEM and XRD, Mr Martin Roe and Mrs Nicola Weston for their help with SEM and Ms Julie Wells for her help in developing TEM images. I would also like to thank Alan Tibbatts of Dunlop Aerospace for his assistance in patent searching.

Special thanks are given to all my family, in particular my Mother and Father and my Gran and Grandpa, for this would not have been possible without their support and encouragement. Sincere thanks are also given to Karen for her understanding, tireless support and patience during the preparation of this thesis. Finally, I would like to thank the countless people who have ensured that my postgraduate days in Nottingham will always be remembered. Although too many to mention, special thanks are given to Neil, Frank, Stuart, Luke, Graham, Matt, Steve and Mia as well as all of the members of Good Skills!

List of Abbreviations

CAEM	Controlled atmosphere electron microscopy
CNF	Carbon nanofibre
CNT	Carbon nanotube
CVD	Chemical vapour deposition
CVI	Chemical vapour infiltration
DL	Dark laminar
DSC	Differential scanning calorimetry
HC	Hydrocarbon
HF	High flow rate ($1.5 \text{ dm}^3 \text{ min}^{-1}$ @ STP)
HPLC	High-performance liquid chromatography
HT	High tension
HTT	Heat treatment temperature
IPA	Isopropan-2-ol
ISO	Isotropic
LF	Low flow rate ($0.2 \text{ dm}^3 \text{ min}^{-1}$ @ STP)
MM	Molar mass (g mol^{-1})
MS	Mass spectrometry
MWNT	Multi-walled carbon nanotube
NG	Mains natural gas (unknown composition)
PAH	Polyaromatic hydrocarbons
PAN	Polyacrylonitrile
PLM	Polarised light microscopy
RL	Rough laminar
SAED	Selected area electron diffraction
SEM	Scanning electron microscopy

SL	Smooth laminar
STP	Standard temperature (0°C) and pressure (1 atm)
SWNT	Single-walled carbon nanotubes
Syn NG	Synthetic natural gas (1.8 vol. % propane; 6.7 vol. % ethane; balance methane)
TEM	Transmission electron microscopy
TGA	Thermogravimetric analysis
XRD	X-ray diffraction
% PU/h	Percentage pick-up per hour

1 Introduction

1.1 The Aim of the Project

The aim of the work reported in this thesis was to investigate the potential implementation of a catalyst in order to try to reduce the time, temperature and cost of manufacture of carbon-carbon composites for use in the aerospace industry as aircraft brake disks.

Currently carbon-carbon composites are manufactured using high temperatures (in excess of 1000°C) and low pressures (ca. 1 kPa) to pyrolytically deposit carbon from carbon containing gases onto 3-dimensional carbon fibre supports (preforms). These manufacturing conditions lead to lengthy manufacturing times which in turn means that carbon-carbon composites are relatively expensive. By implementation of a catalyst into the manufacturing process the cost of manufacturing carbon-carbon composites could, potentially, be reduced by lowering the temperature of manufacture (lower than 900°C) and shortening manufacturing times through increasing the rate of carbon deposition.

1.2 Carbon-Carbon Composites

Carbon-carbon composites began to emerge as a major new engineering material as early as the late 1960s and nowadays carbon-carbon composites are widely used as structural materials and find applications in space vehicle re-entry heat shields, rocket nozzles, aircraft and automotive brake discs and more recently they have also found use in the medical industry [1, 2].

The most commonly used method for the production of carbon-carbon composites is chemical vapour infiltration (CVI). The CVI process generally starts with a matrix of carbon fibres, usually in the form of a preform, in which the fibres can be arranged unidirectionally, bi-directionally or randomly. The preform is then subjected to the carbon-containing precursor, which can be in either a liquid- or gas- phase. The CVI process then involves infiltrating the carbon fibre preform with carbon-containing vapour.

The carbon-containing vapour is thermally degraded at temperatures between 600 and 1500°C; pyrolytic carbon is then deposited onto the carbon fibres within or on the surface of the preform. As more pyrolytic carbon is deposited into the pores within the preform the density of the composite increases, finally the pores become closed to further deposition and surface crusting of the preform begins to take place [3].

At present the fabrication of carbon-carbon composites, in particular for the aerospace industry, is a lengthy process. Due to the need for the preform to be regularly mechanically ground to remove any surface deposits which build up during the densification process and to allow for good infiltration of the densification gas or gases into the pores of the preforms. The densification process can be of the order of thousands of hours. Due to this there is increasing interest in shortening the production time of carbon-carbon composites in order to achieve greater production flexibility and throughput. It has therefore been proposed that the use of

catalysts in the production process could shorten the processing times.

Although there are numerous different CVI methods employed for the fabrication of carbon-carbon composites, the most widely used and most well understood is the isobaric, inductively heated, isothermal CVI process, this technique is used for the densification of carbon-carbon composites, and is the approach used for the densification of aircraft brake discs and therefore was the method employed for carbon deposition on carbon fibre preforms reported in this thesis.

This technique utilises a hot-wall reactor in which the carbon preforms are placed, the preforms are, therefore, radiantly heated under an isothermal process i.e. there is no temperature gradient across the preforms. The pressure in the reactor is also kept constant at either atmospheric pressure or at a reduced pressure. Deposition of carbon, in order to densify the preforms, takes place when the precursor gas or gases are introduced into the reactor. These gases infiltrate the internal porosity of the preforms, and deposition of solid carbon occurs on their internal and external surfaces [4].

The main advantages of isothermal, isobaric CVI are that the method is well established (since the 1960s) and is relatively well understood. Although the total processing time at temperature is high, in the order of 600 – 2000 hours, the method is capable of densifying a large number of preforms, of different shapes and sizes, simultaneously. This, therefore, makes the densification time

per preform relatively low when compared to other methods, which are only capable of densifying a single preform per densification run.

Some of the main disadvantages of isothermal, isobaric CVI are that surface crusting of the preforms occurs before the final required density is reached. This means that, on an industrial scale, the reactor has to be opened up several times before the densification process is complete, in order to permit grinding of the external surfaces of the preforms. This removes surface deposits and opens up the internal pores to further densification. Another disadvantage is that thinner preforms will densify at a faster rate than thicker preforms, which leads to problems in timing the densification process and the positioning of preforms within the reactor. The properties of carbon-carbon composites depend greatly upon the type of microstructure obtained. The main properties of carbon-carbon composites at elevated temperatures are:

- Good wear resistance
- High thermal conductivity with low thermal expansion
- High specific stiffness, toughness and strength
- High thermal shock resistance

All of these properties rely upon obtaining the desired microstructure within the composite. The elements during the CVI process that govern the type of microstructure obtained are:

- Type of carbon fibre preform employed
- The matrix precursor
- The processing history
- Fibre-matrix interactions

In order to obtain the desired properties, the final composite must have a uniform density and a low residual porosity, which is obtained through in-depth pore-filling of the substrate with the matrix [3].

There are three main types of carbon matrix microstructure [3]:

- Smooth laminar (SL)
- Rough laminar (RL)
- Isotropic (ISO)

Another, somewhat less well-known and studied form of carbon matrix microstructure is dark laminar (DL) [5, 6].

The type of microstructure obtained can be determined by observing polished samples under polarised light, from this the extinction angle (A_e) is obtained, this is determined by rotating the sample and marking the degrees through which the sample is turned so that the north-south arms of the Maltese cross align with the east-west arms. It is this extinction angle that is used to determine the type of carbon matrix microstructure that has been obtained; the definitions are stated below [5]:

- For isotropic - $A_e < 4^\circ$;
- For dark laminar - $4^\circ < A_e < 12^\circ$;
- For smooth laminar - $12^\circ < A_e < 18^\circ$;
- For rough laminar - $A_e > 18^\circ$.

It has been found that a SL matrix shows a higher flexural strength than a RL matrix and that a triplex matrix consisting of ISO, SL and RL produces a higher flexural strength than composites that contain mostly RL pyrocarbon in the matrix. It has also been

found that the use of linear carbon molecules in the densification process (C_1 - and C_2 -species) yields a pyrocarbon matrix with a RL structure [6].

1.3 Catalytic Carbon Deposition

The main application for catalytic carbon deposition is for the formation of filamentous carbon, which includes carbon nanotubes (both single walled and multi-walled) and carbon nanofibres.

Research for the formation of nanostructured carbons has centred on using iron, nickel or cobalt or alloys of these, either with each other or with other metals, in particular copper, as the catalyst. The research has investigated and proposed possible mechanisms for the formation of nanostructured carbons, and a number of authors has tried to identify what the optimum conditions for the formation of filamentous carbon are [7-11]. For example variations in gas composition, temperature and catalyst morphology have an effect upon the rate of carbon formation i.e. increasing the temperature and adding hydrogen to the gas mixture can increase the rate of carbon deposition, and nanosized catalyst particles are favourable over larger catalyst particles. The conditions used also affect the type of carbon formed e.g. increasing the temperature to ca. 800°C will favour the formation of graphitic carbon shells forming around the catalyst particles as opposed to the formation of carbon nanofilaments.

It is now widely understood that there are three types of carbon nanofilaments [9, 10]:

1. Platelet nanofibres (with the graphite planes stacked perpendicular to the fibre axis).
2. Herringbone nanofibres (with the graphite planes stacked at an angle to the fibre axis).
3. Nanotubes (formed when the graphite layers are parallel to the fibre axis).

Selective deposition of the different types of carbon nanofilaments is still an issue. Although alluded to as a potential application in some papers, there has been little work reported on the use of metal catalysts for the densification and manufacture of carbon-carbon composites [11-13].

The work by Zielinski and Grow [11] used methane as the carbon deposition gas and although this is relatively cheap they used expensive ferrofluids as the catalyst source and high temperatures of 977°C. The percent mass gains reported are also relatively low with the greatest reported being 24.79 % and the sizes of the carbon fibre supports used were not stated. Work by Downs and Baker [12] reported using a copper-nickel catalyst at relatively low temperatures (600°C) but again the size of the carbon fibre supports used were not stated and in this instance a relatively expensive and reactive gas (ethene) was used as the feedstock gas. McAllister and Wolf [13] reported the use of a nickel catalyst at even lower temperatures (375°C) for the catalytic deposition of carbon, but again they were using an expensive and more reactive feedstock gas (propene), although they did report the size of the carbon fibre preforms to be 0.6 x 0.6 x 0.25 cm,

however, this preform size is relatively small when compared with potential commercial applications.

It has been found that production of carbon fibres by pyrolysis of hydrocarbons requires submicron-sized catalyst particles, which act as nuclei for fibre growth. Catalyst particles with diameters less than 20-30 nm work well and the fibres form more efficiently with decreasing particle size [14].

1.4 Project Summary

A nickel catalyst was selected, along with cobalt and iron, as initial tests showed nickel to have the highest activity towards catalytic carbon deposition. It was also decided that the gases for the catalytic deposition of carbon would be a bottled synthetic natural gas mixture (composition given in section 3.2), to emulate mains natural gas used in industry but without the day-to-day variations in composition. Ethane was also used, due it being a relatively inexpensive saturated straight chain hydrocarbon whilst having a greater reactivity than methane at the temperature range under investigation, which was 650 – 800°C, as this would provide industry with significant savings over the temperatures currently used which are in excess of 1000°C. The effect of the addition of hydrogen to the gas feedstock on the rate of catalytic carbon deposition was also investigated, as was the effect of reaction time. The total gas flow rates investigated were 0.2, 0.25 and 1.5 dm³min⁻¹ @ STP and total deposition times of 3 and 12 hours were used.

The catalyst was impregnated onto carbon fibre substrates using a methanolic solution of nickel nitrate hexahydrate, this procedure was loosely based upon the “incipient wetness technique” which involves the impregnation of a carbon fibre preform with a methanolic solution of the catalyst salt [15].

An optimum set of conditions to yield the highest rate of carbon deposition within the limits defined for a nickel catalyst were determined i.e. temperature, gas flow rate, gas composition and reaction time, using small carbon mat samples. The reactions were then scaled up to larger carbon preform samples to determine the capability and practicality of the process for the formation of carbon-carbon composites.

1.5 Structure of Thesis

The thesis is structured as follows:

Chapter 2 is a detailed review of the literature on the catalytic deposition of carbon detailing the different types of catalysts used, the gases used, the temperatures at which reactions take place, the types of catalyst supports and the different types of carbon deposited under the varying reaction conditions.

Chapter 3 details the experimental procedures used to obtain the results presented in this thesis as well as the apparatus used and the characterisation techniques employed.

Chapter 4 will present the main body of work carried out, which is the catalytic deposition of carbon onto carbon fibre mats using a nickel catalyst under varying reaction conditions of temperature,

gas composition and deposition time. It will present the results obtained followed by a discussion of the relevance of the results within the context of this work and the wider research community.

Chapter 5 presents results relating to the catalytic deposition of carbon, using larger carbon fibre preforms as the nickel catalyst support and these results are presented in tandem with results for densification of the carbon fibre preforms without a catalyst present. The results obtained are then discussed again within the context of this thesis and within the context of the wider research community.

Chapter 6 gives conclusions of the work presented and Chapter 7 discusses how the research could be taken forward and presents ideas for future work.

2 Literature Review

2.1 Introduction

This chapter will look at the different types of catalysts that have been used in order to facilitate the production and/or deposition of carbon, as well as looking at the different methods that have been used or proposed in order to introduce catalysts into the carbon forming process. It will explain in detail the various areas of research surrounding catalytic carbon deposition as well as the formation of carbon-carbon composites along with their applications. It will also give a brief description of carbon and nickel and their properties as well as putting into context the scope of the work in the related fields of research.

2.2 Carbon (C)

Only ten elements have been known since the beginning of recorded history, of which carbon is one. Carbon is a group 14 element which has the atomic number of 6, a molar mass of 12.011 g mol⁻¹ and is tetravalent, with graphite (the most stable allotrope) having a density of 2267 kg m⁻³.

Carbon accounts for only 0.02 % of the mass of the earth's crust but has a relative abundance of 23 % in the human body and is found naturally in three different forms: diamond, graphite and fullerene.

Diamond consists of a covalent network of carbon atoms each of which uses sp³ hybrid orbitals to bond to 4 other carbon atoms to

form an array of σ -bonds with a tetrahedral geometry, a schematic representation of diamond can be seen in Figure 2.1. This structure makes diamond the hardest known substance and gives this form of carbon the highest melting point for any element ($> 3550^{\circ}\text{C}$).

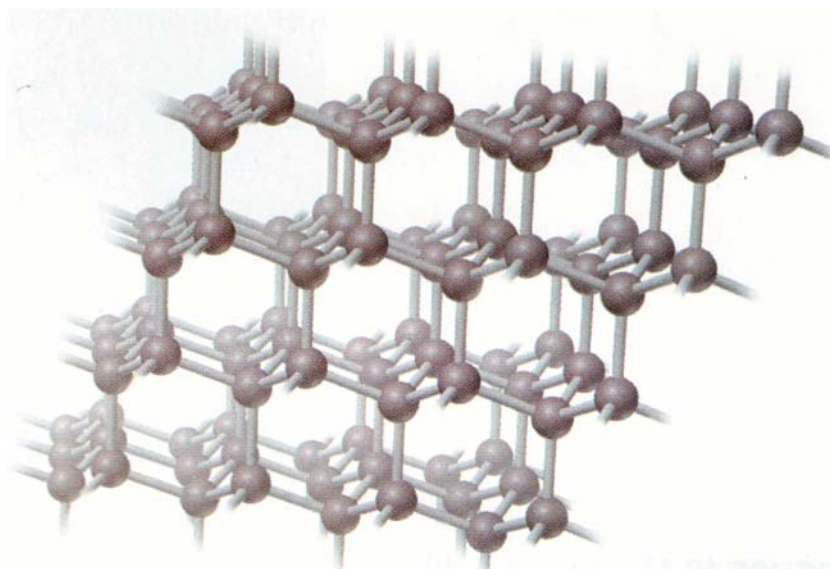


Figure 2.1: Schematic representation of the covalent crystal structure of diamond [16].

Graphite consists of a two-dimensional structure which consists of sheets of six-membered rings in which each carbon atom σ -bonds to 3 others in a trigonal planar arrangement using sp^2 hybrid orbitals. Each carbon atom then uses its remaining p_z -orbital to form a π -bond, because each carbon atom must share its π -bond with each of the three neighbouring carbon atoms, the π -electrons are delocalised in the plane of the sheet [16], the graphite crystal lattice is shown in Figure 2.2.

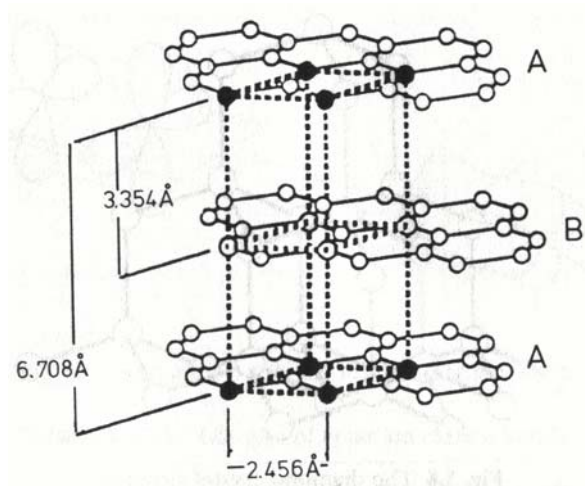


Figure 2.2: The graphite crystal lattice [1].

Recently other allotropes of carbon have been discovered, the first of these was buckminsterfullerene (C_{60}) which was discovered in 1985 by Robert F. Curl Jr., Harold Kroto and Richard E. Smalley [17]. The C_{60} molecule is spherical and has the shape of a soccer football with 12 pentagonal and 20 hexagonal faces where each carbon atom is sp^2 – hybridised and bonded to three other carbon atoms [16], the structure is illustrated in Figure 2.3.

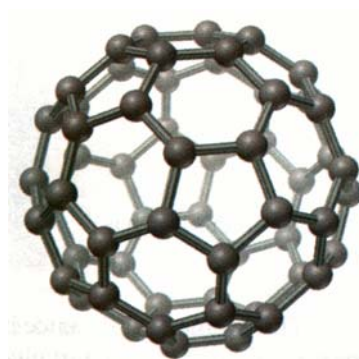


Figure 2.3: Buckminster fullerene [16].

Following this discovery other derivatives of carbon were discovered including C_{70} [16] (an egg shaped molecule) and more

recently carbon nanotubes (both multi-walled and single-walled) [18-20] and carbon nanofibres [21], both of which will be discussed in more detail in sections 2.4.2.1 and 2.4.2.2.

2.3 Nickel (Ni)

Nickel was discovered in 1751 by Alex Fredrik Cronstedt when he extracted it from a mineral called niccolite. It is a transition metal with an atomic number of 28, a molar mass of 58.69 g mol^{-1} , a density of 8908 kg m^{-3} and a melting point of 1455°C .

Nickel is the seventh most abundant transition metal and the twenty second most abundant element in the earth's crust. Nickel is found in most meteorites and is often used to distinguish a meteorite from other minerals. It is a hard malleable metal which is ductile, ferromagnetic and a fair conductor of heat and electricity. Some of its uses include alloying to form stainless steel, coinage, to give glass a green colour, in batteries and in electroplating to provide a protective coating for other metals [22].

2.4 Catalytic Carbon Deposition

2.4.1. Introduction

Although the catalytic deposition of carbon has been a process that has been used for many years it has only recently become a "hot topic" with regards to international research, the research field became especially prominent with the discovery of Buckminster fullerene in 1985 [17], furthered by the discovery of carbon nanotubes in 1993 [19].

Since these two discoveries, research into the field of producing nanosized carbons by catalytic means has intensified and the field is now probably one of the most interesting fields of research today. Although this makes working in the field exciting and challenging a comprehensive review of all the literature is beyond the scope of this thesis. Therefore, the key results from the more recent papers will be presented in terms of the structures of the different types of catalytically deposited filamentous carbon, the different types of catalyst and catalyst supports used, the preparation methods used to catalytically produce filamentous carbon deposits, the growth mechanisms behind filamentous carbon formation and some of the (potential) applications of catalytically grown carbon.

2.4.2. Carbon Structures

This section will discuss the structures of the different types (nanotubes, nanofibres and encapsulation) of carbon that are formed from the catalytic deposition of carbon. It will look at the different types of nanofibres, which have diameters ranging from 50 – 200 nm and lengths of up several millimetres, e.g. platelet and herringbone, and at the different types of nanotubes e.g. single- and multi-walled and bamboo-shaped. Where multi-walled nanotubes can have diameters of 2 – 20 nm and single walled nanotubes have diameters of ~ 1 nm, and both have lengths of up several micrometers [23].

2.4.2.1. Carbon Nanofibres

There are two main types of carbon nanofibres produced from the catalytic deposition of carbon, these are platelet nanofibres and herringbone nanofibres (which can sometime be confused with nanotubes due to the possible presence of a hollow core), see Figure 2.4 (a) and (b), however other types of nanofibres have also been observed, see Figure 2.4 (c).

The main factor in determining the type of carbon nanofibre produced is the morphology of the catalyst particle. Rodriguez *et al.* [10] discussed the effect of catalyst particle morphology on the resulting morphology of the carbon fibre produced. In this work they used bi-metallic iron – copper (7:3) powders which were reacted with an ethylene : hydrogen (4:1) gas mixture at 600°C.

From the resulting carbon fibres, produced from the reaction, the authors described how the morphology of the catalyst particle affected the morphology of the growing carbon fibre, the different observed morphologies are shown in Figure 2.4. If the catalyst particle adopts a rectangular morphology then the graphite planes stack perpendicular to the fibre axis giving a platelet nanofibre (Figure 2.4 (a)), if the catalyst particle is square (or diamond-shaped) then the graphite planes stack at an angle to the fibre axis giving a “herringbone” nanofibre (Figure 2.4 (b)) and if the graphite planes are parallel to the fibre axis nanotubes are formed (Figure 2.4 (c)). In all cases the nanofibres produced were found to be faceted and solid.

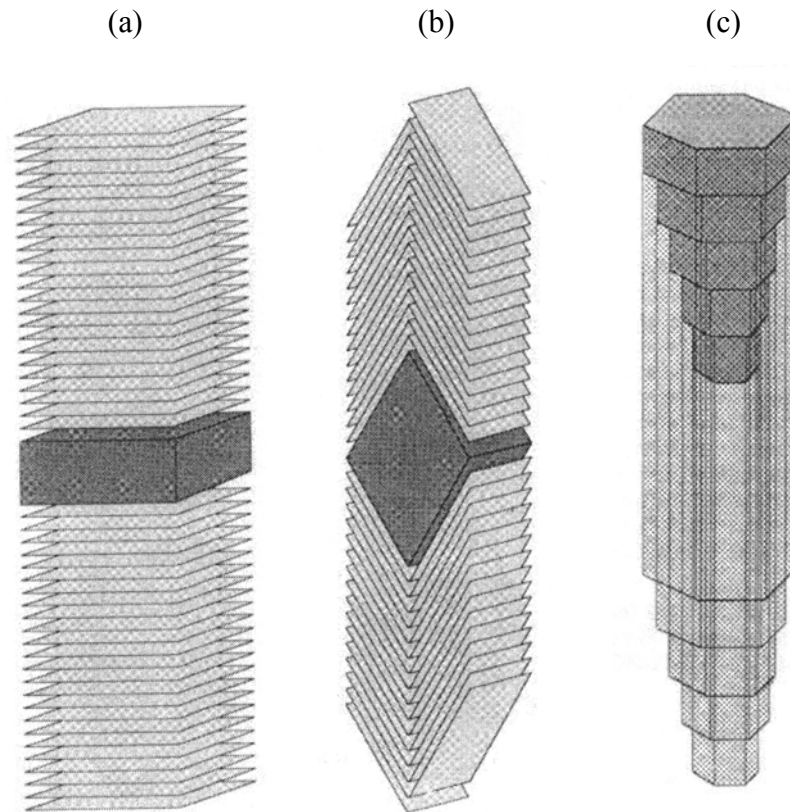


Figure 2.4: Schematic diagrams of the different catalyst morphologies and the respective differences that the catalyst morphologies impart on the carbon fibres produced. (a) Shows a platelet nanofibre; (b) shows a "herringbone" nanofibre and (c) shows a carbon nanofibre growing off an elongated catalyst particle [10].

Baker and co-workers [9] also discussed the relationship between metal catalyst morphology and the structural characteristics of the carbon deposited. Here they used controlled atmosphere electron microscopy (CAEM) to show the various morphological characteristics of different bimetallic catalyst particles during interaction with selected gas mixtures, the bimetallic catalyst particles are prepared by co-precipitation of the respective metal carbonates from metal nitrate solutions using ammonium bicarbonate, a schematic representation of these catalyst particles is shown in Figure 2.5.

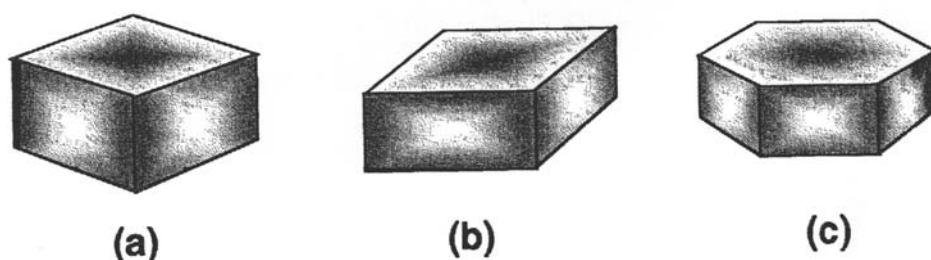


Figure 2.5: Schematic representation of the observed morphological characteristics of various bimetallic particles during interaction with selected gas environments. (a) an Fe-Ni (5:5) particle undergoing reaction in C_2H_4/H_2 (4:1) at $500^\circ C$; (b) a Cu-Fe (2:8) particle heated to $475^\circ C$ in the presence of CO/H_2 (4:1); and (c) a Cu-Co (1:3) particle treated in C_2H_4/H_2 (4:1) at $525^\circ C$ [9].

The way in which the graphite platelets grow off from these morphologically different catalyst particles is the determining factor in the type of carbon filament produced, a schematic representation of the different arrangements observed is shown in Figure 2.6.

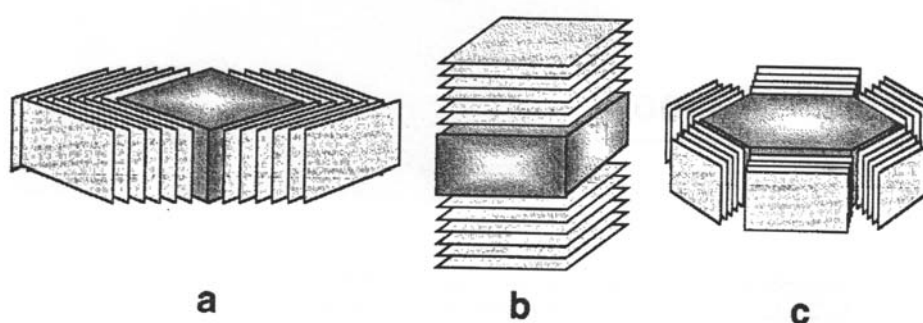


Figure 2.6: Schematic representation of the platelet arrangements generated from the three different catalyst particles shown in Figure 2.5. (a) "herringbone" nanofibre; (b) and (c) platelet nanofibre [9].

In this paper Baker and co-workers not only discuss the mechanisms by which carbon filaments are produced, and how the different catalyst morphologies affect the types of filament produced, but they also discuss the mechanisms by which

encapsulation of the catalyst particles could occur and lead to catalyst deactivation. The authors propose two different mechanisms by which this process could occur and these are shown in Figures 2.7 and 2.8.

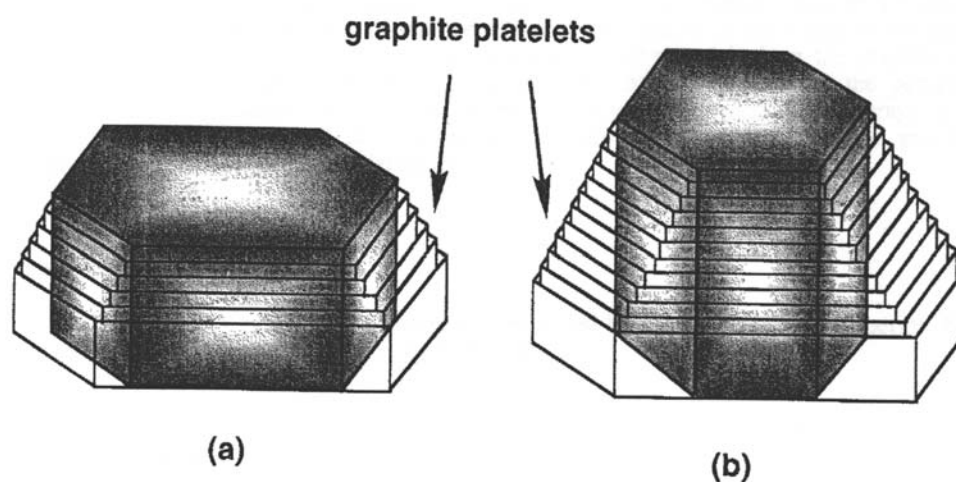


Figure 2.7: Schematic representation of a possible growth mechanism for the shell-like graphitic deposits, where the catalyst particle shape changes, but the overall volume remains the same [9].

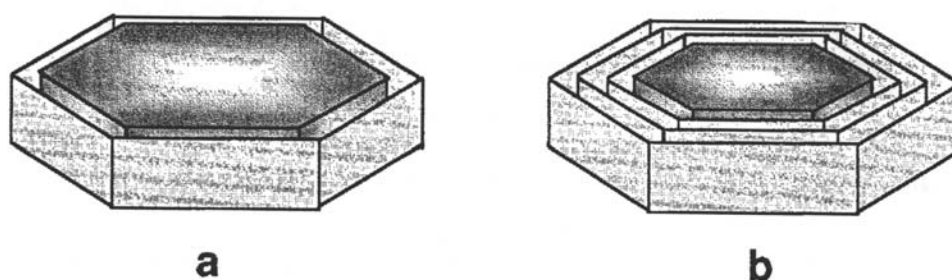


Figure 2.8: Schematic representation of a possible growth mechanism of the shell-like graphitic deposits, where the catalyst particle undergoes a wetting and spreading action with the platelet structures and the particle is progressively depleted in size as the reaction proceeds [9].

This complementary work shows that the morphology of the catalyst particle affects the type of carbon nanofibres produced. They authors show that square or diamond shaped catalyst particles can give rise to both herringbone and platelet nanofibres,

where as rectangular or hexagonal catalyst particles will yield solely platelet nanofibres. However, Rodriguez *et al.* [21] showed that hexagonal catalyst particles could also lead to the formation of nanofibres with a hollow core (these could be mistaken for multi-walled nanotubes) which are produced from elongation of the catalyst particle, whereas Baker *et al.* [9] showed that hexagonal catalyst particles could lead to the formation of a crust of carbon around the catalyst particle therefore deactivating it towards further carbon deposition.

In cases where morphologically similar catalyst particles can lead to the formation of a number of different types of carbon deposits it is likely that the faces of the catalyst particles which are responsible for adsorbing and desorbing the carbon will ultimately determine the type of carbon deposited, although little work has been done to determine which catalyst faces lead to deposition of carbon and which to adsorption of carbon.

2.4.2.2. Carbon Nanotubes

Another form of nano-structured carbons are carbon nanotubes, these consist of multi-walled or single-walled tubes and were first discovered by Iijima [18, 19].

Iijima [18] reported the formation of “helical microtubules of graphitic carbon”. In this work “graphitic carbon needles” were produced ranging from 4 – 30 nm in diameter and up to 1 μm in length. These deposits were grown on the negative end of the carbon electrode used in the dc arc-discharge evaporation of carbon in an argon filled vessel at 13.3 kPa.

The graphitic carbon needles formed consisted of co-axial tubes of graphitic sheets ranging in number from 2 – 50 and in each tube the carbon atom hexagons were observed to arrange about the needle axis in a helical fashion. Images showing how the multi-walled nanotubes are constructed are shown in Figure 2.9 and Figure 2.10. Figure 2.9 shows how multiple graphitic sheets can build up to form the walls of multi-walled nanotubes, Figure 2.9 (a) shows transmission electron micrographs of three different multi-walled carbon nanotubes with 5, 2 and 7 concentric graphitic sheets making up the wall of the tubes.

Carbon nanotubes which are constructed from a single graphitic sheet and therefore only have one co-axial tube making up the walls of the tube are termed – single-walled carbon nanotubes.

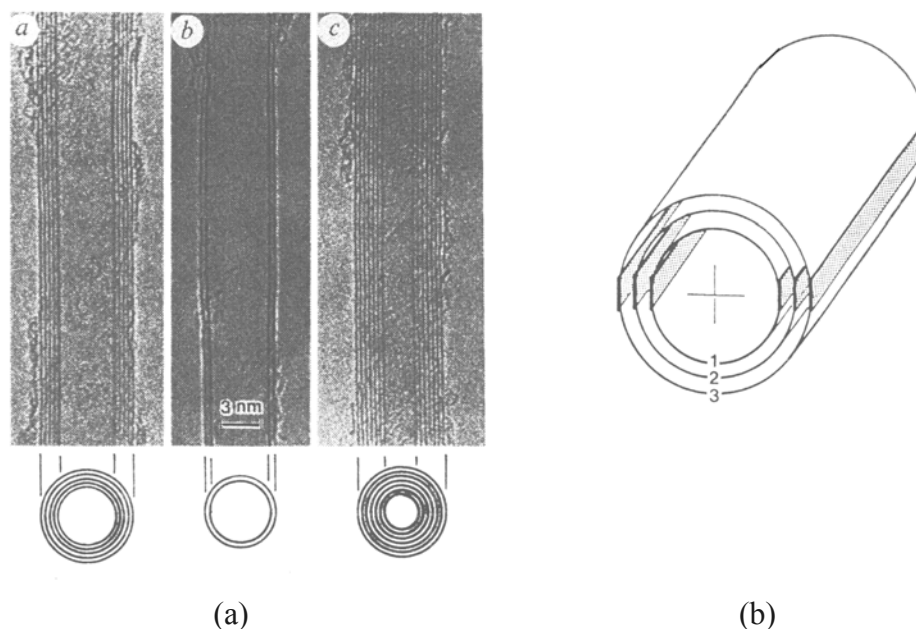


Figure 2.9: (a) shows transmission electron micrographs of multi-walled nanotubes with schematic representations of how they are constructed with 5, 2 and 7 graphitic sheets; (b) shows a schematic representation of how multi-walled nanotubes are constructed of concentric graphitic sheets [18].

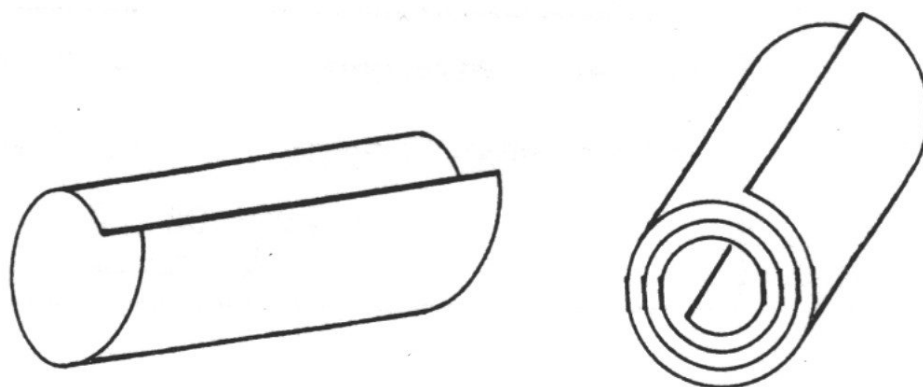


Figure 2.10: Schematic representation of how multi-walled carbon nanotubes can be formed by from a single graphitic sheet which wraps around on itself [18].

As a follow on to this work Iijima and Ichihashi [19] went on to study carbon nanotubes with diameters in the region of 1 nm. In this work they again used dc arc-discharge but with the chamber filled with 1.33 kPa methane and 5.33 kPa argon and with the cathode containing a small piece of iron. On heating the iron melts and forms iron vapour which cools and condenses as iron carbide particles above the cathode.

They found that, using this method, bundles of tubes as well as separate single shelled carbon tubes (single-walled carbon nanotubes) were formed, they postulated that the single shelled carbon nanotubes formed are the precursor for the formation of thicker multi-walled carbon nanotubes.

Another more recently categorised form of carbon nanotubes are “bamboo-shaped” carbon nanotubes, which are the most common member of carbon nanotubes with special structures e.g. bamboo-shaped [5, 24-27], Y-junctions [27] and coils [28-30]. TEM

images of bamboo-shaped carbon nanotubes are shown in Figure 2.11.

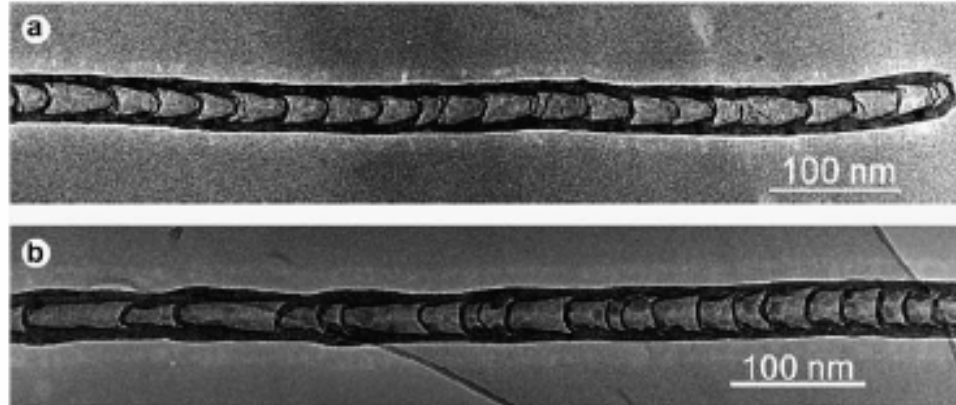


Figure 2.11: TEM images of bamboo-shaped carbon nanotubes constructed with compartments with regular dimensions (a) and with different dimensions (b) [26].

This section has shown that there are various types of nano-structured carbon filaments formed from the catalytic deposition of carbon, these range from larger diameter fibrous deposits to narrower tubular deposits, where the diameter of the catalyst particle is the determining factor in the diameter of the nano-filament produced. Proposed growth mechanisms for the different nano-structured carbon filaments will be discussed later in section 2.4.4.

2.4.3. Preparation Methods

This section will look at different processing techniques used i.e. catalyst, catalyst support, temperature and gas feedstock and how these affect the amount and type of carbon deposited. This section will first highlight the different types of catalysts and catalyst

supports used then, as the work presented subsequently in this thesis will focus upon the use of nickel as a carbon deposition catalyst, this section will look at reported work concerning the use of nickel catalysts for carbon deposition before further discussing work which has been presented using other catalysts for the catalytic deposition of carbon.

One of the first possible discoveries of what could have been carbon nanofilaments (described as “hair-like carbon filaments”) came in 1889 when T.V. Hughes and C.R. Chambers [31] filed a patent describing the use of an iron furnace through which a gaseous carbon compound was passed at elevated temperatures, yielding “loose fibrous or cob-web like” masses of carbon. Although it is likely that the authors were indeed forming carbon nanostructures, as they were passing carbon containing gases over iron at elevated temperatures, the technology required to observe these different forms of carbon was not readily available until the latter half of the 20th century, when the development and availability of electron microscopy led to the emergence of a new scientific discipline – nanoscience. The introduction of electron microscopes has helped lead to the discovery and characterisation of Buckminster fullerene and other carbon nanostructures i.e. nanotubes and nanofibres amongst others.

However before the discovery of fullerenes [17] and nanotubes [18, 19] there was a number of scientists looking at catalytically depositing carbon. Of these, the work by Baker *et al.* [32-40] in the early to mid 1970s was pioneering in the implementation of

catalytic carbon deposition for the formation of filamentous carbon and other carbonaceous deposits utilising a number of different catalysts and carbon precursors.

2.4.3.1. Catalysts and Catalyst Supports Used

The most common catalysts used for the catalytic deposition of carbon are the transition metals: iron, nickel and cobalt; although a variety of other metals has also been used to deposit carbon catalytically these include vanadium, manganese, copper, zinc, molybdenum, zirconium and cerium [41] along with palladium [42] and platinum [43, 44]. A number of alloys has also been used including alloys of iron with nickel or cobalt [9, 45-50] and alloys of iron, nickel or cobalt with copper [7, 9, 10, 51].

Tungsten-rhenium alloy wires have also been used [52] as have platinum-tin alloys [44], however this list is not exhaustive, as it only focuses upon some of the more commonly used catalysts for carbon deposition.

These catalysts have been supported on a variety of different support media, from carbon fibre based supports [11, 13-15, 53, 54] (i.e. individual fibres or preforms) to ceramic supports [41, 44, 55] (i.e. silica or alumina) as well as silicon [42], silicon nitride [43] and magnesium oxide [56], amongst others.

2.4.3.2. Nickel and Nickel – Containing Catalysts

From an industrial perspective the use of methane as a carbon deposition gas feedstock would be desirable, as methane is the main component of natural gas (which is the gas currently used in

industry for the manufacture of carbon-carbon composites). However, due to the relative stability of methane compared to other short-chain hydrocarbons, in particular unsaturated hydrocarbons, the catalytic deposition of carbon from methane does not occur until relatively high temperatures are reached ($\geq 900^{\circ}\text{C}$), and even then the rate of carbon deposition is relatively low. Despite this a number of authors has still attempted to use methane as a carbon precursor to catalytically deposit carbon over nickel.

Baker *et al.* [39] discussed the reaction of methane over nickel and the types of carbonaceous deposits that are formed during this reaction. Here they used controlled atmosphere optical microscopy utilising a piece of nickel foil (approx. 5 mm wide) as the catalyst, this was then reacted with methane at 80 kPa between 750 and 1060°C for up to 12 hours.

In this work the authors found that at 850°C carbon deposits were apparent after 5 min and these carbonaceous clusters grew in size and coverage with time. These clusters were found not to be fibrous in nature, however at 900°C and after 2 hours, fibrous growths were observed (2 μm in width and up to 50 μm in length), these fibrous deposits expanded in width and increased in length over time.

Tekunova and Tesner [52] also looked at depositing carbon from methane over nickel. Here they used a nickel sheet as the catalyst, with methane flowing at $0.500 \text{ dm}^3 \text{ min}^{-1}$ @ STP as the carbon precursor. The reactions were carried out at 1000°C and the authors claimed that deposition rates for the nickel catalyst reached

steady state after 4 hours with the formation of amorphous carbon films reaching a thickness of 3 μm .

Kong, Cassell and Dai [57] also discussed the chemical vapour deposition of methane for the production of single walled carbon nanotubes. In this work they used nickel oxide (NiO) or a nickel oxide / cobalt oxide alloy (NiO/CoO 1:1) these were supported on either alumina or fumed silica. They took approximately 10 mg of the supported catalysts and reacted them at 1000°C in methane (6.15 $\text{dm}^3 \text{min}^{-1}$ @ STP).

They found that the catalysts supported on alumina produced a mixture of individual single walled nanotubes and also small bundles of nanotubes, whereas the catalysts supported on silica only produced small bundles of single walled nanotubes.

However, for all of the work carried out by Baker *et al.* [39], Tekunova and Tesner [52] and Kong *et al.* [57] the reaction temperatures used were in excess of 850°C and at these temperatures methane will pyrolytically decompose to form solid carbon without the presence of a catalyst, therefore with all of this work it is difficult to determine whether the carbon being deposited was deposited *via* catalytic means or pyrolytic means or a combination of the two (which is more likely).

Despite the results of the previous authors [39, 52, 57], other authors continued to persevere with the deposition of carbon from methane over nickel.

Guerts and co-workers [47] used an FeNi alloy as a catalyst which was exposed to a multi-component gas mixture comprised of

hydrogen, carbon monoxide, methane, carbon dioxide and water vapour. Prior to carbon deposition the catalyst samples were heated in flowing hydrogen from room temperature to the reaction temperature of 627°C at a rate of 7°C per minute. After reaching the reaction temperature the catalysts were kept in flowing hydrogen for 100 min prior to the introduction of the reaction gas mixture. The reaction gas mixture was then either kept constant for the entire run or was systematically and incrementally changed, the total flow rate of the gases was 1.2 dm³ min⁻¹ @ STP. The authors found that the carbon filaments produced from the reactions consisted of an alloy catalyst particle at the tip of the fibre – not the pure metal. They also observed that the overall weight gain due to carbon deposition decreased as the nickel content in the alloy was increased.

Tsai *et al.* [55] discussed the formation of carbon nanofibre films on metallic nanowire arrays. In this work they used a nickel nanowire array with a thickness of 100 µm and a diameter of 30 – 40 nm. They exposed this to a mixture of methane and hydrogen (0.009 and 0.041 dm³ min⁻¹ @ STP respectively) at 5.3 kPa and 650°C. They found that under the described conditions they could grow carbon nanofibres *via* the tip-growth mechanism without the undesired production of soot.

Liao and Ting [58] looked at the effect of nickel catalyst characteristics on the growth of carbon nanowires. In this work the authors used thin films of nickel (10 – 286 nm) supported on silicon substrates. These catalysts were exposed to a mixture of methane

and hydrogen (1:9) at 450 – 510°C in a plasma for 3 min. The amorphous nickel thin films were capable of producing carbon nanowires with diameters of ~ 40 nm.

Fenelonov *et al.* [51] reported that a nickel catalyst was capable of depositing carbon with relatively high yields (up to 300 grams of carbon per gram of catalyst) from a methane gas feedstock at 550°C. They found that during the carbon deposition process the catalyst particles grew in size from 0.25 – 0.5 μm to 3 – 5 μm .

However, the size of these particles is not in the size range usually stated as being required for the deposition of carbon nanofilaments, there is therefore some scepticism as to whether the results obtained were true results, mainly due to the reaction temperature used, and it was also extremely unlikely that the carbon deposited would be filamentous in nature, due to the size of the catalyst particles used. There is also reason to be sceptical about the work carried out by Guerts *et al.* [47], Tsai *et al.* [55] and Liao and Ting [58], who claimed to be able to deposit carbon over nickel using methane as the carbon precursor at temperatures of 627, 650 and 450 – 510°C respectively, as ΔG for the decomposition of methane becomes negative at 538°C, meaning that the decomposition of methane is not thermodynamically feasible at temperatures below 538°C, and even at temperatures above 538°C, the reaction will not be kinetically feasible until the required activation energy for the reaction to proceed is available. So the temperatures used by these authors were likely to be too

low to induce the catalytic deposition of carbon, over nickel from methane, to any appreciable degree.

However, in the work carried out by Guerts *et al.* [47] the carbon deposited could be from the decomposition of carbon monoxide and/or carbon dioxide.

From an industrial point of view the use of short-chain saturated hydrocarbons for the catalytic deposition of carbon would be preferred (for cost and ease of supply reasons), and as methane is a relatively poor carbon precursor for the catalytic deposition of carbon, in that it only offers small reductions in temperature and relatively low rates of carbon deposition, the next logical step would be to investigate the potential of ethane as a carbon precursor for the catalytic deposition of carbon.

Rodriguez *et al.* [49] discussed the deposition of carbon over iron-nickel alloy particles and how the temperature and additives to the gas mixture affect the type of carbon formed. They used iron-nickel alloys, with 8:2 and 5:5 atomic ratios, as the catalysts, these had surface areas of 1 m²/g and diameters of ca. 1 µm, 0.4 g of the catalyst powders were exposed to a mixture of ethane and helium (1:1) at temperatures ranging from 815°C to 865°C. They found that lower temperatures favoured the production of carbon nanofibres and higher temperatures favoured the production of graphitic shell-like encapsulating carbon. Although no rates for carbon deposition were given, the authors found that on increasing the temperature from 815 to 865°C the ratio of pyrolytically deposited carbon to catalytically deposited carbon increased and

that by increasing the ratio of iron in the alloy the ratio of solid carbon formed increased (as highlighted in Tables 2.1 and 2.2), this is in contrast to the work by Guerts *et al.* [47] who found that by increasing the nickel concentration in an iron-nickel alloy the rate of carbon deposition increased when methane was used as the carbon precursor. They also found that if they added H₂S to the gas mixture then this favoured, almost exclusively, the formation of graphitic shell-like carbon.

Temp. /°C	Catalytic Carbon	Pyrolytic Carbon	CH ₄	C ₂ H ₄	C ₂ H ₆	C ₃ and C ₄
815	9.5	15.8	42.4	19.7	11.9	0.95
840	3.7	30.7	55.2	6.3	3.6	0.20
865	1.4	37.5	47.7	3.4	10.1	0.0

Table 2.1: Product distribution (wt. %) for the decomposition of ethane over an Fe-Ni (5:5) alloy powder [49].

Temp. /°C	Catalytic Carbon	Pyrolytic Carbon	CH ₄	C ₂ H ₄	C ₂ H ₆	C ₃ and C ₄
815	54.0	1.0	22.8	9.8	12.4	-
840	25.5	24.0	39.4	6.2	4.9	-
865	25.4	29.7	39.6	3.2	2.0	-

Table 2.2: Product distribution (wt. %) for the decomposition of ethane over an Fe-Ni (8:2) alloy powder [49].

Although, as highlighted previously, some work has been carried out looking at catalytic carbon deposition over nickel with short-chain saturated hydrocarbons as the carbon precursors the majority of the reported work surrounding the catalytic deposition of carbon over nickel has focussed upon using more reactive unsaturated hydrocarbons, the most common of these is acetylene.

For almost all of the reactions carried out using acetylene as the carbon precursor the reactions are carried out at sub-atmospheric

pressures, and the work is normally carried out using controlled atmosphere electron microscopy (CAEM), which involves the incorporation of a reaction cell to the sample chamber of a transmission electron microscope, the reaction cell allows the sample under microscopic investigation to be heated and exposed to reactive gas atmospheres whilst being viewed *in situ*.

Baker and co-workers [32] discussed the nucleation and growth of carbon filaments from the decomposition of acetylene over nickel. They used a nickel catalyst which was in the form of a nickel strip. The reactions were carried out using CAEM, for the deposition of filamentary carbon the temperature used was 597°C and the acetylene pressure was varied from 50 – 260 Pa. They observed that at 597°C the nickel particles were mobile and became detached from the support, this allowed the carbon filaments to grow from underneath the nickel particles and force them away from the support surface (now commonly referred to as “tip growth”). They also noted that increasing the acetylene pressure from 50 - 260 Pa did not increase the rate of carbon deposition. The filaments produced were typically 30 nm in diameter and had lengths varying from 0.53 – 1.1 µm.

In a further study [59] using CAEM with acetylene as the carbon precursor. It was found that the onset of filament growth occurred at 510°C in 266.6 Pa of acetylene and that almost all of the filaments produced were formed by the tip-growth mechanism, which agrees with the results reported by Baker *et al.* [32], with only a few being formed *via* the root-growth mechanism.

Yokomichi and co-workers [60] also used pure nickel to catalytically deposit carbon nanotubes and amorphous carbon films simultaneously by thermal chemical vapour deposition. Here they used 30 nm thick nickel films supported on Si or SiO₂, which were etched in NH₃ gas at 800°C, prior to carbon deposition in acetylene (0.010 dm³ min⁻¹ @ STP and 4 Pa) at 600 – 900°C, although the reactions were carried out at sub-atmospheric pressures, instead of using CAEM the reactions were carried out in a silica glass reaction tube. From the reactions the authors concluded that:

- A. The growth of carbon materials is promoted by nickel.
- B. Nanotube diameter is equal to nickel catalyst particle diameter.
- C. Carbon nanofibres are fabricated if the nickel grain size is > 100 nm.
- D. Amorphous carbon is formed if the nickel grain size is larger than 1 µm.

Nickel containing alloys have also been used to catalytically deposit carbon from acetylene. Baker and Chludzinski [61] again used CAEM to study the reaction of deposited nickel – iron particles with acetylene. They found that the formation of carbon filaments from 5 to 50 nm in diameter and 300 nm in length began at 480°C and as the temperature was increased the size and number of filaments also increased. In this work the authors also show that the formation of carbon filaments on nickel – iron is much more prominent than either of the pure metals alone.

Kim *et al.* [62] attempted to determine the role of catalyst composition on the structure of the carbon deposits formed using nickel-copper catalysts over the temperature range of 450 – 700°C. They again used CAEM to carry out the experiments with the metal catalyst in either a 1:1 Ni:Cu ratio; pure copper; copper rich or nickel rich in order to determine the effect of catalyst composition on the growing carbon filaments. The experiments were carried out in 266.6 Pa of acetylene.

The authors showed that for nickel rich catalyst particles the growth of carbon filaments commenced at 285°C following the structural transformation of the catalyst particles from globular to faceted. In this study the filaments grew in a bidirectional fashion with the catalyst particles being located in the body of the filament.

They noted that as the temperature was increased there was a corresponding increase in the size and number of new filaments being deposited, this growth of filaments slowed remarkably at 700°C with the loss in activity being more pronounced at 740°C.

For the copper rich samples the reactivity pattern was similar in many respects to that of the nickel rich system, however, in this system the catalyst particles produced coiled “spring-like” carbon filaments.

They also noted that when pure copper was used as the catalyst carbon deposition did not occur up to 950°C, this deposition is likely to be due entirely to the pyrolytic deposition of carbon.

This body of work has shown that acetylene can be used as the carbon precursor to catalytically deposit carbon over a nickel

containing catalyst at pressures from 4 to 266.6 Pa at temperatures ranging from 285 to 900°C.

Another common short-chain unsaturated hydrocarbon which is used to deposit carbon over nickel containing catalysts is ethylene.

Kim and co-workers [7] used nickel and nickel-copper alloys to deposit carbon filaments from ethylene. They found that the carbon filaments produced had diameters in the range of 25 to 100 nm and that diamond shaped catalyst particles were located within the filament structures.

In this study the authors noted that the period of catalytic activity is related to the amount of catalyst present and that the weight of the carbon deposit reached a maximum at about 200 to 250 times that of the original weight of catalyst (50 – 100 mg). They also found that adding an inert carrier gas (i.e. argon or helium) to the reaction gas mixture had no effect upon the amount of hydrocarbon which was converted to carbon. Over a nickel catalyst the authors found that the addition of hydrogen to an ethylene gas feed increased the weight of carbon deposited if hydrogen was added up to 50 %, however, if further hydrogen was added to the ethylene gas feed then the amount of carbon deposited steadily declined.

Although the authors conclude that it is not clear as to why the addition of hydrogen promotes carbon deposition with nickel catalysts, they postulated that it may be possible that the hydrogen is preventing the polymerisation of adsorbed ethylene molecules on the metal surface and therefore reducing the potential for

deactivation of the catalyst by the formation of a graphite overlayer.

Rodriguez *et al.* [63] looked at the deactivation of copper – nickel catalysts due to changes in the surface composition of the catalyst alloy particles. Here the catalyst particles were prepared from co-precipitation of the metal carbonates from the nitrate solution mixed in the desired quantities, using ammonium bicarbonate. The powdered catalyst samples (50 mg) were then reacted in ethylene/hydrogen mixtures at temperatures ranging from 550 to 900°C.

In this work the authors showed that the deactivation of the alloy particles is a complex process which depends on a number of different factors. They showed that if hydrogen is added to ethylene then the deactivation of the catalyst particles occurs at higher temperatures and that lowering the temperature can rejuvenate a deactivated catalyst, they postulate that this phenomenon is due to the re-organisation of the alloy particle back to its original composition after it was found that separation of the alloy occurs much more readily in ethylene than it does in hydrogen.

Park and co-workers [45] looked at carbon deposition over iron – nickel alloy catalysts when exposed to ethylene – hydrogen gas mixtures. The Fe-Ni bimetallic powders with compositions (7:3, 3:7 and 2:8), were exposed to ethylene at $0.040 \text{ dm}^3 \text{ min}^{-1}$ @ STP plus hydrogen and argon to a total flow of $0.100 \text{ dm}^3 \text{ min}^{-1}$ @ STP at 600°C.

They found that the composition of the Fe-Ni catalysts influenced the crystalline nature and structure of the carbon filaments produced and that, as found by Rodriguez *et al.* [63] and Kim *et al.* [7], the addition of hydrogen improved the catalytic behaviour. They also found that increasing the temperature from 600°C to 725°C favoured the decomposition of ethylene and adding 5 % nickel to a Fe-Ni (3:7) catalyst increased the amount of solid carbon formed from 4.6 to 38.5 wt.% with respect to the catalyst, this agrees with the work carried out by Guerts *et al.* [47] who also found that increasing the nickel content in an Fe-Ni alloy increases carbon deposition, however, this finding is disputed by Rodriguez *et al.* [49], who found that increasing the nickel content in an Fe-Ni alloy decreases the rate of formation of carbon.

As well as short-chain hydrocarbons, other carbon precursors have been used in order to try to deposit carbon catalytically over nickel or nickel-containing catalysts. These include carbon oxides, either alone [50, 64] or with hydrocarbons [46], as well as longer-chain alkenes i.e. 1-butene, 1,3-butadiene [65] and xylene [48].

2.4.3.3. Nickel – Free Catalytic Carbon Deposition

As with nickel and nickel containing catalyst, the catalytic deposition of carbon has also been carried out over a number of other catalysts, these mainly focus upon the transition metals and in particular iron and cobalt, using a variety of different carbon deposition conditions of temperature and carbon precursor. The majority of the work using nickel free catalysts focuses upon using acetylene over iron or cobalt containing catalysts.

Baker and co-workers [33] looked at the formation of filamentous carbon over iron, cobalt and chromium, using acetylene as the carbon precursor. Here they observed that all filaments had a catalyst particle at their growing end (tip-growth) and that it was this particle which determined the fibre diameter. They found that fibre diameters ranged from 10 – 150 nm and that fibre lengths ranged from 0.5 – 8 μm over temperatures ranging from 512°C to 972°C. Their results showed that growth rates for the iron and cobalt systems were similar to those of the nickel system and that growth times to completion are dependant on reaction temperature, at 652°C filament growth was observed for up to 10 min whereas at 972°C the growth of the filaments ceased after only 30 sec, this would be expected as at higher temperatures the rate of reaction would be higher and therefore the formation of a carbon layer around the catalyst particle would form more quickly.

The authors confirmed this by stating that high magnification images of filaments that had ceased to grow showed that in all cases the catalyst particles had become encapsulated by a layer of carbon. Although Baker *et al.* [32, 33] found that the decomposition of acetylene on nickel, iron and cobalt exhibited similar growth mechanisms i.e. the catalyst particle determined the diameter of the filament and in all cases the filament had a catalyst particle at its tip, for the chromium catalyst a different growth mechanism was observed.

In the case of chromium catalysts carbon deposition did not occur until 802°C and in this case carbon deposition was observed

whilst the chromium catalyst particle stayed in contact with the support and the carbon was extruded through the catalyst particle (root-growth) [33], today these two growth mechanisms have been more clearly defined as “tip-growth” and “root-growth” respectively.

In order to rate the efficiency of acetylene as a carbon precursor for carbon deposition other experiments were carried out using different carbon precursors, these were: ethylene, benzene (with hydrogen carrier gas), 1, 3 – butadiene, allene and methyl acetylene, all of these carbon precursors yielded poor amounts of deposited carbon in comparison to acetylene at 725°C and 8 kPa, by comparison of weight gains, post-reaction, due to carbon deposition [37], these results are shown in Table 2.3.

<u>Hydrocarbon</u>	<u>Deposited Carbon Yield Relative to Acetylene</u>
Ethylene	0.01
Benzene (+H ₂)	0.03
1,3 – Butadiene	0.10
Allene	0.16
Methyl Acetylene	0.59
Acetylene	1.00

Table 2.3: Variation of deposited carbon yield from various hydrocarbons relative to acetylene, calculated from weight change measurements [37].

The results reported in the previous two papers by Baker and co-workers [32, 33] led them to try to optimise the process by determining the optimum production conditions for filamentous carbon using the cobalt catalyst with acetylene. In this paper [36] the authors varied the temperature of reaction, the acetylene

pressure and flow rate and the reaction time, they also investigated the effect of preheating the gases and the effect of adding hydrogen to the acetylene in a 1:1 ratio.

They found that, using 800 Pa of acetylene for 10 min, at temperatures ranging from 525 – 925°C, the maximum yield of filamentous carbon occurred at 725°C, here the fibres also exhibited the maximum mean width of 122.5 nm, they also noted that there did not appear to be any correlation between fibre length and reaction temperature. After determining that the optimum temperature for the reaction was 725°C they varied the acetylene pressure from 0.8 – 26.7 kPa, in doing this they found that the optimum pressure was between 8.0 and 13.3 kPa, they also noted that in raising the pressure there was no appreciable shift in the optimum temperature of 725°C. In varying the flow rate of the acetylene they found that the optimum flow rate was in the range 0.010 – 0.040 dm³ min⁻¹ @ STP and that flow rates outside of this range gave inferior yields. When deposition times were varied from 10 – 240 min under the previously determined optimum conditions of temperature pressure and flow rate, it was found that there was a dramatic increase in filament yield when the deposition time was increased from 10 – 30 min, but that a further increase in deposition time to 240 min only gave a marginal increase in filament yield. Pre-heating the acetylene to either 550°C or 650°C also improved the yield of carbon filaments as did the addition of hydrogen to the gas mixture when pre-heated to the same

temperatures, which again agrees with previous reports [32, 33, 35, 37-39].

The surface state of an iron catalyst on the formation of carbon filaments was also studied [66]. In this work CAEM was again used with acetylene to study the formation of carbon filaments, the catalysts studied for the formation of the carbon filaments were pure Fe, FeO and Fe₂O₃. In order to produce essentially pure FeO a piece of pure Fe foil was heated in steam at 800°C for 3 hours, from the weight gain data for this it was concluded that in this time a 0.13 mm thick piece of Fe foil was converted into FeO which is rough and faceted in nature. The deposits formed from the reactions of this foil in acetylene produced predominantly carbon filaments. In this work, one of the main discussion points was the role that the oxide takes in dramatically increasing the rate of carbon formation, here the authors speculated that:

"The oxygen atoms in the surface will be readily accessible to extraction by protons generated by the hydrocarbon decomposition reaction and as a results the oxide could rapidly attain at the surface an iron-rich sponge-like arrangement i.e. the role of the FeO is that of a precursor for a high surface area Fe catalyst formed in situ."

The reasoning behind this lies in the observed data that shows that after reaction of the FeO and Fe₂O₃ only metallic iron and iron carbide remain in the sample indicating that the chemical state of the iron after reaction is essentially the same for all catalyst

precursors, therefore the differences in activity must be due to differences in effective surface areas.

In a continuation to using an iron catalyst – work was reported using either α -iron or γ -iron supported on either graphite or silica, acetylene as the carbon precursor and CAEM to carry out experiments [67].

For the α -iron/graphite – acetylene system they found that the formation of carbon filaments by the tip-growth mechanism commenced at 530°C and continued in a uniform manner up to 765°C when the formation of filaments ceased, this observed inactivity continued up to 865°C when the filaments began to grow again, however at this temperature the filaments were formed through the root-growth mechanism and the particles which had produced filaments at lower temperatures did not regain their activity.

For the α -iron/silica – acetylene system it was found that it was necessary to heat the samples in hydrogen prior to reaction in order to achieve sufficient nucleation of the α -iron particles. After the nucleation step in hydrogen at 650°C it was found that the growth of carbon filaments from acetylene commenced at 530°C and the growth characteristics observed were the same as for the α -iron/graphite – acetylene system, whereby the mechanism for filament growth was by a tip-growth mechanism at 530°C.

In the γ -iron/graphite – acetylene system the formation of carbon filaments commenced at a lower temperature than previously observed of 380°C and filament growth ceased at 685°C,

in this system the filament also grew by the tip-growth mechanism as previously observed for the other two systems, however in this case almost all of the catalyst particles were responsible for filament growth as opposed to approximately one quarter of catalyst particles, which was observed the α -iron system.

In the γ -iron/silica – acetylene system filament formation was not observed until 650°C and there was no appreciable increase in the rate of formation when the temperature was raised to 935°C, it was also noted that in this system filament growth was extremely slow when compared to the other systems and it was revealed that less than 5 vol. % of the catalyst particles were responsible for filament formation.

Baker and Waite [38] investigated carbonaceous deposits formed from the decomposition of acetylene on platinum-iron catalysts. Here they used the same CAEM as mentioned previously [32, 33] and deposited the Pt-Fe catalyst from a metal wire of composition 54 % Pt : 46 % Fe onto graphite or silica supports.

The Pt-Fe alloy films were divided into particles by treatment in 70 Pa of hydrogen or argon at 647°C. Acetylene was then introduced at ambient temperature and at 70 Pa, as the temperature was increased the authors observed that at 417°C the alloy particles changed shape from irregular to spherical and movement of material was observed in the particles, this movement was due to the separation of the Pt and the Fe to leave a dense iron embryo surrounded by a lighter platinum “apron” (with the relative width of the iron embryo to the platinum apron being 1:7), this

arrangement is shown in Figure 2.12. This behaviour was immediately followed by the growth of carbon filaments.

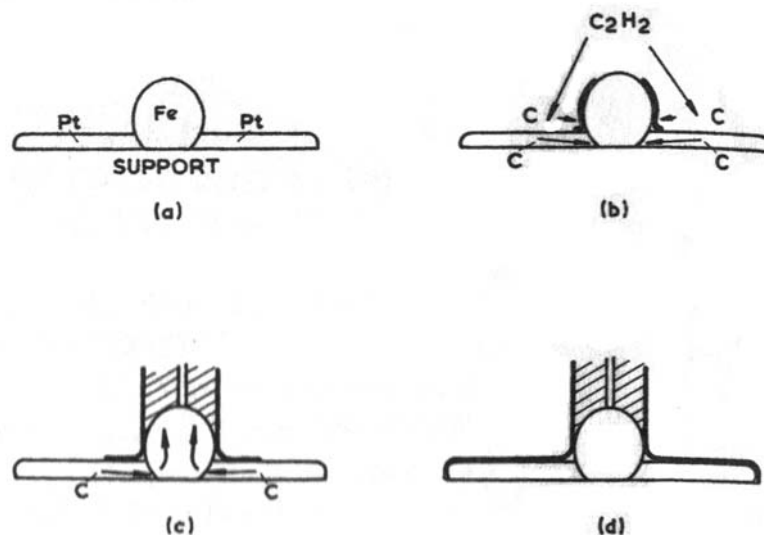


Figure 2.12: Mechanism of carbon filament formation from a platinum-iron catalyst [38].

It was noted that the diameter of the filaments was approximately equal to that of the iron core and not the entire catalyst particle. Filament growth continued up to $717^{\circ}C$ at which point the amount of amorphous carbon deposits formed became appreciable and prevented the contact of the acetylene with the catalyst. This shows that platinum is inactive to the catalytic deposition of carbon from acetylene and forms an inactive barrier around the carbon so that deposition will not occur until the two components of the alloy separate.

However, this hypothesis is in contradiction to the work carried out by Owens *et al.* [68] who looked at using platinum as a carbon deposition catalyst. They used platinum wires and platinum

supported on graphite. The carbon deposition was carried out in either acetylene or ethylene. The authors concluded that the addition of hydrogen to the deposition gas mixture increased the rate of carbon deposition, but they inferred that this could be due to a different type of carbon being formed (as hydrogen concentration increased the amount of amorphous carbon deposited increased), as opposed to the hydrogen keeping the metal surface clean, due to the lack of an increase in the formation of methane with the introduction of hydrogen. They also infer that instead of keeping the metal surface clean the hydrogen is capable of reconstructing the surface of the platinum, and it is this reconstruction of the catalyst particle which is responsible for the increase in carbon deposition with the addition of hydrogen.

As well as iron, cobalt, chromium and platinum, the use of vanadium and molybdenum as carbon deposition catalysts has also been reported. Baker *et al.* [69] moved from studying the formation of carbon on iron sub-group metals and looked at the production of filamentous carbon over vanadium and molybdenum using acetylene as the carbon precursor.

In this work the authors again use CAEM with acetylene as the carbon precursor and either strips of vanadium or molybdenum foil or monolayer films of the metals on graphite as the catalyst.

The authors show that both vanadium and molybdenum are active catalysts for the catalytic growth of carbon filaments. In both cases it was found that there was an upper temperature limit above which the formation of carbon filaments ceased, for vanadium this

was 825 – 845°C and for the molybdenum this was 680°C. The authors attribute this loss of activity to the formation of a metal carbide, which is likely, as they also show that both VC and Mo₂C are inactive catalyst for the deposition of carbon filaments.

Again as with the nickel containing catalysts the use of ethylene as a carbon precursor was also studied, usually in conjunction with the added carbon precursor – carbon monoxide – and with iron or cobalt containing catalysts.

Rodriguez *et al.* [70] discussed the promotional effect of carbon monoxide on the decomposition of ethylene over an iron catalyst. In this work the authors used the same apparatus as described in the previous study [63] using a powdered iron catalyst (50 mg) but in this work the catalyst was exposed to either pure CO, CO-H₂, C₂H₄-H₂ or CO-C₂H₄-H₂ mixtures at 600°C for periods of up to 5 hours.

Carneiro *et al.* [71] reported the growth of carbon nanofibres from the iron – copper catalysed decomposition of CO/H₂ and C₂H₄/H₂ mixtures. In this work they used powdered Cu – Fe catalysts prepared by co-precipitation with compositions of 1:9, 3:7, 5:5, 7:3, 9:1 and pure Fe, 100 mg of each of these bimetallic powders or pure Fe were exposed to CO/H₂ (4:1 or 1:4) or C₂H₄/H₂ at temperature ranging from 500°C to 750°C.

They found that the reactions carried out using Fe alone produced low rates of carbon deposition whereas the bimetallic powders increased the rate of carbon deposition for the experiments carried out in C₂H₄/H₂, for the experiments carried out

in CO/H₂ the addition of copper had little effect upon the rate of overall carbon deposition.

The authors propose that three reactions could be contributing to the amount of CO converted to carbon after one hour at 600°C when hydrogen is added to the gas mixture, these are:

1. Boudouard reaction: $2\text{CO} \rightarrow \text{C} + \text{CO}_2$; this occurs at high CO:H₂ ratios.
2. CO hydrogenation: $\text{CO} + \text{H}_2 \rightarrow \text{C} + \text{H}_2\text{O}$; this occurs with equimolar mixtures of CO and hydrogen when about half of the solid carbon formed is from CO hydrogenation.
3. CO methanation: $\text{CO} + 3\text{H}_2 \rightarrow \text{CH}_4 + \text{H}_2\text{O}$; this occurs at high H₂:CO ratios where CO hydrogenation and methanation become the dominant reaction pathways.

When ethylene was introduced into the reactive gas mixture it was found that iron was a poor catalyst for the decomposition of ethylene when compared to nickel and cobalt, this was in contrast to iron being the most active catalyst for the decomposition of carbon monoxide. When the iron powder was reacted in a C₂H₄-H₂ (3:1) mixture the activity (the mass wt. % of solid carbon produced, which was determined using mass change measurements and confirmed by carbon mass balance using gas chromatography to monitor the gases exiting the reactor) was 0.43 wt. % and remained at this level for 1 hour, however the addition of carbon monoxide into the mixture to give CO-C₂H₄-H₂ (1:3:1) increased the activity from 0.43 wt. % to 68.0 wt. % over a 30 minute period.

From this it was deduced that the addition of CO may induce changes to the surface morphology of the iron catalyst.

It was also found in this work that if the carbon monoxide was present from the start the activity was still high, but when the carbon monoxide was removed from the gas mixture the activity dropped back to levels comparable with the previous experiment, however when the carbon monoxide was re-introduced the activity rose again to the previously shown high levels. This showed that the activation – deactivation process was reversible and that the high activity was only observed when the carbon monoxide was present.

Following the reactions the carbonaceous deposits formed were examined using TEM and they were found to consist of a network of carbon filaments with diameters ranging from 10 to 300 nm and lengths up to 100 μm .

Chambers *et al.* [72] discussed the effect that the addition of copper to cobalt would have upon the catalytic effect of cobalt. They used copper – cobalt alloys which were prepared by co-precipitation to form bi-metallic granules with an average particle size of 1 μm , 50 mg of these granules were reacted in ethylene – hydrogen gas mixtures at 600°C.

The authors found that the addition of copper to cobalt enhanced the catalytic activity of cobalt towards filamentous carbon production, as was found by Carneiro and co-workers [71], when using an iron – copper catalyst; they also noted that the addition of

hydrogen to the gas mixture induced catalytic behaviour and also extended the lifetime of the catalyst.

Lim and co-workers [73] reported a method for the high yield preparation of carbon nanofibres over Co-Mo catalysts. The catalysts were prepared by dissolving cobalt nitrate and ammonium molybdate in water, the solution was then impregnated onto carbon black or titanium dioxide.

The resulting powdered catalyst grains (110 – 130 mg) were reduced in 20 vol. % hydrogen with the balance helium for 2 hours. They were then exposed to either C₂H₄/H₂ or CO/H₂ at 0.200 dm³ min⁻¹ @ STP. The Co-Mo (9:1) catalyst either on carbon black or titania gave high carbon nanofibre yields, up to 43 g carbon/g catalyst from CO and 57 g carbon/g catalyst from C₂H₄ at temperatures of 530°C and 480°C respectively. It was also found that the carbon yield decreased as the temperature was raised to 600°C.

Again the use of short-chain saturated hydrocarbons i.e. methane and propane, has also been proposed – mainly using iron as a catalyst.

Zielinski and Grow [11] reported the use of an iron based catalyst for the decomposition of methane to form carbon. Here they used two different ferrofluids:

1. EMG 805 – a water based ferrofluid.
2. EMG 905 – a mineral oil based ferrofluid.

Both of the ferrofluids contained magnetite particles with diameters of 7 – 10 nm. In these experiments polyacrylonitrile (PAN) fibres were soaked in dilutions of the ferrofluids before being dried to leave magnetite particles on the surfaces of the fibres. The impregnated fibres were then reacted in varying concentrations of methane and nitrogen at varying flow rates at 977°C for 4 or 8 hours.

The authors concluded that the magnetite particles promoted the deposition of carbon from methane on PAN fibres and stated that the deposition was independent of ferrofluid used and gas flow rate, however, the number of active magnetite sites was important to the rate of deposition. The authors also inferred that there was the possibility that this method may be used to enhance the production of carbon-carbon composites.

Ting and Huang [74] also reported the use of iron particles (100 ± 20 nm) to catalyse the deposition of carbon in order to thicken chemical vapour deposited carbon fibres. In this work the authors used methane or propane as the carbon containing gas and varied its concentration (17 – 83 %) in hydrogen, they used reaction temperatures of 800, 900, 1000, 1100, 1200 and 1300°C.

They found that the thickening of the carbon fibres increased and then decreased as the temperature was raised from 800 to 1300°C. The optimum temperatures reported were 1100°C for methane and 1200°C for propane with optimum hydrogen concentrations at 60 vol. % for methane and 70 vol. % for propane.

Although in this work the author has tried to report the optimum conditions for carbon deposition over iron, as for the work carried out by Zielinski and Grow [11], the temperature conditions used meant that the methane and propane would have been depositing carbon *via* pyrolytic means and the iron particles were likely to be providing an increased number of nucleation points for this deposition to take place on.

Wilson and co-workers [75] used plasma chemical vapour infiltration to produce carbon nanotubes using an iron catalyst which was exposed to a plasma of argon to which ~ 5 % methane was added at 0.020 – 0.080 dm³ min⁻¹ @ STP. From this it was determined that multi-walled carbon nanotubes were formed along with other carbon products, however if hydrogen was intentionally added, the growth of nanotubes ceased. Melt tests showed that the temperature at the catalyst could be as low as 450°C, as has been shown previously, this would be a surprising temperature for the decomposition of methane to occur at.

As well as the short-chain saturated hydrocarbons i.e. methane and propane and unsaturated hydrocarbons i.e. ethylene and acetylene, other authors have reported the use of carbon monoxide [76] as the carbon precursor with an iron containing catalyst and the use of xylene [42] using palladium and iron as the catalysts.

2.4.4. Growth Mechanisms

This section will discuss some of the mechanisms that have been proposed in order to explain how the utilisation of a catalyst

could facilitate the deposition of carbon from a gaseous carbon containing precursor.

Following their observations Baker *et al.* [32] proposed a mechanism for the growth of carbon filaments, they noted that all of the filaments produced, using a nickel catalyst, had a nickel catalyst particle at one end and that part of the surface of the nickel particle was shielded towards gas adsorption by the carbon filament. They also noted that in cases where the filament growth had ceased there was an encapsulating layer of carbon surrounding the catalyst particle thus preventing the catalyst particle from coming into contact with the gas phase.

They observed that flocculent deposits (see Figure 2.13) of amorphous carbon built up around the nickel catalyst particles prior to filament growth this led to the postulation that there were three separate growth regions that lead to the formation of carbon filaments:

1. an initial growth period;
2. a region of constant growth rate and
3. a tailing off period.

This theory led towards the mechanism for carbon filament growth as highlighted in Figure 2.13. Here the flocculent amorphous carbon deposits are taken into solution by the metal catalyst particle, this drives the catalyst particle away from the support and changes the morphology of the particle from spherical to ovular. The acetylene then decomposes on the catalyst surface and the

deposited carbon travels through the catalyst particle and is deposited on the opposite side of the particle to form the carbon filament. Once the catalyst particle becomes saturated with carbon a layer of carbon will form on the exposed face of the catalyst particle preventing further decomposition of the acetylene, stopping the catalytic deposition of carbon.

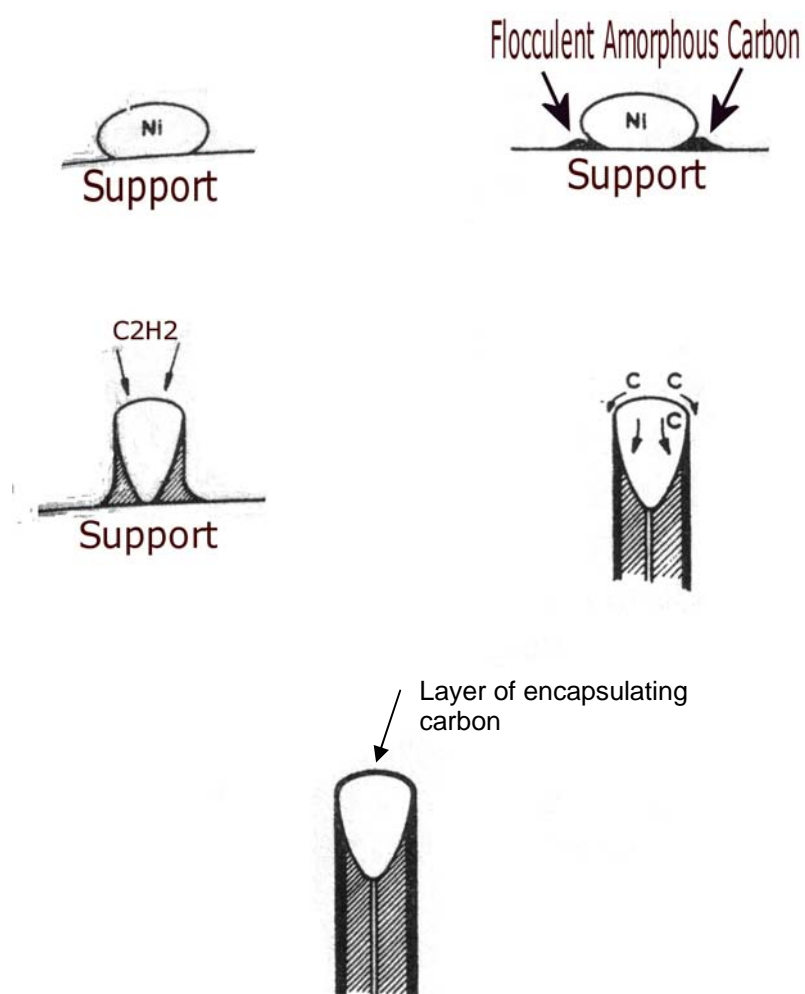


Figure 2.13: Stages in the growth of carbon filaments from a nickel catalyst particle [32].

As the acetylene decomposition is an exothermic process and as it is unlikely to decompose on the shielded regions of the catalyst

surface as readily as on the exposed regions, a temperature gradient is set up across the particle. The acetylene then decomposes on the exposed catalyst surface and the deposited carbon goes into solution and travels across the temperature gradient set up across the catalyst particle and deposits at the shielded surface. This growth is responsible for the distortion of the catalyst particle, from spherical to ovular, as well as being responsible for the removal of the catalyst particle from the support.

Although Baker *et al.* [32] speculate that the diffusion of carbon could be temperature driven due to the establishment of a temperature gradient across the catalyst particle, this is unlikely to be a significant factor due to the extremely small (nanoscale) size of the catalyst particles, however, the local heat of adsorption could play a small role in establishing a temperature gradient.

As the rate determining step for the reaction is postulated to be the diffusion of carbon through the catalyst particle, then as the particle becomes saturated with carbon there will be a build up of carbon at the exposed surface leading to the formation of a layer of carbon around the catalyst particle, which in turn prevents further carbon deposition and causes the formation of filaments to cease, this mechanism is outlined in Figure 2.13.

A mechanism for the formation of carbon on Pt-Fe alloys using acetylene at 70 Pa and 417°C is shown in Figure 2.12.

Here the authors [38] observed that before filament growth occurs there is a separation of the two metals on the support surface. Carbon is then adsorbed on the Pt and travels across the

temperature gradient to the cooler Pt-Fe interface, here the carbon will build up and be steadily transferred into the Fe particle where it will diffuse through and be deposited as a carbon filament. The rate determining step is the diffusion of the carbon through the Fe particle and as heat is imparted to the Fe particle the rate of the reaction will steadily increase. In this investigation the authors also noted that small inclusions of metal particles were carried away with the growing filament, this meant that the iron core was steadily becoming smaller in diameter and size and when the iron core became depleted the growth of the carbon filament ceased, this mechanism also showed some tapering of the filaments prior to the end of growth.

The authors [39] went on to suggest a growth mechanism for the deposition of carbon from methane over a nickel foil, where the carbon is in solution in the metal at the reaction temperature and precipitates out during the cooling stage of the reaction, they suggested that the yield of carbon deposited will increase with:

1. the duration of the experiment, probably to some limit;
2. increasing deposition temperature;
3. increased cooling time and
4. may be influenced by the thickness of the nickel foil, either directly or indirectly through increased heat capacity.

They also postulated that they failed to see the formation of filamentous carbon similar to when a nickel catalyst was used in the decomposition of acetylene because when a hydrocarbon (other

than methane) decomposes it transfers heat to the metal catalyst particle due to the exothermic nature of the reaction, this allows a temperature gradient to be set up across the catalyst particle and carbon is taken into solution by the metal and diffuses across the temperature gradient to the cooler regions where it precipitates out. However, in the case of methane the decomposition reaction is endothermic thus not allowing the formation of a temperature gradient across the catalyst particle and therefore the postulated conditions for filament growth are not achieved.

However, when Keep, Baker and France [40] investigated the formation of carbon from propane over nickel they found that the formation of filamentous carbon was possible despite the decomposition of propane also being an endothermic reaction.

Here they showed that at pressures of ca. 40 kPa and temperatures of between 450 and 700°C there was the formation of filamentous carbon deposits from the decomposition of propane over a nickel foil catalyst. They attribute this to a postulation that propane decomposes to form radicals which can react to form intermediate products such as ethylene, propylene and benzene and they speculate that the final carbon deposition is attributed to the decomposition of these intermediate species. As the decomposition of ethylene, propylene and benzene are exothermic reactions, this would allow the formation of filamentous carbon by the previously postulated mechanism whereby a temperature gradient is set up across the catalyst particles [32], again, whether

this would have a pronounced effect is debatable due to the small catalyst particle size.

Rostrup-Nielsen and Trimm [8] also discussed and reviewed some of the proposed mechanisms for carbon filament formation over nickel containing catalysts and agreed with the theory put forward by Baker and co-workers [39] that the carbon is taken into solution and passes through the nickel to be deposited on the other side of the catalyst particle. However, they not only mentioned a temperature gradient across the catalyst as being the driving force for deposition but also that the driving force for the carbon to travel across the catalyst particle could be due to a concentration gradient being established across the particle, this is a more feasible theory than the theory which involves the establishment of a temperature gradient across the catalyst.

Baker *et al.* [69] went on to provide evidence for the previously speculated hypothesis that the rate determining step for the production of carbon filaments is the diffusion of carbon through the catalyst, whereby the carbon is taken into solution on a particular face of the catalyst particle, passes through the catalyst particle to be deposited as solid carbon on a different face of the catalyst particle. Here they show that the measured activation energy for catalytic filamentous carbon growth is in good correlation with the activation energy for the diffusion of carbon through the respective metals, this is shown in Table 2.4.

<u>Catalyst</u>	<u>Activation Energy For:</u>	
	<u>Catalysed Filament Growth (kJ/mol)</u>	<u>Diffusion of Carbon (kJ/mol)</u>
Vanadium	115.5 ± 12.6	116.3
Molybdenum	162.3 ± 16.7	171.5
α-iron	67.4 ± 8.4	43.9 – 69.0
Cobalt	138.9 ± 16.7	145.2
Nickel	145.2 ± 16.7	138.1 – 145.6

Table 2.4: Comparison of measured activation energies for filament growth in acetylene at 266.6 Pa from 600 - 900 °C, with those for carbon diffusion in the corresponding metal catalyst [69].

The different mechanisms possible for the formation of carbon filaments are shown in Figure 2.14. It shows the tip-growth mechanism (nanotubes) – termed “whisker like”, the mechanism by which a diamond shaped catalyst particle is responsible for the formation of two separate fibres (nanofibres) – termed “bi-directional”, the mechanism by which a similar shaped diamond like catalyst particle is responsible for the formation of four separate nanofibres – termed “multi-directional”, and also the formation of branched fibres which occur through the breaking up of a single catalyst particle as the nanotube grows.

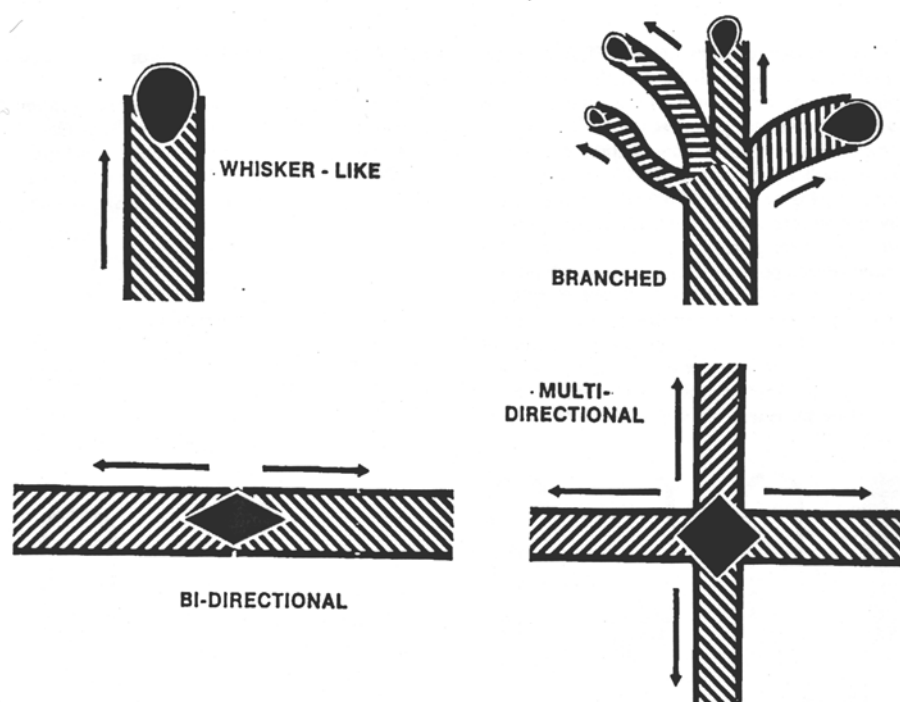


Figure 2.14: Schematic representation of the different types of growth observed in carbon filaments; the black shapes represent catalyst particles [77].

Figure 2.15 shows how the interaction between the metal catalyst and the support affects whether the growth mechanism observed is tip-growth or root-growth. If the interaction between the metal catalyst and the support is weak then the catalyst particle can become separated from the support and the fibre grows *via* a tip-growth mechanism, however if the interaction between the metal catalyst and the support is strong then the fibre is extruded through the catalyst particle as the catalyst particle remains in contact with the support and the fibre is grown *via* a root-growth mechanism, however the interaction between the metal catalyst and the support can be affected by temperature, as was reported with α -iron supported on graphite [67], as the temperature was

increased from 765 to 865°C the mechanism of filament growth changed from tip-growth to root-growth.

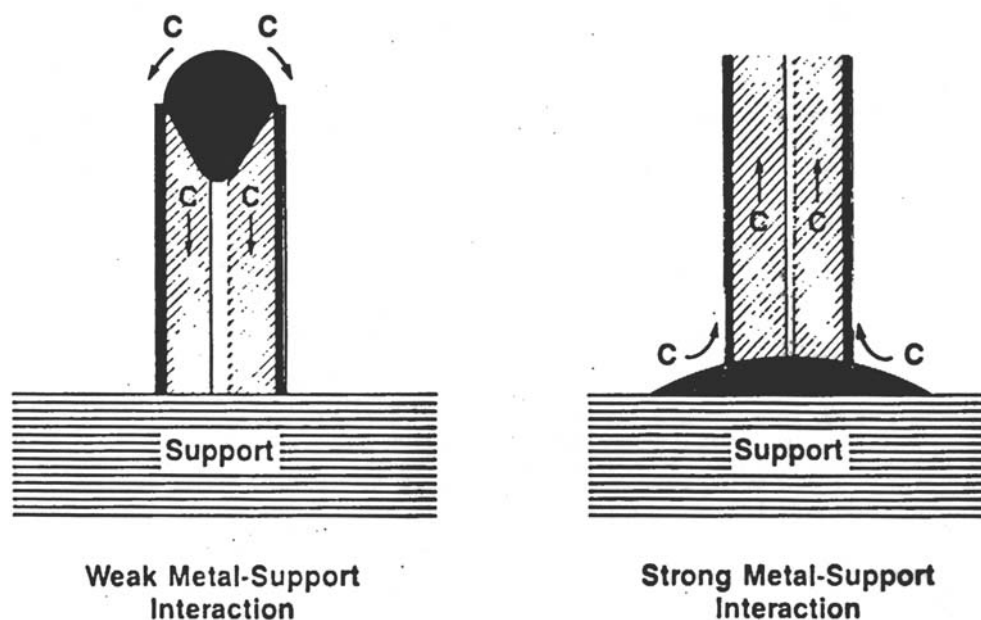


Figure 2.15: Influence of the metal-support interaction on the mode of growth of filamentous carbon [77].

2.4.5. Applications of Catalytically Deposited Carbon

The applications of catalytically deposited carbon have not, as yet, come to complete fruition, however the majority of the early interest in catalytic carbon deposition, in particular the deposition of filamentous carbon, has focussed upon using carbon nanotubes and, more so, carbon nanofibres for the storage of hydrogen for use in fuel cell applications.

Chambers and co-workers [78] discussed a novel application for the potential use of carbon nanofibres to store hydrogen. The carbon nanofibres have small graphitic platelets which are 3 – 50 nm in width. They state that this material is capable of storing 20

dm³ of hydrogen at STP per gram of carbon when exposed to hydrogen at 12.67 MPa and 25°C.

The way in which the authors state that the carbon nanofibres can do this is due to weak Van der Waals forces between the platelets which allow the graphite layers to expand and accommodate hydrogen in a multilayer formation. By lowering the pressure to nearly atmospheric the authors state that almost all of the hydrogen stored can be released at room temperature.

If the storage of hydrogen in this capacity was possible it could have major implications in the design and manufacture of a new breed of fuel cells, however this work has not been substantiated by the subsequent publishing of further work in the area.

The topic of hydrogen storage in graphitic nanofibres was again discussed [79]. Here the authors found that they could predominantly produce “herringbone” graphitic nanofibres when they used a Cu-Ni (2:8 and 1:9) catalyst exposed to ethylene-hydrogen (4:1) at 600°C. They found that the graphitic nanofibres produced had short range crystalline order and significant dislocations which improved their hydrogen adsorption capacity, however if the fibres were reduced or oxidised *in situ* then this could remove excess water and further improve the possible hydrogen storage levels. The topic of hydrogen storage in carbon nanofibres is still a hotly debated topic, with opinions as to whether it is possible being divided.

However, carbon nanofibres and nanotubes are now emerging as potential materials of interest in other fields, in particular in the

field of micro-processing and circuitry due to their ability to conduct electricity and their high strength to weight ratio.

They are also being considered as potential materials for the structural reinforcement of composite materials and work surrounding the use of catalytically deposited carbon forms in the formation of carbon-carbon composites will be discussed in section 2.5.

2.5 Carbon-Carbon Composites

2.5.1. Introduction

Carbon-carbon composites are fabricated by depositing carbon from a carbon-containing gas at high temperatures, typically $\geq 1000^{\circ}\text{C}$, onto a carbon preform, which consists of a two- or three-dimensional weave of carbon fibres.

Carbon-carbon composites began to emerge as a major new engineering material as early as the late 1960s [1]. But they have now found applications as racing car brakes and clutches, hot glass transfer elements, protective shielding, vacuum/inert gas furnace insulation, hot pressing moulds, metal sintering trays, electronic circuit board thermal planes and semiconductor manufacturing components, amongst others [2].

This section will discuss the different types of furnaces and processing methods used to fabricate carbon-carbon composites. It will also look at the different microstructures of the deposited carbon and discuss the effect of microstructure upon the properties of the composite. The densification process and the types of

preforms used will also be discussed as will the effects of catalysts on the densification process along with ways of introducing catalysts into the densification system.

2.5.2. Chemical Vapour Infiltration (CVI) Process

The most commonly used method for the production of carbon-carbon composites is chemical vapour infiltration (CVI). The CVI process generally starts with a matrix of carbon fibres, usually in the form of a preform, in which the fibres can be arranged unidirectionally, bi-directionally or randomly. The preform is then subjected to the carbon-containing precursor, which can be either a liquid or gas. The CVI process then involves infiltrating the carbon fibre preform with carbon-containing gas or vapour. The carbon-containing gas or vapour is thermally degraded at temperatures between 600 and 1500°C; pyrolytic carbon is then deposited onto the carbon fibres within or on the surface of the preform. As more pyrolytic carbon is deposited into the pores within the preform the density of the composite increases, finally the pores become closed to further deposition and surface crusting of the preform begins to take place [3]. The different mechanisms for the filling of the pores can be seen in Figure 2.16.

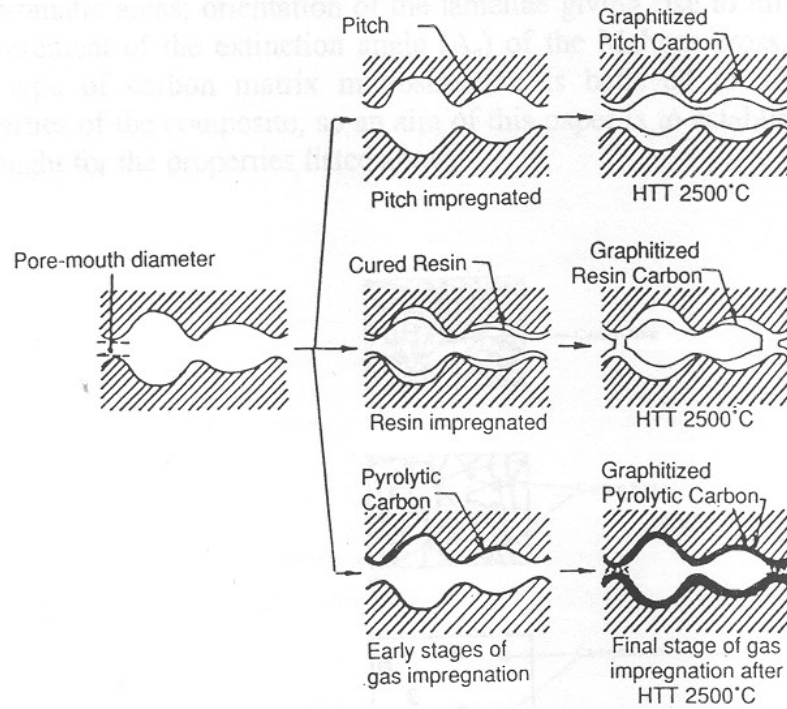


Figure 2.16: Carbon preform pore filling mechanisms (HTT = Heat Treatment Temperature) [1].

2.5.3. Carbon Deposited & Effect of Processing Parameters

The properties of carbon-carbon composites depend greatly upon the type of carbon texture obtained. Texture is a description of the symmetry of the carbon layers at long range. The texture can be isotropic as in glassy carbon, concentric as in carbon blacks, axis-symmetric as in carbon fibres or planar as it is in pyrocarbon [80]. The main properties of carbon-carbon composites at elevated temperatures are:

- Good wear resistance
- High thermal conductivity with low thermal expansion
- High specific stiffness, toughness and strength
- High thermal shock resistance and damping characteristics

All of these properties rely upon obtaining the desired carbon texture within the composite. The elements during the CVI process that govern the type of microstructure obtained are:

- Type of carbon fibre preform employed
- The matrix precursor
- The processing history
- Fibre-matrix interactions

In order to obtain the desired properties, the final composite must have a uniform density and a low residual porosity, which is obtained through in-depth pore-filling of the substrate with the matrix [3].

There are three main types of carbon matrix microstructure that are commonly known [3]:

- Smooth laminar (SL)
- Rough laminar (RL)
- Isotropic (ISO)

The characteristic images of the three main types of carbon matrix, viewed using polarised light microscopy (PLM) are shown schematically in Figure 2.17. Another, somewhat less well-known and studied form of carbon matrix microstructure is dark laminar (DL) [5, 6].

The formation of the SL microstructure occurs at the lowest temperatures and for short residence times, and when viewed under PLM they exhibit a smooth Maltese cross. For longer

residence times the RL microstructure is observed, this has a high reflectance when viewed using PLM and exhibits a contrasted Maltese cross, the RL microstructure has the highest crystallinity, it is graphitisable and has the best properties, especially thermal conductivity. However, if the residence time is too long then the SL microstructure is again observed [80]. The presence of the RL microstructure also improves the toughness of carbon-carbon composites [5].

As the temperature is increased the formation of an intermediate texture occurs, the DL (or granular) microstructure, if this is deposited in appreciable amounts then anisotropy is lost. Further increases in the temperature result in the formation of the isotropic microstructure, when viewed under PLM the images remain completely extinguished [80].

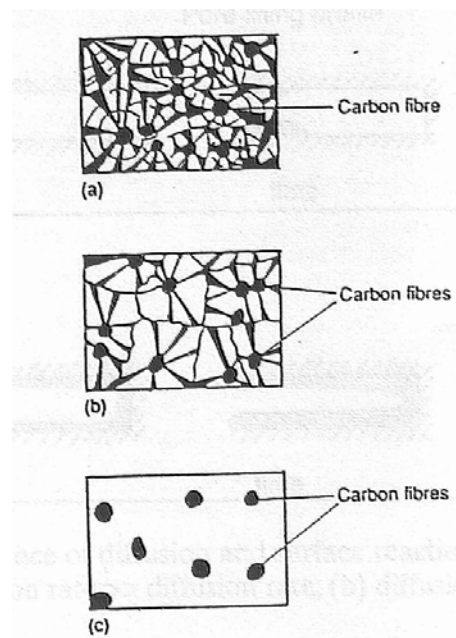


Figure 2.17: Schematic representation of the main types of carbon microstructures derived using CVD. (a) rough laminar; (b) smooth laminar and (c) isotropic [3].

The type of microstructure obtained is determined by observing polished samples under polarised light; from this the extinction angle (A_e) is obtained. It is this extinction angle that is used to determine the type of carbon matrix microstructure that has been obtained; the definitions are stated earlier in section 1.2.

It has been found that a SL matrix shows a higher flexural strength than a RL matrix and that a triplex matrix consisting of ISO, SL and RL produces a higher flexural strength than composites that contain mostly RL pyrocarbon in the matrix. It has also been found that the use of linear carbon molecules in the densification process (C_1 - and C_2 -species) yield a pyrocarbon matrix with a RL structure [6].

Hou *et al.* [81] also found that “the internal friction of carbon-carbon composites decreases with increasing density and decreasing porosity”. The RL matrix also provides a higher internal friction, while ISO provides a lower internal friction. The internal friction is also dependent on the fibre volume fraction within the composite and as the fibre volume fraction increases so does the internal friction.

Although the properties of carbon-carbon composites can be tailored by controlling the type and amount of deposited pyrocarbon within the matrix it is not possible to achieve the highest strength and toughness within a single composite [82].

One of the main problems associated with the densification of carbon-carbon composites is the premature closure of pores, which occurs when the rate of surface reaction is greater than the rate of

diffusion, as shown in Figure 2.18, this prevents the complete densification of the preform and leads to the existence of voids within the internal structure of the preform, making the preform feel “spongy” to the touch. Once the pores become closed, the deposition of carbon takes place on the outer surfaces of the preform, which leads to the requirement for the preforms to be removed from the densification furnace and their surfaces mechanically ground to re-open the pores to further deposition, this of course leads to delays in densification and increased densification times.

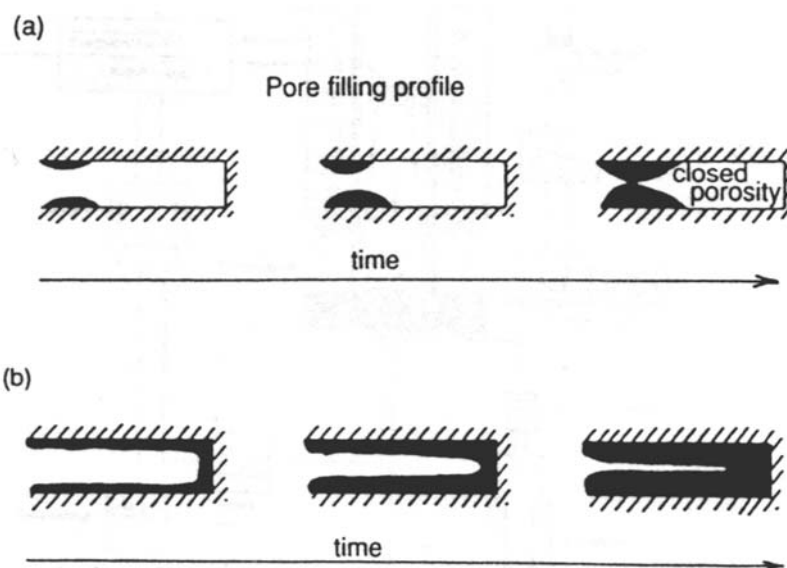


Figure 2.18: The balance of diffusion and surface reaction kinetics, idealised depictions: (a) surface reaction rate $>$ diffusion rate; (b) surface reaction rate $<$ diffusion rate [3].

In order to try to combat this, the densification parameters need to be optimised i.e. temperature, pressure and carbon precursor.

It is known that increasing the temperature will favour the deposition of carbon on the hotter surfaces of the preform as

opposed to diffusion, thus leading to pore closure [83]. However, changes in the carbon precursor and its partial pressure, as well as the total pressure within the furnace, are much more complex phenomena, and predictions and assumptions of their effects upon the rate of deposition and infiltration cannot easily be deduced.

As methane is the most common gas used for the pyrolytic densification of carbon in the manufacture of carbon-composites it would be valuable to study the effect that this carbon precursor has on the rate of carbon deposition, work by Benzinger and Hüttinger [84] showed that increasing the partial pressure of methane whilst keeping the total pressure in the furnace constant (20 kPa) caused an increase in the rate of infiltration and therefore the degree of pore filling. Increased methane partial pressures were also found to be optimum for homogeneous infiltration.

In a continuation to this work [85] the authors also showed that by increasing the total pressure in the furnace the rate of diffusion is increased and as a result the degree of pore filling is enhanced. It was also found [86] that adding hydrogen to the methane gas feedstock improved the rate of diffusion and again the degree of pore filling.

2.5.4. Types of Furnaces Used

One of the main processes used to fabricate carbon-carbon composites is chemical vapour infiltration (CVI); and in a review article by Golecki [4] he identified that there are eleven general types of CVI furnace, these are:

1. Isothermal, isobaric CVI
2. Plasma enhanced, isothermal or thermal gradient, reduced pressure CVI
3. Thermal gradient, radiantly heated, isobaric CVI
4. Thermal gradient, inductively heated, isobaric CVI
5. Liquid immersion, thermal gradient, atmospheric pressure, isobaric CVI
6. Forced flow, isothermal CVI
7. Forced flow, thermal gradient, atmospheric pressure CVI
8. Pulsed pressure, isothermal CVI
9. Microwave heated, isobaric or forced flow CVI
10. Catalyst enhanced, isothermal, isobaric CVI
11. Particle transport enhanced, isothermal, isobaric CVI

An overview of these different types of CVI methods is shown in Figure 2.19.

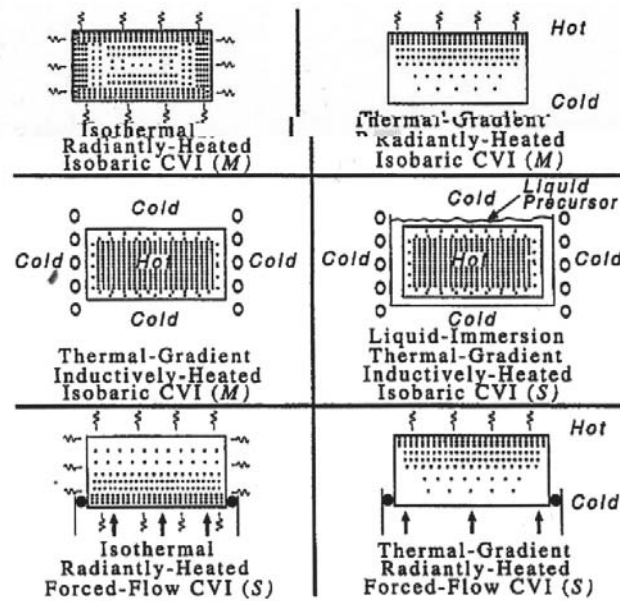


Figure 2.19: Principles of the main chemical vapour infiltration methods used within the different furnaces employed for the densification of carbon-carbon composites [4].

From these eleven types of furnace outlined above there are two methods of heating commonly used in CVI, the first is isothermal heating (see (a) and (c) in Figure 2.19) and the second is thermal gradient heating (see (b) and (d) – (f) in Figure 2.19).

Isothermal heating is where there is no temperature gradient across the preform in any direction and thermal gradient heating is where a temperature gradient is set-up across one of the dimensions of the preform. The preform can also be inductively heated (see (b) and (e) in Figure 2.19) or radiantly heated (see (a), (c), (d), and (f) in Figure 2.19). Inductively heated preforms are heated directly by the induction coils whereas radiantly heated preforms are heated using a hot-wall furnace.

For the purposes of this thesis there are three types of furnace of interest. These will be discussed in the next three sections.

2.5.4.1. Isothermal, Inductively Heated, Isobaric CVI

This technique is the most widely used technique for the densification of carbon-carbon composites, and is the approach used for the densification of aircraft brake discs.

This technique utilises a hot-wall reactor in which the carbon preforms are placed, the preforms are, therefore, radiantly heated under an isothermal process i.e. there is no temperature gradient across the preforms. The pressure in the reactor is also kept constant at either atmospheric pressure or at a reduced pressure. Deposition of carbon, in order to densify the preforms, takes place when the precursor gas or gases are introduced into the reactor.

These gases infiltrate the internal porosity of the preforms, and deposition of solid carbon occurs on their internal and external surfaces. When the precursor gas decomposes, e.g. if methane is used as the precursor gas (as it commonly is) a simplified formula for the mechanism of decomposition and deposition of carbon can be written as:



Equation 2.1 is a much-simplified representation of the actual densification process, wherein it has been found that the precursor gases that lead to the deposition of carbon are usually larger carbon-containing compounds such as ethene, propylene and benzene [4].

The main advantages of isothermal, isobaric CVI are that the method is well established (since the 1960s) and is relatively well understood. Although the total processing time at temperature is high, in the order of 600 – 2000 hours, due to the low rate of carbon deposition. The method is capable of densifying a large number of preforms, of different shapes and sizes, simultaneously. This, therefore, makes the densification time per preform relatively low when compared to other methods, which are only capable of densifying a single preform per densification run.

Some of the main disadvantages of isothermal, isobaric CVI are that surface crusting of the preforms occurs before the final required density is reached. This means that, on an industrial scale, the reactor has to be opened up several times before the densification process is complete, in order to permit grinding of the external surfaces of the preforms. This removes surface deposits and opens up the internal pores to further densification. Another disadvantage is that thinner preforms will densify at a faster rate than thicker preforms, which leads to problems in timing the densification process and the positioning of preforms within the reactor.

2.5.4.2. Thermal Gradient, Inductively Heated, Isobaric CVI

One of the first uses of thermal gradient, inductively heated, isobaric CVI was to produce carbon-carbon composite parts for rockets. The main advantage of early thermal gradient, inductively heated, isobaric CVI was that it decreased the infiltration times of isothermal, isobaric CVI by a factor of, approximately, two.

Although this was the case, the infiltration times were still quite long and control of deposition rate and infiltration conditions was not easy.

In recent studies an AlliedSignal Inc. patented [87] method claims to be able to densify a preform of dimensions 10.8 cm od x 4.4 cm id x 3.0 cm, in 26 hours using a one cycle process. The preforms were heated so as to produce an inside out thermal gradient and cyclopentane vapour was used as the precursor gas. The process used was determined to have significant potential for scale up and may find use in a variety of applications. Problems could occur in scale up though due to the use of an expensive precursor gas and with the handling of a vapour instead of a gas.

The advantages of recent thermal gradient, inductively heated, isobaric CVI include the ability to carry out single cycle densifications at least ten times faster than isothermal, isobaric CVI, and multiple preforms, of different size and shape, can be densified per run. The process is also capable of producing well-densified thick preforms (> 25 mm in thickness).

One of the thermal gradient, inductively heated CVI reactors used to achieve this and investigate the science behind it is the AlliedSignal patented [87] thermal gradient, inductively heated CVI reactor, as shown in Figure 2.20.

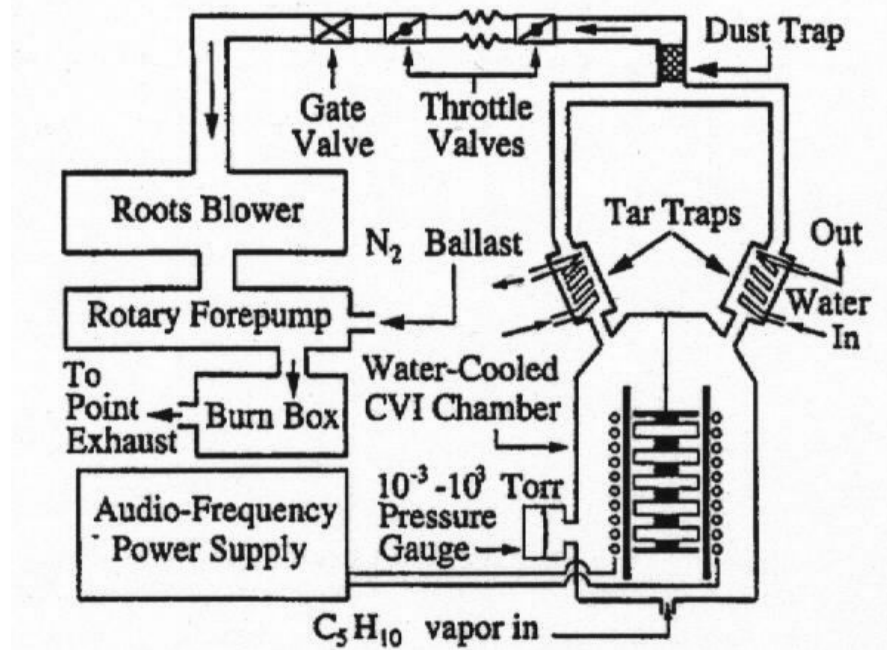


Figure 2.20: Simplified schematic diagram of AlliedSignal patented inductively heated, thermal gradient CVD reactor [4].

The process is particularly suitable for medium batch size runs, in order to produce densified preforms with a turn around time of less than one week. The only real disadvantage of this method of production is that different shaped preforms, with different lateral dimensions, may require different coil configurations [4].

2.5.4.3. Catalyst Enhanced CVD

The rate of deposition of carbon from hydrocarbons is known to be considerably increased on the surface of many metals; three of the main metal catalysts used to increase the rate of carbon deposition are iron, cobalt and nickel. These metals have been used to decompose methane at temperatures as low as 500 – 900 °C, whereas on carbon alone the deposition rate at these temperatures is practically insignificant [4].

Although the area of catalytic deposition of carbon is well studied and could be described as a “hot-topic”, the use and implementation of catalytically grown carbon in the manufacture of carbon-carbon composites is something that has not been well documented and has only been alluded to, as was shown in section 2.4.

Work by McAllister and Wolf [13] discussed the catalytic deposition of carbon over a nickel catalyst, using propylene as the carbon precursor, for the infiltration of carbon fibre substrates. The carbon fibre substrates were injected with methanolic solutions of nickel nitrate hexahydrate, using the incipient wetness technique, which was then decomposed and reduced in hydrogen (500°C) to yield nickel catalyst particles on the substrate.

They found that nickel could be used to deposit carbon catalytically within carbon fibre structures at temperatures as low as 375°C, and concluded that this reduction in temperature along with a reduction in infiltration times from hundreds of hours to less than 10 hours would provide huge economical advantages for industry, this led to the work being patented [15].

However, the gas used (propylene) is a reactive unsaturated hydrocarbon and it is unlikely that the same results would be obtained with the natural gas which is currently used in industry, which mainly consists of methane. The authors also found that the use of the incipient wetness technique did not provide a uniform catalyst distribution and that the results obtained had a poor degree of reproducibility, even when using very small scale carbon

fibre supports, with masses of 15 mg for rayon felts and 165 – 175 mg for PAN felts, indicating that the feasibility of scaling up this process to an industrial scale is poor.

Downs and Baker [12] also discussed the catalytic deposition of carbon onto carbon fibres using a copper-nickel catalyst at 600°C, however, the same concerns arise as to whether this method could feasibly be used in the industrial production of carbon-carbon composites, as again they use an unsaturated hydrocarbon (ethylene) and only deposit carbon onto individual 2D carbon fibres.

The use of methane has however been suggested and patented for the catalytic production of carbon-carbon composites using nickel or iron containing catalysts [53]. However, in this patent they state that the carbon fibre substrates are heating to temperatures in excess of 950°C during carbon deposition, it is therefore debatable as to the effect that the catalyst is having as pyrolytic carbon will also be deposited at those temperatures, and as current manufacturing processes currently use temperatures ca. 1100°C, then it is also unlikely that the costs involved in implementing a catalyst could be recouped by the small reduction in manufacturing temperature.

2.6 Summary

This section has shown that the most common types of catalysts used for the production of carbon are the transition metals and the most commonly used of these are the iron sub group metals of nickel, cobalt and iron, however these are not the only

metals that have been reported for the catalytic deposition of carbon. It has also been reported that the oxides of the metals can be used as catalyst precursors, but during the carbon forming process these oxides are usually under a reducing atmosphere and will, therefore, reduce to the metals. The formation of carbide phases has also been reported.

The main types of gases used for the formation of carbon are typically short-chain hydrocarbon gases, and these can either be saturated hydrocarbons e.g. methane, ethane, propane or unsaturated hydrocarbons e.g. ethylene and acetylene, although the use of longer chain hydrocarbons e.g. xylene, 1-butene and 1,3-butadiene, has also be reported.

The majority of the literature concerned with the deposition of carbon centres on the production of filamentous carbon. Although the production of amorphous carbon and “graphitic shell-like” carbon has also been reported, the problems with forming this type of carbon are that it is sometimes possible for the carbon to encapsulate the catalyst particle, thus preventing further catalytic carbon growth.

Some of the (potential) main applications for the filamentous forms of carbon are in hydrogen storage, nano-circuitry and the formation and reinforcement of carbon-carbon composites.

Although there are numerous different CVI methods employed for the fabrication of carbon-carbon composites, the most widely used and most well understood is the isobaric, inductively heated, isothermal CVI process.

There have also been four types of carbon matrix microstructures reported, of these the rough laminar microstructure is the most desirable for the production of carbon-carbon composites. The main types of gases used for the formation of carbon-carbon composites are typically short chain hydrocarbon gases e.g. methane, ethane and propane, which are the main constituents of natural gas.

The implementation of a catalyst for the production of carbon-carbon composites has been shown to have potential, but currently the process involved in producing catalyst loaded carbon fibre preforms on a large scale still have to be overcome.

3 Experimental

3.1 Introduction

This chapter will explain in detail the materials and methodology used from production through to characterisation of the samples to be discussed in this thesis. It will cover the types of materials used, the catalyst impregnation methods used for the different samples, the carbon deposition methods used and the characterisation techniques employed, which include thermogravimetric analysis – mass spectrometry (TGA-MS), x-ray diffraction spectroscopy (XRD), scanning electron microscopy (SEM), transmission electron microscopy (TEM) and polarised light microscopy (PLM), along with a description of how the samples were prepared for each characterisation technique.

3.2 Materials Used

This section describes the materials and chemicals used and how they will be referred to throughout the thesis.

The materials used were:

1. Methanol – Fisher Scientific - analytical reagent grade – purity of 99.99 %.
2. Iron nitrate – Aldrich in the form of iron (III) nitrate nonahydrate – purity ≥ 99.99 % - molar mass = 404.00 g mol⁻¹.
3. Cobalt nitrate – Aldrich in the form of cobalt (II) nitrate hexahydrate – purity ≥ 98 % - molar mass = 291.03 g mol⁻¹.

4. Nickel nitrate – Aldrich in the form of nickel (II) nitrate hexahydrate – purity of 98.3 % - molar mass = 290.81 g mol⁻¹.
5. IPA – isopropan-2-ol – Fisher Scientific – HPLC grade – purity of 99.99 %.
6. Nitrogen – BOC gases – oxygen free – purity of 99.998 %.
7. Hydrogen – BOC gases – purity of 99.99 %.
8. Methane – BOC gases – purity of 99.5 %.
9. Ethane – BOC gases in the form of a liquefied gas – purity of 99.0 %.
10. Synthetic natural gas – BOC gases – contains 1.8 vol. % propane (purity of 99.0 %), 6.7 vol. % ethane (purity of 99.0 %) and balance methane (purity of 99.5 %).
11. Main natural gas – unknown composition and purity.
12. Carbon fibre mat and carbon fibre preform consisting of PAN based carbon fibres with diameters of 7 µm – kindly supplied by Dunlop Aerospace.

Iron-, cobalt- and nickel- nitrates are termed collectively as “catalyst salts” and the corresponding pure metals as “catalysts” for ease of reading in the remainder of this chapter – it should, however, be noted that on no occasion were mixed metal catalysts used.

3.3 Catalyst Impregnation

3.3.1. Carbon Fibre Mats

Carbon fibre mat consisting of carbon micro-fibres each with a diameter of approximately 7 μm was cut into circular disks approximately 50 mm in diameter, 3 mm thick and weighing approximately 1 g. The individual carbon mats were then weighed before being impregnated with methanol in order to determine the amount of methanol that was required to wet the top surface of each individual carbon fibre mat, after impregnation the methanol was evaporated off in a muffle furnace (Elite Thermal Systems model BCF11/8 - controlled using a Eurotherm 2416 controller – used throughout for the evaporation of methanol) at 70°C in air.

Once the mass of the carbon fibre mat was known the mass of the catalyst salt required to yield 20 wt. % catalyst on the mat could be determined from Equation 3.1.

Mass of carbon fibre mat = 80 % total mass

Therefore;

Mass of catalyst = mass of carbon fibre mat / 4

So;

Moles of catalyst = mass of catalyst / molar mass of catalyst

And, therefore;

Mass of catalyst salt = moles of catalyst x molar mass of catalyst salt

Equation 3.1: *Used to calculate mass of catalyst salt required to yield 20 wt. % catalyst.*

Knowing the mass of catalyst salt required and the volume of methanol needed to saturate the mat, a 5 cm³ solution containing the correct concentration of catalyst salt in methanol could be made and the required volume injected over the carbon fibre mat using a 5 cm³ syringe. After injection of the methanolic solution of catalyst salt the methanol was evaporated off at 70°C in air to yield catalyst salt particles on the surface of the mat. The mat was then weighed and from this the weight percent catalyst on the mat was determined, using Equation 3.2.

$$M_{\text{catalyst salt}} = M_{\text{support}} - M_{\text{impregnated support}}$$

So;

$$M_{\text{catalyst}} = (M_{\text{catalyst salt}} / MM_{\text{catalyst salt}}) \times MM_{\text{catalyst}}$$

And;

$$\text{wt. \% catalyst} = (M_{\text{catalyst}} / (M_{\text{support}} + M_{\text{catalyst}})) \times 100 \%$$

where:

M_{support} = mass of carbon mat or preform.

$M_{\text{impregnated support}}$ = mass of carbon mat or preform after impregnation with catalyst salt.

$M_{\text{catalyst salt}}$ = mass of catalyst salt.

M_{catalyst} = mass of catalyst.

$MM_{\text{catalyst salt}}$ = molar mass of catalyst salt.

MM_{catalyst} = molar mass of catalyst.

Equation 3.2: Used to determine the weight percent catalyst on the carbon fibre mat.

The catalyst salt was decomposed to the metal oxide at 500°C under nitrogen before being reduced to the pure metal catalyst during the carbon deposition process, as described in section 3.4.1.

3.3.2. Carbon Fibre Preforms

The carbon fibre preforms consisted of a number of carbon fibre mats which were stacked up and needled together. Each individual preform was cylindrical and approximately 50 mm in diameter, 30 mm in length and 28 g in mass, consisting of PAN fibres each with diameters of 7 μm .

In order to determine the volume of methanol that the preforms could hold, each preform was placed into 100 cm^3 of methanol in a 250 cm^3 glass beaker which was then covered with Parafilm[®] laboratory film and the preform was allowed to stand for 10 minutes in order to allow the methanol to infiltrate the pores of the preform. The preform was then removed from the beaker and the volume of methanol remaining in the beaker was determined, hence the volume of methanol remaining in the preform can be deduced from:

$$\text{vol. methanol in preform} = 100 \text{ ml} - \text{vol. methanol remaining}$$

The volume of methanol required to saturate each preform was approximately 50 cm^3 . This volume was used to determine the concentration of catalyst salt required to yield 1 wt. % catalyst on the preform, using Equation 3.3.

Mass of carbon fibre preform = 99 % total mass

Therefore;

$$\text{Mass of catalyst} = \text{mass of carbon fibre preform} / 99$$

Equation 3.3: *Used to determine the mass of catalyst salt required to yield 1 wt. % catalyst.*

In order to impregnate the preform a 50 cm³ solution containing the desired amount of catalyst salt in methanol was made up and 20 cm³ of the solution was taken and injected into the centre of the preform using a 50 cm³ syringe, the methanol was then evaporated off at 70°C in air in order to yield catalyst salt particles in the centre section of the preform, the preform was then weighed and from this the weight percent catalyst on the preform was calculated using Equation 3.2.

As the preform can hold approximately 50 cm³ of methanol, and only 20 cm³ of the methanolic catalyst salt solution was injected into the centre of the preform, this meant that the metal catalyst loading in the centre section of the preform was approximately 2.5 times the average total loading for the preform. A schematic diagram of the localised catalyst loading on the preform is shown in Figure 3.1.

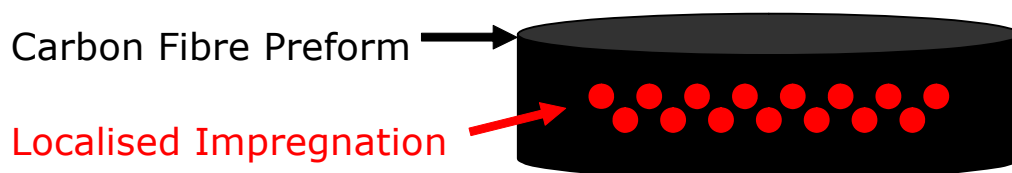


Figure 3.1: Schematic representation of a carbon fibre preform with metal catalyst particles located at the centre.

The deposited catalyst salt was decomposed to metal oxide, before being reduced to pure metal catalyst during the carbon deposition process as described in section 3.4.2.

3.4 Carbon Deposition

3.4.1. Carbon Fibre Mats

After the carbon fibre mat was impregnated with catalyst salt, it was densified in a tube furnace (Carbolite horizontal tube furnace – controlled using 2 Eurotherm controllers (models 810 and 211) connected using a K-type thermocouple – see Figure 3.2) at temperatures ranging from 650°C – 800°C. The catalyst impregnated carbon fibre mat was placed on top of a steel support boat which was pushed into the centre of the tube furnace (in the “hot zone”) the furnace was then purged with nitrogen ($1 \text{ dm}^3 \text{ min}^{-1}$ @ STP) for 30 minutes, heated to 500°C over a period of 1 hour, held at 500°C for a further 30 minutes, in order to allow decomposition of the catalyst salt to metal oxide, before being heated to the required reaction temperature (650 – 800°C) over a period of 30 minutes, this entire process was carried out under a nitrogen ($1 \text{ dm}^3 \text{ min}^{-1}$ @ STP) atmosphere at atmospheric pressure.

Once at the pre-determined reaction temperature (650–800°C) the nitrogen was switched off and the carbon deposition gas mix (either methane, ethane or synthetic natural gas with or without hydrogen at pre-determined flow rates, as outlined in Table 3.1) was passed through the tube furnace for a period of up to 4 hours, the carbon deposition gas mix provided a reducing atmosphere which reduced the metal oxide to metallic catalyst.

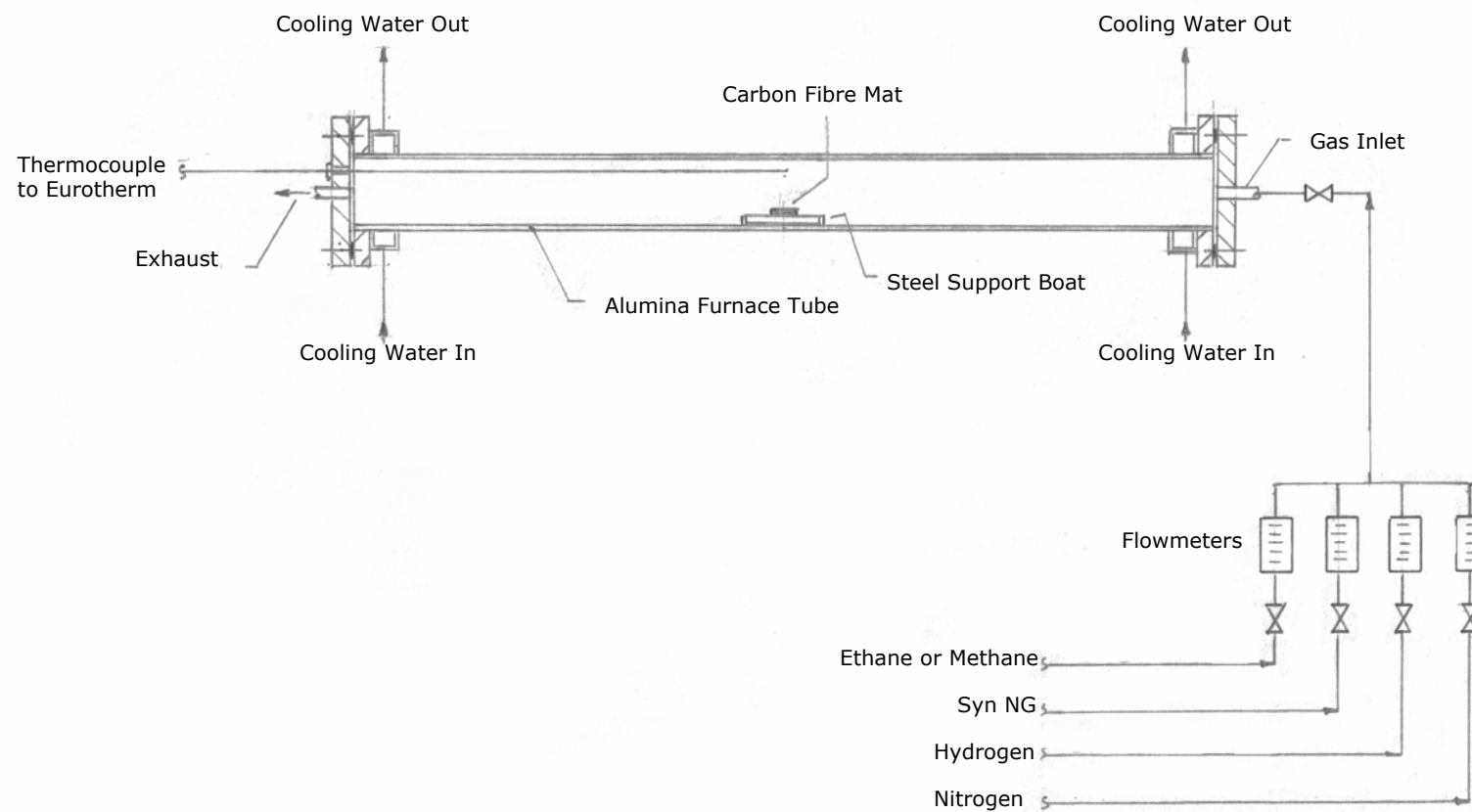


Figure 3.2: Schematic representation of the tube furnace.

After 3 hours the carbon deposition gas mix was switched off and the nitrogen ($0.25 \text{ dm}^3 \text{ min}^{-1}$ @ STP) was switched back on, the furnace was then allowed to cool to room temperature. Throughout the experiment the specific flow rates of all of the individual gases were controlled using gas specific calibrated gas flowmeters (Platon).

The carbon fibre mats were weighed prior to impregnation, after impregnation and after carbon deposition; from this the percentage pick-up per hour (see Equation 3.4) can be calculated for each of the samples.

$$\%PU / h = \left(\frac{m_f - m_p}{m_p \times t} \right) \times 100\% \quad \text{Equation 3.4}$$

where:

%PU/h = percentage pick-up per hour

m_f = final mass of mat or preform

m_p = previous mass of mat or preform

t = densification time

Table 3.1 shows which carbon deposition gas mixtures were investigated and at which temperatures, for experiments carried out using nickel as the metal catalyst with a loading of 20 wt. %, as the bulk of this thesis will focus upon reactions carried out using nickel as the catalyst, each of these experiments were repeated 6 times to ensure statistical significance in the results obtained. The reactions carried out using cobalt and iron as the catalysts are outlined in Table 3.2.

Deposition Gas Used	Ratio HC:H ₂ (Vol. %) (Total Gas Flow Rate @ STP)	Temperature Used /°C			
		650	700	750	800
Ethane	100:0 (0.25 dm ³ min ⁻¹)	X	X	X	X
Ethane + Hydrogen	80:20 (0.25 dm ³ min ⁻¹)	X	X	X	X
	60:40 (0.25 dm ³ min ⁻¹)			X	
	40:60 (0.25 dm ³ min ⁻¹)			X	
	20:80 (0.25 dm ³ min ⁻¹)			X	
Syn NG	100:0 (0.25 dm ³ min ⁻¹)	X	X	X	X
Syn NG + Hydrogen	80:20 (0.25 dm ³ min ⁻¹)	X	X	X	X
	60:40 (0.25 dm ³ min ⁻¹)			X	
	40:60 (0.25 dm ³ min ⁻¹)			X	
	20:80 (0.25 dm ³ min ⁻¹)			X	

Table 3.1: Table showing the experimental parameters that have been investigated for the carbon mat experiments using nickel as the catalyst (marked X).

3.4.2. Carbon Fibre Preforms

Carbon fibre preforms either impregnated with catalyst (catalytic) or without catalyst (non-catalytic) have been investigated at a range of different temperatures (800 – 1150°C)

using methane ($1.5 \text{ dm}^3 \text{ min}^{-1}$ @ STP) or synthetic natural gas ($1.5 \text{ dm}^3 \text{ min}^{-1}$ @ STP or $0.25 \text{ dm}^3 \text{ min}^{-1}$ @ STP) as the densification gas for varying densification time periods. The carbon fibre preforms were placed into a vertical isothermal, isobaric, induction heated furnace (Radyne HF induction heating generator 300 BTE – operated at 30 kW, 450 kHz, 2 amps and 9 kV – controlled using a Eurotherm 2132 controller connected using a K-type thermocouple – see Figure 3.3).

The furnace consisted of an outer silica glass tube which was 500 mm l x 130 mm od x 3 mm wall thickness (wl). The tube ends were sealed using brass end caps with nitrile o-rings (BS430 Fenner FPT UK Ltd.), each end cap was water cooled. The bottom end cap had a gas inlet through which the densification gases flowed and the top end cap had inlets for 3 thermocouples and an exhaust pipe.

Inside the outer silica glass tube was an inner silica glass tube (175 mm l x 75 mm od x 2 mm wl) on top of which was seated a circular disc of insulating board (H91 Sindanyo[®] - Tenmat) (110 mm dia x 16 mm thk). On top of this sat a graphite tube (kindly supplied by Dunlop Aerospace) which acted as the “hot-walled” furnace section. The graphite tube had dimensions of 120 mm l x 110 mm od x 5 mm wl, within the graphite tube sat the preform, supported on a silica glass tube (45 mm l x 30 mm od x 3 mm wl). The graphite tube was sealed with another disc of insulating board with the same dimensions as the previous one. The reaction gases flowed through this set-up via the gas inlet in the bottom end cap, through the centre of the inner silica glass tube, through a hole

drilled into the insulating board, through the centre of the preform support silica glass tube and then through the preform, where reactions took place, before passing out through a hole in the upper disc of insulating board, through which the thermocouple entered the reaction vessel and the preform.

The exhaust tube also had a diaphragm vacuum pump (Pfeiffer Vacuum Ltd., model MVP015-2) attached to it, which was used to reduce the amount of air in the furnace. This was done by flowing nitrogen through the furnace ($1 \text{ dm}^3 \text{ min}^{-1}$ @ STP), followed by reducing the pressure in the furnace using the vacuum pump then back filling with nitrogen, this process was repeated 3 times. The set-up of the furnace is shown in Figure 3.3.

For all of the experiments (catalytic and non-catalytic) the furnace was purged with nitrogen for 30 minutes before being inductively heated to the reaction temperature (800°C – 1150°C) under nitrogen ($0.5 \text{ dm}^3 \text{ min}^{-1}$ @ STP), once at the reaction temperature the gas was switched from nitrogen to methane ($1.5 \text{ dm}^3 \text{ min}^{-1}$ @ STP) or synthetic natural gas ($1.5 \text{ dm}^3 \text{ min}^{-1}$ @ STP or $0.25 \text{ dm}^3 \text{ min}^{-1}$ @ STP) and the reaction was allowed to proceed for the pre-determined reaction time before the methane or synthetic natural gas was switched back to nitrogen ($0.5 \text{ dm}^3 \text{ min}^{-1}$ @ STP) and the furnace allowed to cool to room temperature.

The preform was weighed before experimentation, after catalyst impregnation (if applicable) and after densification; from this the percentage pick-up per hour was determined.

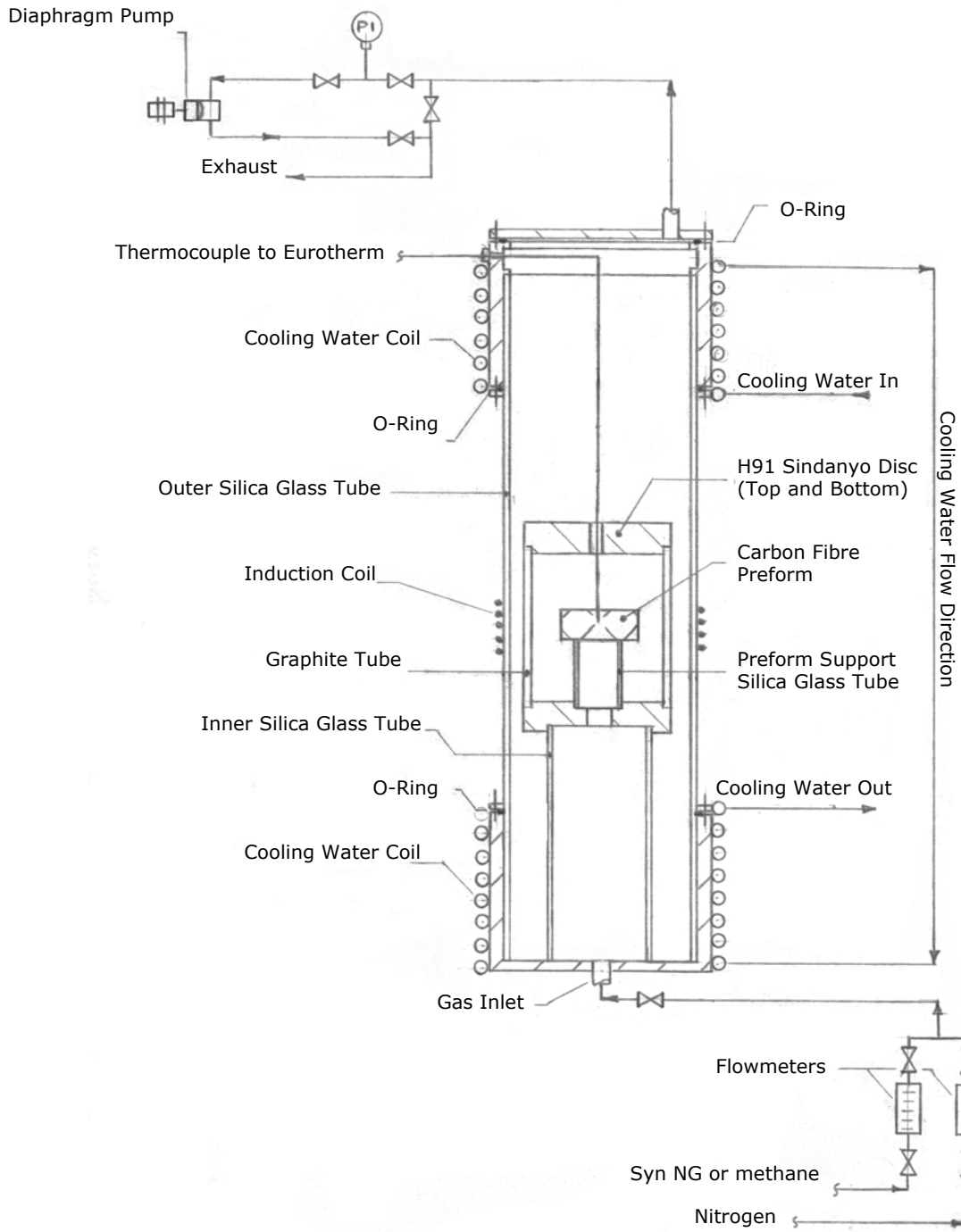


Figure 3.3: Schematic representation of the induction furnace.

3.5 Characterisation

3.5.1. TGA-MS

TGA-MS analysis was carried out using a TA Instruments Q600 simultaneous DSC/TGA with a horizontal beam balance connected to a quadrupole mass spectrometer (Hiden Analytical Ltd. HPR QIC-20 gas analysis system), which is capable of monitoring the changes in intensity of specified m/z values, where m/z is the mass to charge ratio (m/ze). However, as multiply charged ions are rarely produced, relative to singly charged ions, then z can normally be taken as 1 and as e is a constant (the charge of one electron), m/z gives the mass of the ion [88].

Samples for analysis were prepared in one of two ways: for the as received nickel nitrate hexahydrate the crystals were placed directly into the alumina sample pan; for the samples from the carbon fibre mat, bundles of fibres were pulled from the carbon fibre mat (either as received, after impregnation with nickel nitrate or after densification in hydrocarbon) using tweezers and then, if required, the removed fibres were cut into smaller bundles using scissors, before being placed in an alumina sample pan. The sample size used varied from 4.59 to 15.78 mg.

Before the experiments were carried out, the two samples pans were placed onto the balance arms and tared. One of the pans was then loaded with the sample for analysis and replaced on the balance arm, this allowed accurate determination of the mass of the sample for analysis. The furnace was then closed and purged with

nitrogen for 30 min before starting the experiment. For all of the experiments carried out the reaction program was setup and ran as follows:

1. select nitrogen at $0.1 \text{ dm}^3 \text{ min}^{-1}$ @ STP
2. equilibrate at 50°C
3. ramp to 500°C at $15^\circ\text{C min}^{-1}$
4. hold at 500°C for 30 min
5. ramp to 750°C at $15^\circ\text{C min}^{-1}$
6. select 5 vol. % hydrogen in nitrogen at $0.05 \text{ dm}^3 \text{ min}^{-1}$ @ STP
7. hold at 750°C for 30 min
8. select nitrogen at $0.1 \text{ dm}^3 \text{ min}^{-1}$ @ STP
9. cool to room temperature

During the experiment the mass changes with respect to the initial sample mass were recorded as a weight percent with respect to the sample temperature and the gases released from the furnace were continuously monitored using the mass spectrometer. From this, observed mass losses could be attributed to the evolution of specific gases and hence the determination of the reactions occurring could be deduced.

In order to obtain reference background data and to allow determination of sample induced changes, in both mass and evolved gases analysed, a TGA-MS experiment was run with two empty samples pans loaded into the furnace. From this, evolved gas data was obtained using the MS.

3.5.2. XRD

Powder XRD patterns were taken using a Siemens D500 Kristalloflex 810 diffractometer operated at 40 kV and 20 mA utilising a CuK_α radiation source ($\lambda = 0.154 \text{ nm}$). Data were collected using a step mode with step intervals of 0.02° over a 2θ range of $20 - 80^\circ$ with a dwell time of 3 seconds.

In order to prepare the samples for XRD analysis a small section of each of the samples to be examined was cut out and was ground into a fine powder using a pestle and mortar. The powder was then pressed into a hollowed out Perspex[®] sample holder and flattened using a glass microscope slide. A schematic representation of the powder diffraction set-up can be seen in Figure 3.4.

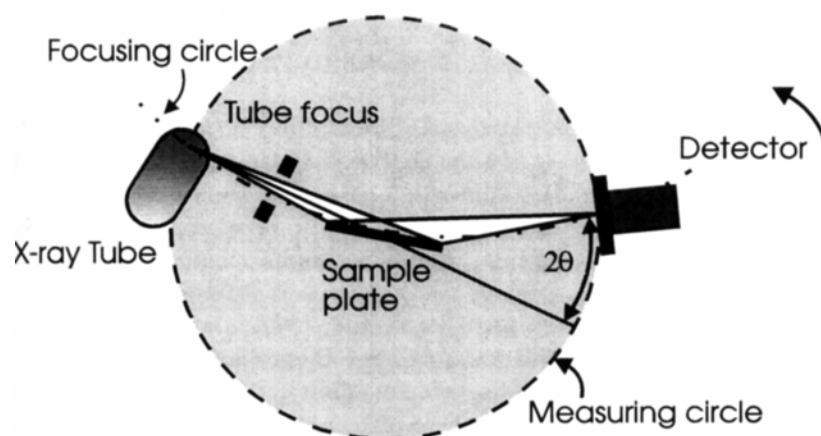


Figure 3.4: Schematic representation of a typical powder XRD set-up [89].

In XRD the sample is rotated at a constant angular velocity θ and when the Bragg condition is fulfilled maximum x-ray diffraction

occurs at an angle of 2θ [16, 89-91]. This relationship is expressed by Bragg's law as shown in Equation 3.5.

$$n\lambda = 2d \sin \theta \quad \text{Equation 3.5}$$

where:

n = integral number; λ = wavelength of incident radiation;

d = separation of the lattice planes; θ = incident Bragg angle.

X-rays striking a powder sample are diffracted, as governed by the Bragg equation (Equation 3.5). From this each lattice separation of a particular orientation gives rise to a cone of closely spaced diffractions. These cones, therefore, give rise to a powder diffraction which is expressed as a series of peaks corresponding to Bragg allowed reflections from a variety of crystal planes [89].

The data collected were qualitatively analysed in order to determine the chemical state of the nickel as well as the relative graphiticity of the catalytically deposited carbon to the carbon fibres from either the carbon fibre mat or preform.

3.5.3. SEM

SEM analysis was carried out using a Phillips XL 30 microscope operated at 20 keV using either a secondary electron or backscattered electron detector. A schematic diagram of a typical SEM set-up is shown in Figure 3.5.

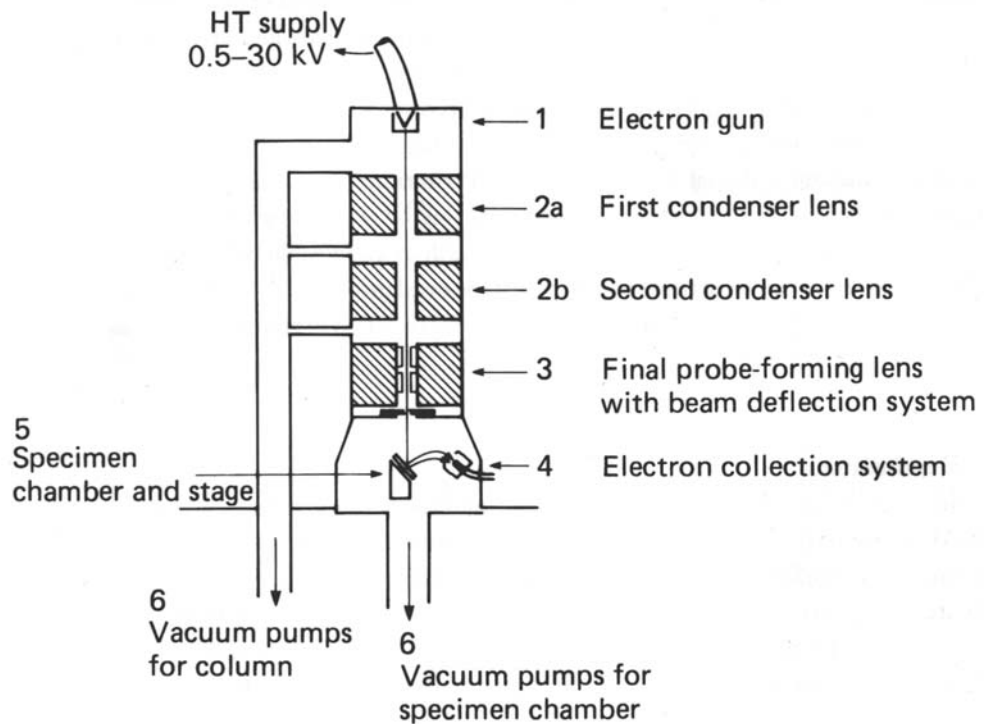


Figure 3.5: Schematic representation of a typical SEM column [92].

In order to collect images from the samples, small sections of each sample were removed and were fixed onto aluminium SEM stubs using sticky carbon tabs for the mats and conductive carbon cement (Neubauer Chemikalien) for the preforms. The prepared samples were then placed into the vacuum chamber of the microscope and images were collected at varying magnifications.

3.5.4. TEM

TEM analysis was carried out in a JEOL FX II microscope operating at 200 keV. During TEM analysis samples were analysed using selected area electron diffraction (SAED), this technique relies upon the fact that the electron beam, after diffraction by the specimen, forms a diffraction pattern (rings or spots), in the back

focal plane of the objective lens. If an aperture of diameter D is placed into the first intermediate image only electrons coming from a part of the object of diameter D/M will pass through, where M is the magnification of the objective lens. With this selecting aperture in place diffraction patterns are formed only by those electrons originating from the chosen small area of the object [92].

The samples for TEM analysis were prepared by shaking either the carbon fibre mat or preform in order to release some of the catalytically deposited carbon. A small amount of the resulting powder (5 – 10 mg) was placed into a vial containing 10 cm³ of IPA; this was then sonicated for 5 minutes in order to obtain a suspension of the catalytically deposited carbon and to aid the dispersion of the sample over the TEM grid. Two or three drops of the suspension were dropped onto a 3 mm diameter holey carbon coated copper TEM grid (300 mesh) and the IPA was allowed to evaporate off at room temperature, leaving the sample for examination on the TEM grid. The TEM grid was then placed onto the specimen holder and was inserted into the vacuum chamber of the microscope. The samples were then observed at varying magnifications. A schematic representation of a TEM is shown in Figure 3.6.

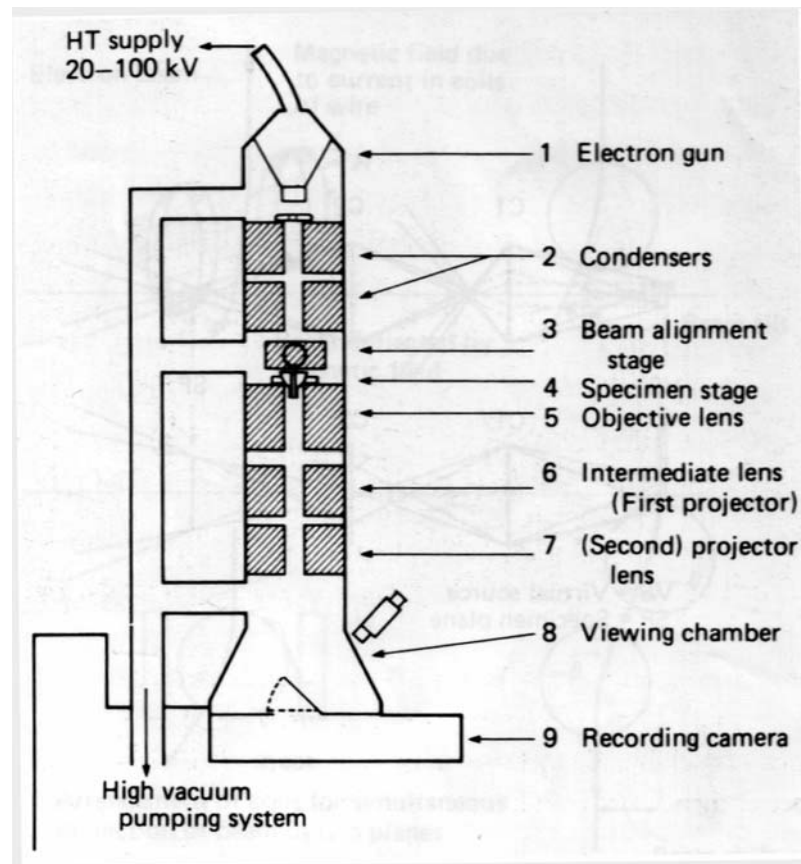


Figure 3.6: Schematic diagram of a high-resolution transmission microscope [92].

3.5.5. PLM

PLM (Nikon Optiphot) was only used for the carbon preform samples. The samples were prepared by cutting sections out of the samples and mounting them in epoxy resin using the instructions and equipment supplied in a Struers Epofix kit. This involved mixing 15 parts resin with 2 parts hardener in the desired quantities for two minutes ensuring that no air bubbles became trapped in the mix. After two minutes the resin mix was poured over the sample which was located in a plastic mould and the resin mix was allowed to go off for over 8 hours (overnight).

The sample was then released from the mould and the surface for examination was ground and polished down to 1 μm , using diamond polishing grit, before being examined on the microscope at magnifications varying from 50 x – 400 x.

The wave model of light describes light waves vibrating at right angles to the direction of travel, this is known as “common light”. In plane polarised light there is only one vibration direction (see Figure 3.7) which the human eye – brain system has no sensitivity to, so plane-polarised light can only be detected by an intensity or colour effect. In a polarising microscope, shown schematically in Figure 3.7, there are two polarising filters – the polarizer and the analyser. The polarizer is usually rotatable through 360° and the analyser is usually aligned north-south. When both the polarizer and analyser are in the optical path, they are said to be crossed and a dark field of view is present in the eye pieces [93].

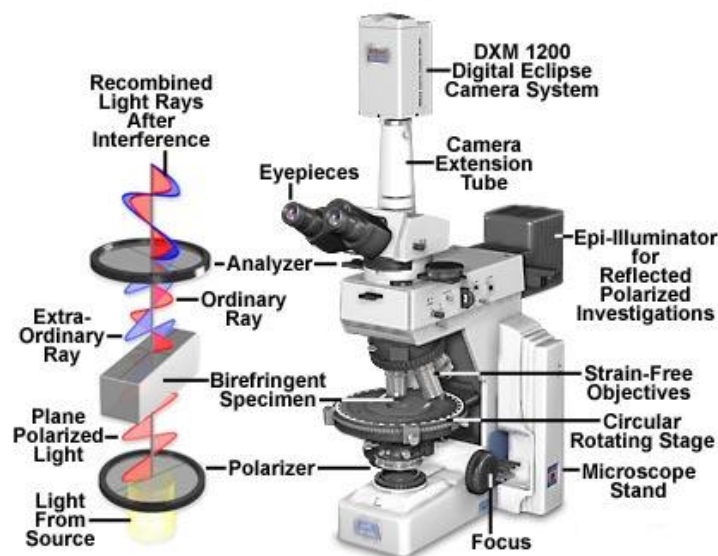


Figure 3.7: Schematic illustration of a typical polarised light microscope [93].

4 Carbon Deposition on Carbon Fibre Mats

4.1 Introduction

This chapter will present the results which have been obtained through the work carried out during the Ph.D. using carbon fibre mats as the catalyst support. It will present data obtained from original screening, mass change measurements, carried out in a horizontal tube furnace, thermogravimetric analysis coupled with a mass spectrometer (TGA-MS), x-ray diffraction (XRD), scanning electron microscopy (SEM) and transmission electron microscopy (TEM). The chapter will then go on to discuss the results (section 4.3) presented and will provide scientific explanations for the presented results as well as putting the results into context with regards to the published literature. Tables for the results presented are listed in the relevant appendices.

4.2 Results

4.2.1. Original Screening

In order to determine a suitable catalyst, temperature range, deposition time and gas feedstock to be investigated a number of preliminary experiments were carried out. These tested nickel, iron and cobalt catalysts at 600 and 700°C using methane and mains natural gas plus hydrogen for 1 and 3 hour deposition times. The deposition rates recorded under varying carbon deposition conditions are outlined in Table 4.1.

<u>Catalyst</u>	<u>Temp. (°C)</u>	<u>Gas Feed</u>	<u>Time (h)</u>	<u>% PU/h</u>
10 wt. % Ni	700	CH ₄	1	-21.28
10 wt. % Fe	700	CH ₄	1	-22.61
10 wt. % Co	700	CH ₄	1	-29.73
20 wt. % Ni	600	NG + H ₂	3	11.08
20 wt. % Fe	600	NG + H ₂	3	2.58
20 wt. % Co	600	NG + H ₂	3	4.21

Table 4.1: Percentage pick-up per hour (%PU/h) values obtained from preliminary experiments carried out under the outlined conditions. NG = mains natural gas.

The data presented in Table 4.1 show that the deposition rate decreased in the order Ni > Fe > Co at 700°C with methane as the gas feedstock and when mains natural gas plus hydrogen was used as the gas feedstock at 600°C the rate of deposition was shown to increase in the order Ni > Co > Fe.

4.2.2. Carbon Deposition

4.2.2.1. Effect of Deposition Temperature and Gas Mixture

This section will present the variation in carbon deposition rate obtained from the reaction of carbon fibre mats, all of which were impregnated with nominally 20 wt. % nickel, in gas mixtures of ethane (0.25 dm³ min⁻¹ @ STP), synthetic natural gas (0.25 dm³ min⁻¹ @ STP), ethane (0.20 dm³ min⁻¹ @ STP) plus hydrogen (0.05 dm³ min⁻¹ @ STP) or synthetic natural gas (0.20 dm³ min⁻¹ @ STP) plus hydrogen (0.05 dm³ min⁻¹ @ STP) at temperatures of 650, 700, 750 and 800°C over 3 hours. The graph in Figure 4.1 shows how

the mean percentage pick-up per hour varies with temperature for a specific gas or gas mixture over a carbon deposition period of 3 hours. Tables of the data used to compile all of the following graphs (Figure 4.1 – Figure 4.4) can be found in Appendix 1.

Figure 4.1 shows that as the temperature of deposition was increased from 650°C to 800°C the mean percentage pick-up per hour increased from 5.5 to 56.0 % for ethane and from - 3.0 to 33.7 % for synthetic natural gas, and at all temperatures the ethane gave a higher mean percentage pick-up per hour than the synthetic natural gas. Both the plot for the ethane and the plot for the synthetic natural gas exhibit similar patterns from 650 – 750°C, whereas from 750°C to 800°C the mean percentage pick-up per hour of the synthetic natural gas plateaus off whilst the mean percentage pick-up per hour for the ethane continues to increase.

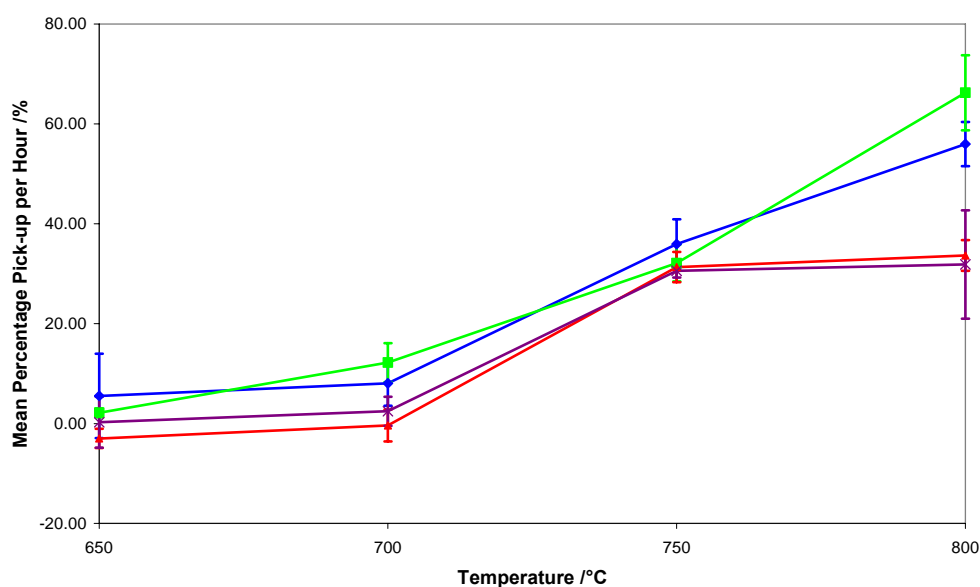


Figure 4.1: Mean percentage pick-up per hour versus temperature for a reaction carried out in ethane (blue), ethane plus hydrogen (green), synthetic natural gas (red) or synthetic natural gas plus hydrogen (violet) for 3 hours with 20 wt. % nickel, error bars represent the standard deviation from the mean.

Figure 4.1 also shows that as the temperature of deposition was increased from 650°C to 800°C the mean percentage pick-up per hour increased from 2.2 to 66.3 % for ethane plus hydrogen and from 0.3 to 31.9 % for synthetic natural gas plus hydrogen, and at all temperatures the ethane gave a higher mean percentage pick-up per hour than the synthetic natural gas. However, without the presence of hydrogen, as the temperature is increased from 750°C to 800°C the mean percentage pick-up per hour for the synthetic natural gas plus hydrogen levels off whereas the mean percentage pick-up per hour for the ethane plus hydrogen continues to increase.

4.2.2.2. Effect of Hydrogen Addition

This section presents results obtained from the reaction of carbon fibre mats, all of which were impregnated with nominally 20 wt. % nickel, with varying ratios of hydrogen added to the carbon deposition gas feedstock (mixtures of ethane or synthetic natural gas) at a temperature of 750°C for 3 hours. The flow rates for the gases used in each case are shown in Table 4.2.

Vol. % Hydrocarbon	Flow Rate (dm ³ min ⁻¹ @ STP)	
	Hydrocarbon	Hydrogen
100	0.25	n/a
80	0.20	0.05
60	0.15	0.10
40	0.10	0.15
20	0.05	0.20

Table 4.2: Gas flow rates used for the carbon deposition gas feedstock with varying hydrogen : hydrocarbon ratios.

The graph in Figure 4.2 shows how increasing the hydrogen content in the carbon deposition gas mixture affects the mean percentage pick-up per hour for reactions carried out at 750°C for 3 hours.

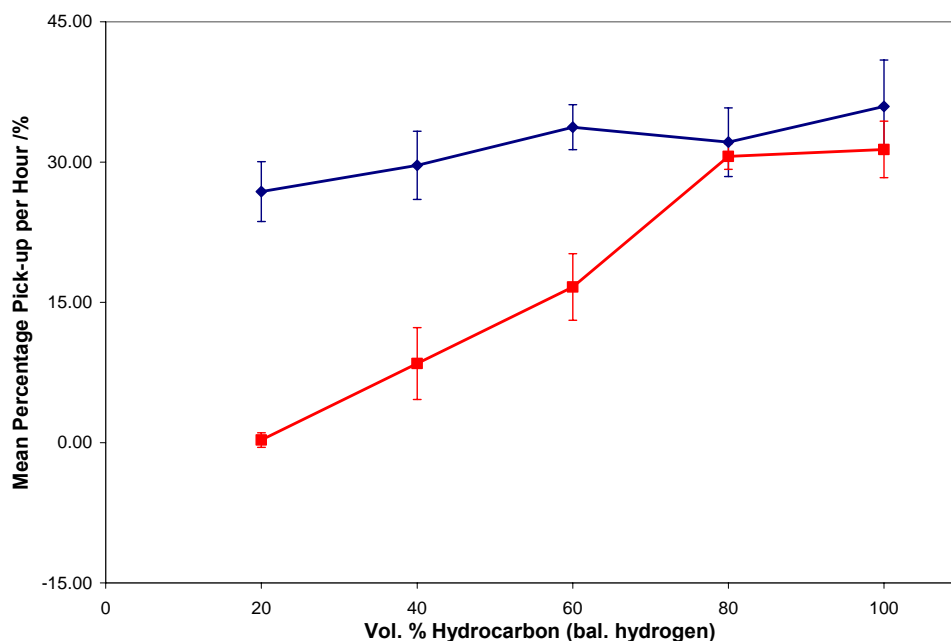


Figure 4.2: Effect of hydrogen concentration on carbon deposition rate for a reaction carried out in ethane plus hydrogen (blue) or synthetic natural gas plus hydrogen (red) at 750°C for 3 hours with 20 wt. % nickel, error bars represent the standard deviation from the mean.

Figure 4.2 shows that the addition of 20 vol. % hydrogen to either ethane or synthetic natural gas has little effect upon the mean percentage pick-up per hour when compared to the gases alone. Further increasing the vol. % hydrogen in synthetic natural gas showed a marked decrease in the mean percentage pick-up per hour from 30.6 % at 20 vol. % hydrogen to 0.3 % at 80 vol. % hydrogen, whereas the same increase in the vol. % hydrogen in ethane had a much less dramatic influence on the mean percentage

pick-up per hour, with a decrease from 33.7 % at 60 vol. % hydrogen to 26.9 % at 20 vol. % hydrogen.

4.2.2.3. Effect of Reaction Time

Results obtained from the reaction of 20 wt. % nickel impregnated carbon fibre mats in gas mixtures of ethane ($0.20 \text{ dm}^3 \text{ min}^{-1}$ @ STP) or ethane ($0.20 \text{ dm}^3 \text{ min}^{-1}$ @ STP) plus hydrogen ($0.05 \text{ dm}^3 \text{ min}^{-1}$ @ STP) at temperatures of 750°C and 800°C for periods of up to 12 hours are shown in Figures 4.3 and 4.4. Samples were weighed at regular intervals (2, 3 or 4 hours).

Figure 4.3 shows that the addition of 20 vol. % hydrogen to ethane at 750°C increased the percentage pick-up per hour, after 3 hours of deposition, from 28.0 % to 45.3 %, however, after 6 hours of deposition and up to 12 hours of deposition the percentage pick-up per hour values for the two gas feedstock's were comparable.

For the same reaction at 800°C (Figure 4.4) the percentage pick-up per hour values were comparable at all times during deposition and it can be seen that without a nickel catalyst present the percentage pick-up per hour obtained is negligible.

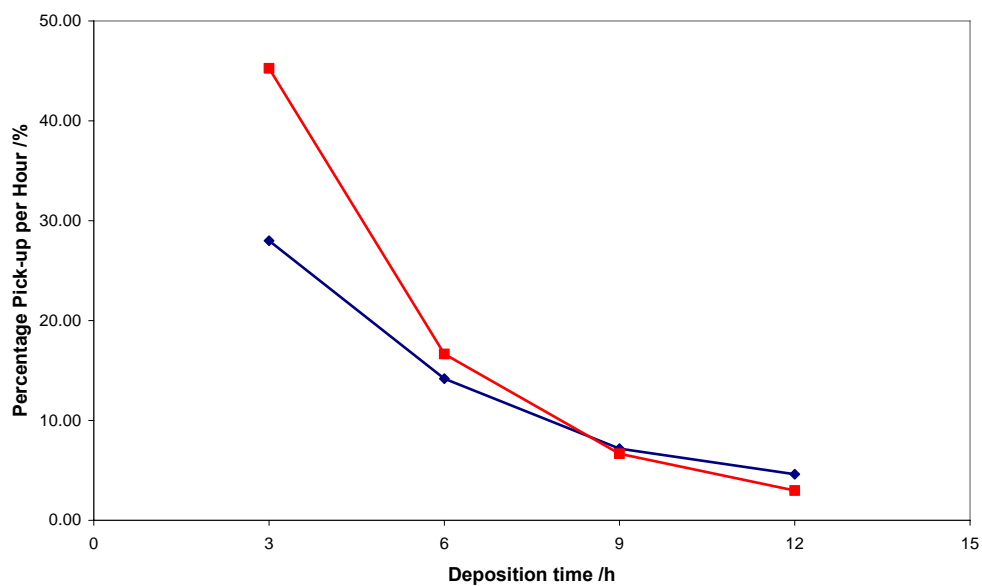


Figure 4.3: Carbon deposition rate on nickel impregnated carbon fibre mats during CVD carried out in ethane (blue) or ethane plus hydrogen (red) at 750°C for 12 hours with 20 wt. % nickel.

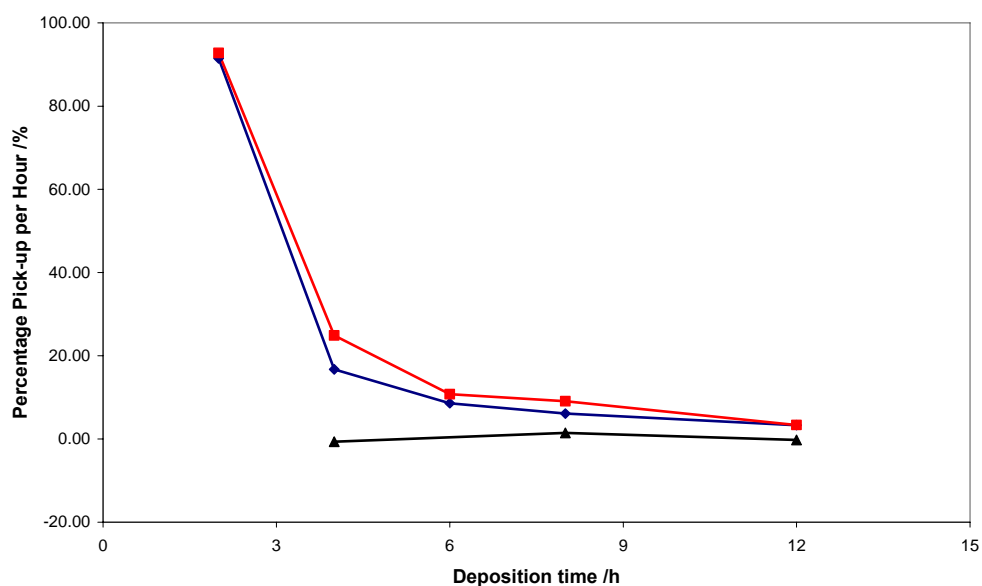


Figure 4.4: Carbon deposition rate on nickel impregnated carbon fibre mats during CVD carried out in ethane (blue) or ethane plus hydrogen (red) at 800°C for 12 hours with 20 wt. % nickel, with the same experiment without a catalyst present (black) shown for comparison.

4.2.3. TGA-MS

This technique was used to determine the chemical state of the nickel catalyst during the reaction process (i.e. during heating from room temperature to 750°C), and when exposed to a reducing atmosphere (i.e. 5 % hydrogen in nitrogen). The TGA was coupled to a mass spectrometer which was used to analyse the gases exiting the TGA as the experiment proceeded. The TGA-MS experiments consisted of samples which were heated to 750°C in nitrogen (0.10 dm³ min⁻¹ @ STP) then when at 750°C the reactant gas was switched from nitrogen to hydrogen (5 vol. % in nitrogen - 0.05 dm³ min⁻¹ @ STP). After reaction for 30 min the gas was switched back to nitrogen (0.10 dm³ min⁻¹ @ STP) and the samples were allowed to cool.

The MS data obtained is shown in Figure 4.5. Once the temperature reached 750°C, in all cases, the hydrogen (5 vol. % in nitrogen) was introduced into the furnace. A table showing which gases the m/z values correspond to is shown in Table 4.3. It was not possible to obtain carbon monoxide data due to the peak at m/z = 28 being saturated by the nitrogen peak (m/z = 28) from the nitrogen carrier gas.

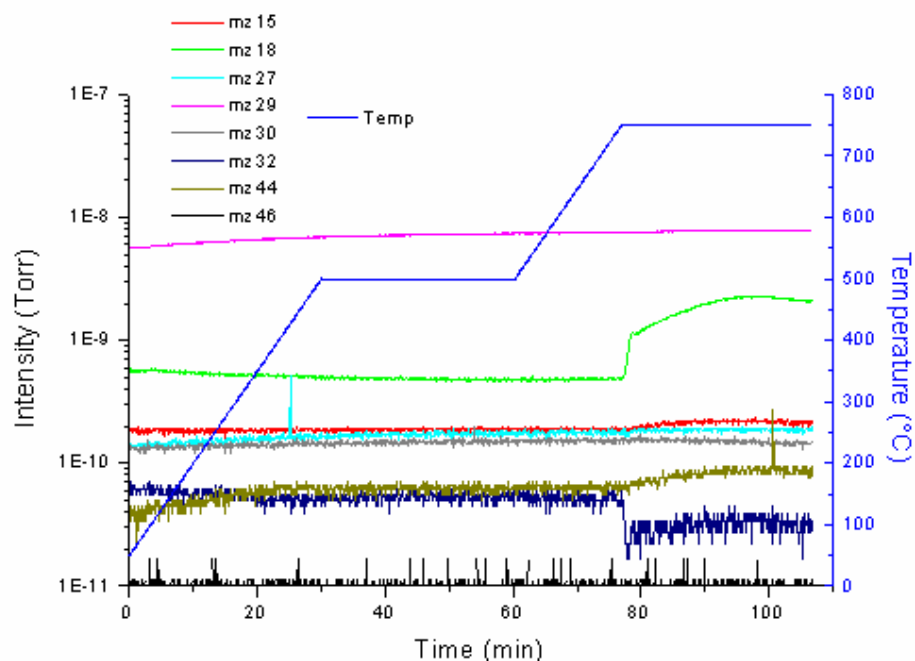


Figure 4.5: TGA-MS data for a blank run showing the MS data and indicating which gases were evolved. N_2 switched to 5 vol. % H_2 in N_2 at $750^\circ C$.

<u>m/z</u>	<u>Ion Monitored</u>	<u>Corresponding Evolved Gas</u>
15	CH_3^+	Mainly Methane/Some Ethane & Propane
18	H_2O^+	Water Vapour
27	$C_2H_3^+$	Ethane and Propane
29	$C_2H_5^+$	Propane and Ethane
30	NO^+/C_2H_6	Nitric Oxide, Ethane or Nitrogen Dioxide
32	O_2^+	Oxygen
44	CO_2^+/C_3H_8	Mainly Carbon Dioxide/Some Propane
46	NO_2^+	Nitrogen Dioxide

Table 4.3: Table indicating which evolved gases or ions correspond to which m/z value in the mass spec traces in Figures 4.5 – 4.10.

Figure 4.5 showed little activity in the concentrations of the gases under observation until the hydrogen was introduced at $750^\circ C$, upon the introduction of hydrogen there was a decrease in m/z = 32, coupled with increases in m/z = 15, 18, 27 and 44; with

the most noticeable change being in the $m/z = 18$ line (water) which showed a marked and sustained increase.

The TGA-MS data for the as received carbon fibre mat, shown in Figure 4.6, showed a small weight loss of ca. 7 % after 20 minutes (Figure 4.6 (a)) which corresponded with an increase in the $m/z = 18$ line of the MS data (Figure 4.6 (b)) at approximately 100°C. Following this there was little change in both the TGA and MS data until the hydrogen was introduced at 750°C, then an increase in the rate of weight loss was observed (Figure 4.6 (a)) along with increases in the MS data (Figure 4.6 (b)) for $m/z = 15, 18, 27, 30, 32$ and 44 as well as a small decrease in $m/z = 29$.

For the as received nickel nitrate hexahydrate, the TGA-MS data, shown in Figure 4.7, there was a weight loss of ca. 45 % after approximately 13 minutes (Figure 4.7 (a)), accompanied by an increase in the $m/z = 18$ line in the MS data (Figure 4.7 (b)), this was followed by another weight loss of ca. 30 % after 20 minutes (Figure 4.7 (a)) and this weight loss was accompanied with increases in the MS data for $m/z = 15, 18, 30, 32, 44$ and 46 . the data for both the TGA and MS then remained stable until the hydrogen was introduced at 750°C, at which time there was a further weight loss of ca. 6 % (Figure 4.7 (a)) and increases in the MS data for $m/z = 15, 18, 27, 30, 32$ and 44 .

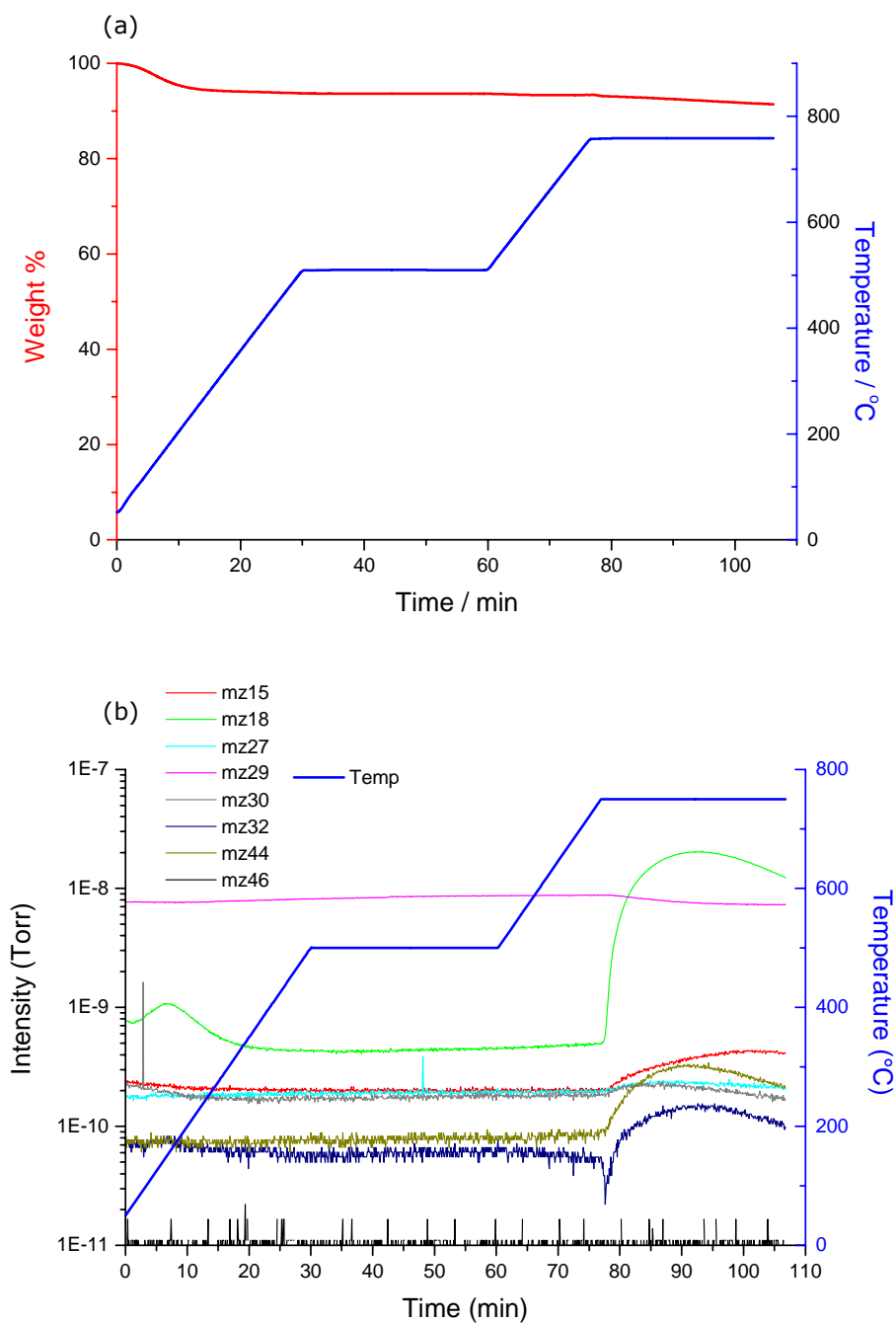


Figure 4.6: TGA-MS data for the as received carbon fibre mat. (a) Shows the TGA data and how the weight percent of the carbon fibre mat changes with temperature; (b) shows the corresponding MS data. N_2 switched to 5 vol. % H_2 in N_2 at 750°C.

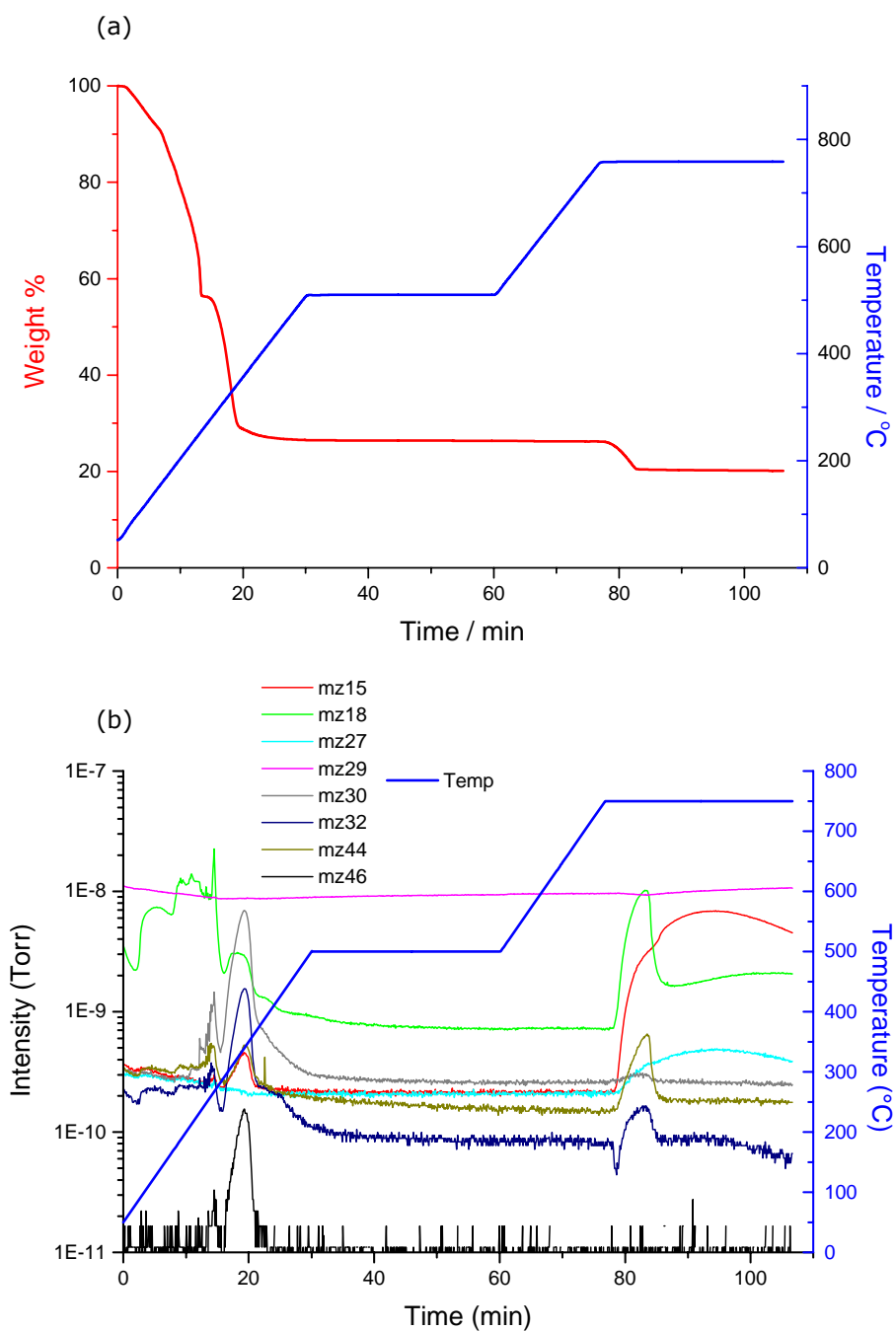


Figure 4.7: TGA-MS data for the as received nickel nitrate hexahydrate. (a) Shows the TGA data and how the weight percent of the nickel nitrate hexahydrate changes with temperature; (b) shows the corresponding MS data. N_2 switched to 5 vol. % H_2 in N_2 at 750°C.

Figure 4.8 shows that TGA-MS data for a carbon fibre mat sample which had been impregnated with nickel nitrate hexahydrate, the patterns seen in the data correspond with the

patterns seen in Figure 4.7 up to 600°C at which point a peak is seen in the $m/z = 44$ line (Figure 4.8 (b)) along with a corresponding weight loss of ca. 5 % (Figure 4.8 (a)), following this the trend, again, follows that observed in Figure 4.7.

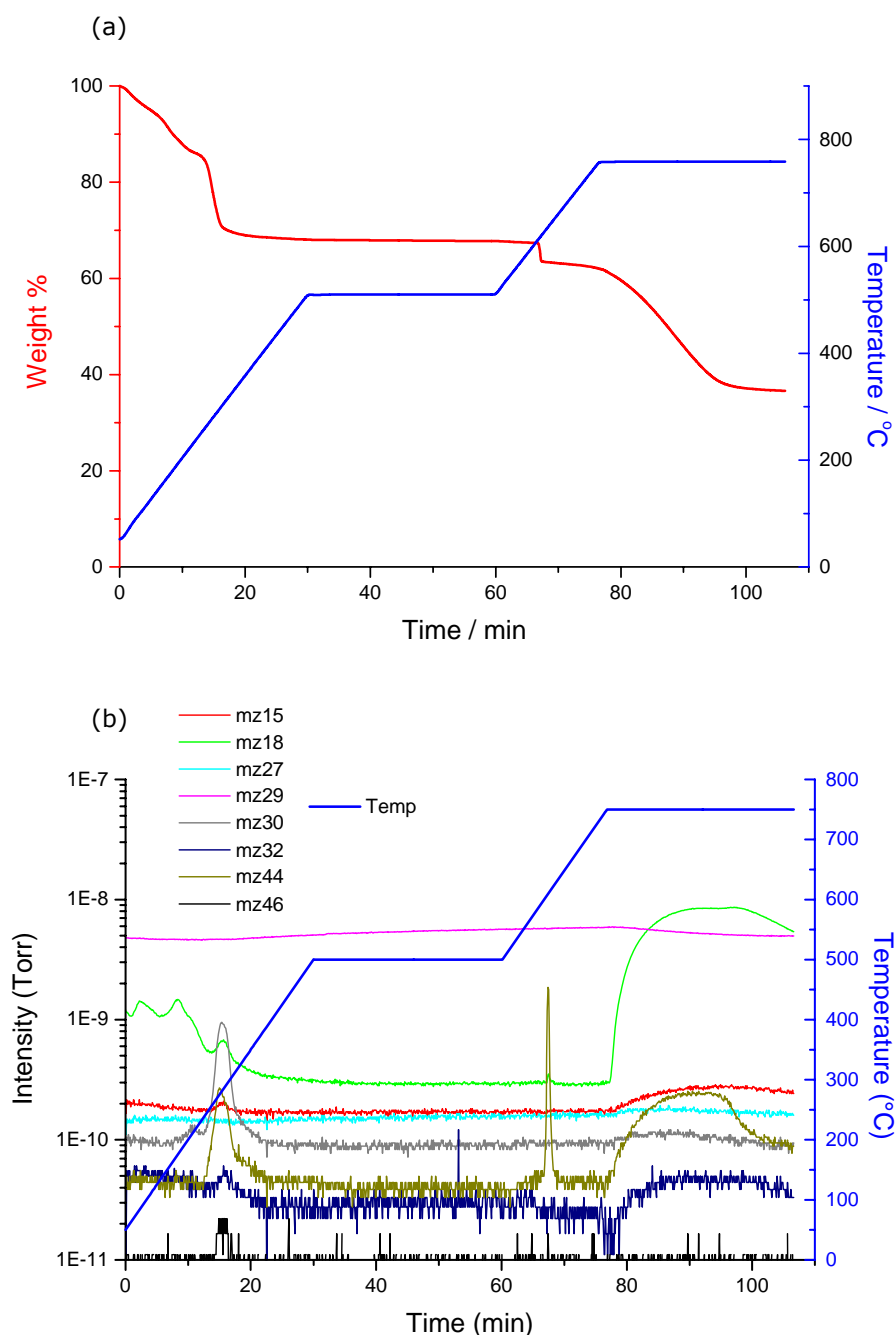


Figure 4.8: TGA-MS data for the carbon fibre mat impregnated with nickel nitrate hexahydrate. (a) Shows the TGA data and how the weight percent of the impregnated carbon fibre mat changes with temperature; (b) shows the corresponding MS data. N_2 switched to 5 vol. % H_2 in N_2 at 750°C.

Figure 4.9 shows the TGA-MS data for a carbon fibre mat sample which had been impregnated with nickel and densified in ethane plus hydrogen at 650°C for 3 hours, these reactions conditions led to a relatively low percentage pick-up per hour of 1.76 %. Here the TGA data (Figure 4.9 (a)) obtained showed a small percentage weight loss of ca. 5 % up to 10 minutes with a corresponding peak in the $m/z = 18$ line (Figure 4.9 (b)). There was then little change in the TGA-MS data until the hydrogen was introduced at 750°C, upon introducing the hydrogen the rate of weight loss increased (Figure 4.9 (a)) and this was coupled with a sharp increase in the $m/z = 18$ line and smaller increases in the $m/z = 15, 27$ and 44 as well as a small decrease in the $m/z = 32$ line (Figure 4.9 (b)).

Figure 4.10 shows the TGA-MS data for a carbon fibre mat sample which had been impregnated with nickel and densified in ethane plus hydrogen at 800°C for 3 hours, these reactions conditions led to a relatively high percentage pick-up per hour of 75.22 %. In this sample the TGA data (Figure 4.10 (a)) showed a negligible weight loss up to 750°C the point at which the hydrogen was introduced. The MS data (Figure 4.10 (b)) showed steady declines in the $m/z = 15, 18, 30, 32$ and 44 lines up to 750°C. Once the hydrogen was introduced at 750°C there was a sharp weight loss of ca 55 % (Figure 4.10 (a)) coupled with increased MS intensities for the $m/z = 18, 27, 30, 32$ and 44 and a small loss in intensity for $m/z = 29$ (Figure 4.10 (b)).

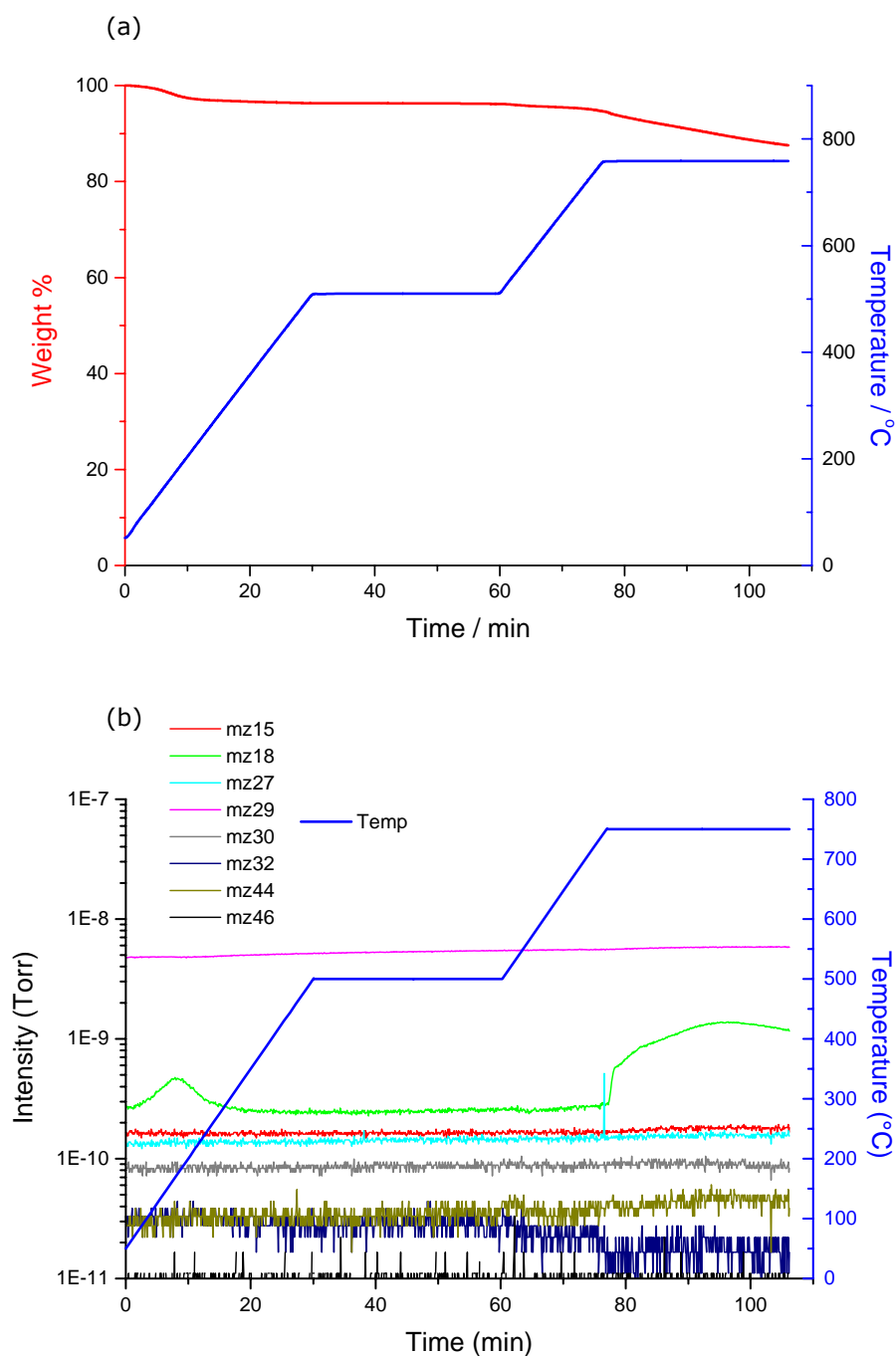


Figure 4.9: TGA-MS data for a carbon fibre mat impregnated with 16.8 wt. % nickel and densified in ethane (80 %) plus hydrogen (20 %) at 650°C for 3 hours to yield a percentage pick-up per hour of 1.76 %. (a) Shows the TGA data and how the weight percent of the "low" carbon deposition carbon fibre mat changes with temperature; (b) shows the corresponding MS data. N_2 switched to 5 vol. % H_2 in N_2 at 750°C.

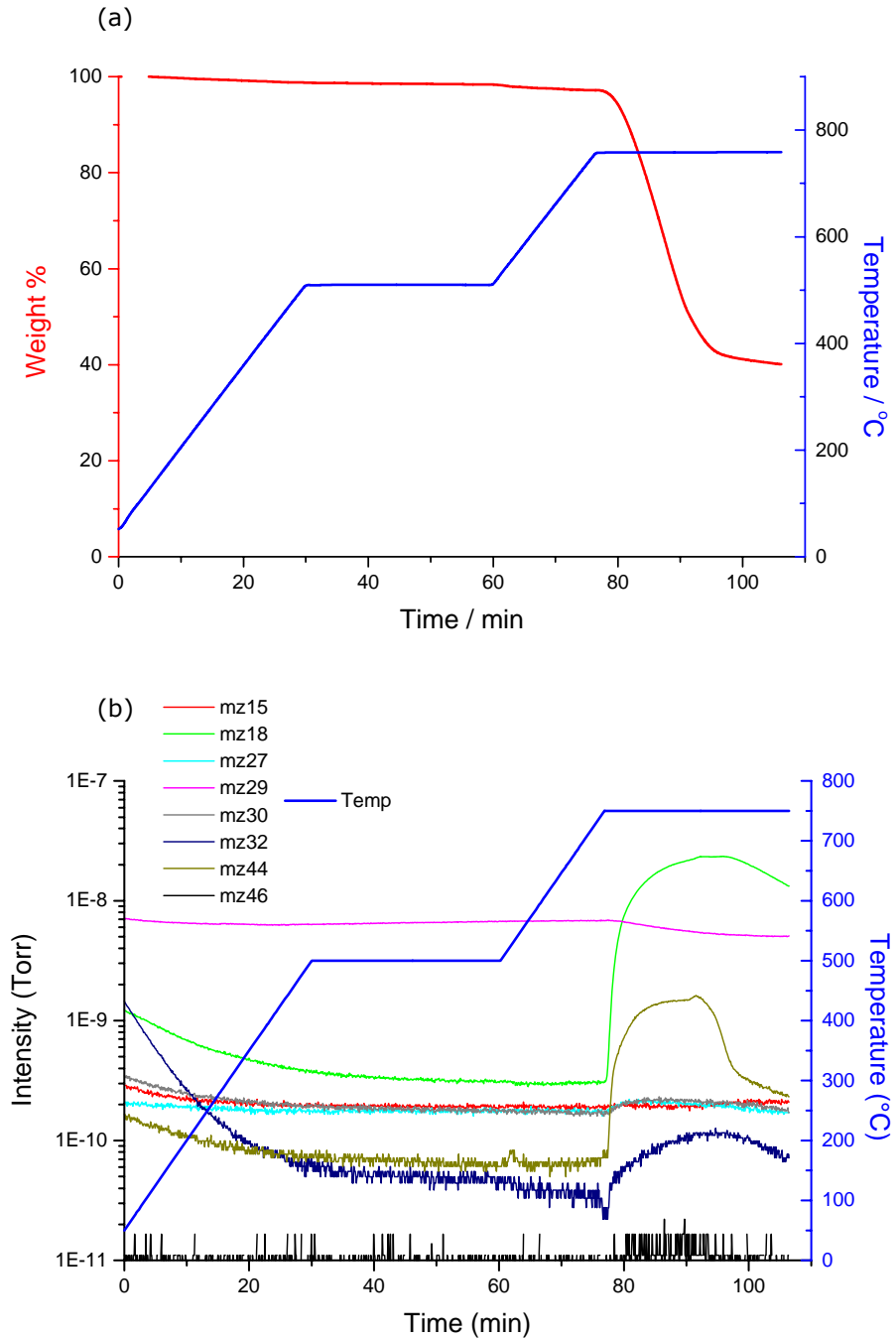


Figure 4.10: TGA-MS data for a carbon fibre mat impregnated with 19.9 wt. % nickel and densified in ethane (80 %) plus hydrogen (20 %) at 800°C for 3 hours to yield a percentage pick-up per hour of 75.22 %. (a) Shows the TGA data and how the weight percent of the "high" carbon deposition carbon fibre mat changes with temperature; (b) shows the corresponding MS data. N_2 switched to 5 vol. % H_2 in N_2 at 750°C.

4.2.4. XRD

XRD was used to determine the state of the nickel catalyst at the different stages of the reaction process and also to investigate whether the catalytically deposited carbon was more graphitic than the carbon fibres of the mat.

The samples investigated were the as received carbon fibre mat (Figure 4.11 A), a carbon fibre mat impregnated with nickel nitrate hexahydrate (Figure 4.11 B), the impregnated carbon fibre mat following reduction of the nickel nitrate through heating the mat to 700°C in nitrogen (Figure 4.11 C) and two carbon fibre mats which have been densified: 1. in ethane (80 %) plus hydrogen (20 %) at 650°C for 3 hours giving a relatively low carbon deposition of 1.76 % pick-up per hour (entitled: low carbon deposition – Figure 4.11 D) and 2. in ethane (80 %) plus hydrogen (20 %) at 800°C for 3 hours giving a relatively high carbon deposition of 61.97 % pick-up per hour (entitled: high carbon deposition – Figure 4.11 E).

The results from the XRD analyses are shown in Figure 4.11 which outlines the samples which contain peaks corresponding to either carbon or nickel or a combination of the two and shows the sample after impregnation with nickel nitrate hexahydrate which contains peaks corresponding to carbon and nickel (II) nitrate hexahydrate.

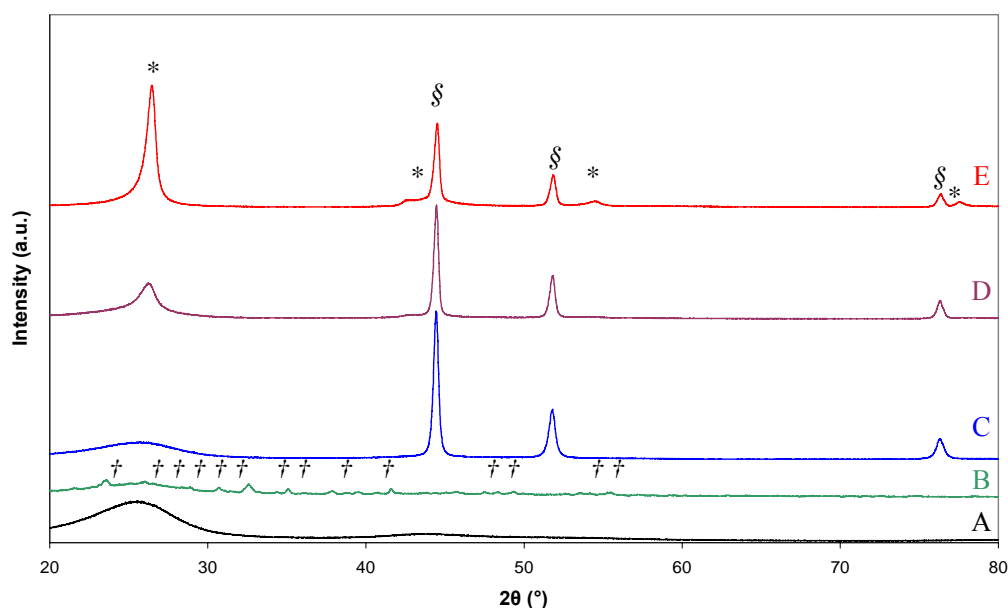


Figure 4.11: XRD patterns of the carbon fibre mat at different stages of the reaction process: *A* – as received carbon fibre mat; *B* – carbon fibre mat impregnated with nickel nitrate hexahydrate; *C* – after reduction of the nickel nitrate at 700°C; *D* – After carbon deposition (low carbon deposition); *E* – After carbon deposition (high carbon deposition). Peaks due to carbon, nickel and nickel nitrate hexahydrate are indicated by the symbols *, § and † respectively.

Figure 4.11 A shows a very broad peak at 26.4° 2θ which was present in all of the samples investigated. Figure 4.11 B showed a series of low intensity reflections. Figure 4.11 C showed reflections at 44.5°, 51.9° and 76.4° 2θ as well as having the broad peak as shown in Figure 4.11 A. Figure 4.11 D and E also show reflections at 44.5°, 51.9° and 76.4° 2θ as well as the aforementioned peak at 26.4° 2θ, however this peak becomes narrower in Figure 4.11 D when compared to Figure 4.11 A and C and narrower still in Figure 4.11 E, Figure 4.11 E also showed low intensity reflections at 44.4, 54.5 and 77.2° 2θ. The XRD patterns in Figure 4.11 D and E are indicative of all of the patterns for the carbon fibre mats after carbon deposition, in each case as the amount of catalytically

deposited carbon increased so did the relative intensity of the carbon peaks and the carbon peak at $26.6^\circ 2\theta$ narrowed accordingly.

4.2.5. SEM

SEM was used to investigate the deposits on the carbon fibre mats, analysing samples after: impregnation with nickel nitrate; reduction of the nickel nitrate to nickel metal; catalytic carbon deposition.

4.2.5.1. Prior to Catalytic Carbon Deposition

4.2.5.1.1 **As Received Carbon Fibre Mat**

Figure 4.12 shows a carbon fibre mat in the as received state, the surface of the carbon fibres, which had a diameter of approximately $7\ \mu\text{m}$, were smooth and free from deposits.

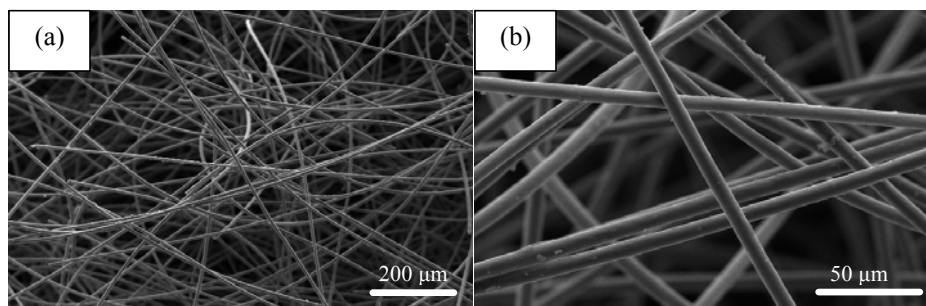


Figure 4.12: (a) and (b) SEM images of the top surface of the as received carbon fibre mat.

4.2.5.1.2 **After Impregnation**

Figure 4.13 shows images of the carbon fibre mat after impregnation with nickel nitrate hexahydrate. Large clusters ($> 50\ \mu\text{m}$ in diameter) of the nickel salt were dispersed over the surface of the carbon fibre mat. At the intersections of fibres the clusters of

the nickel salt were relatively large in size (up to 100 μm) with smaller clusters (ca. 10 – 20 μm) of the nickel salt gathered along individual fibres.

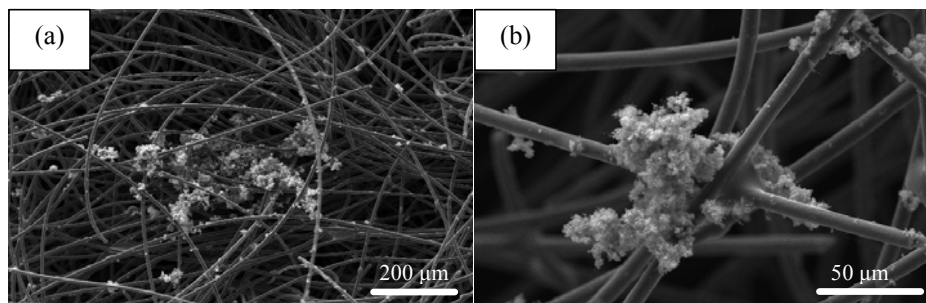


Figure 4.13: SEM images of (a) the top surface of a carbon fibre mat after impregnation with nickel nitrate hexahydrate; (b) a nickel nitrate hexahydrate cluster at an intersection between fibres.

4.2.5.1.3 After Reduction

Figure 4.14 shows SEM images of the carbon fibre mat after reduction of the nickel nitrate hexahydrate to metallic nickel. The metallic nickel particles are shown to be dispersed across the top surface of the mat and the small clusters of metallic nickel particles along individual fibres seem to be in close contact with the carbon fibres from the carbon fibre mat. Although the nickel nitrate has decomposed and been reduced to metallic nickel there was no visible “pitting” of the fibres or degradation of the carbon fibre surfaces.

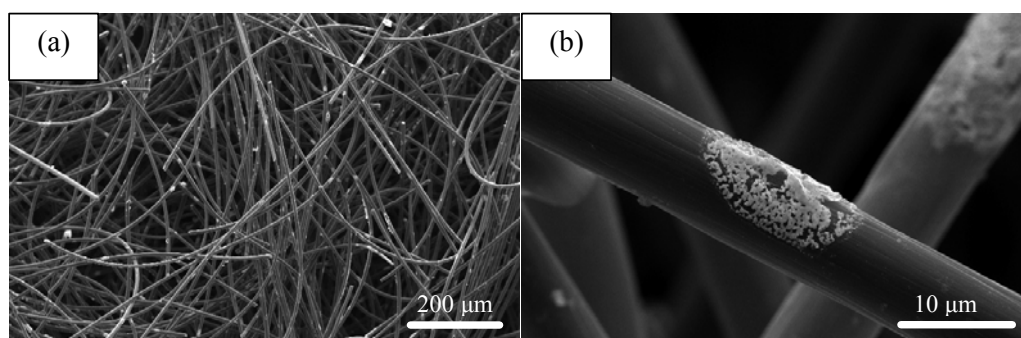


Figure 4.14: SEM images of (a) the top surface of a carbon fibre mat after reduction of the nickel nitrate hexahydrate to form metallic nickel; (b) a metallic nickel deposit.

4.2.5.2. After Catalytic Carbon Deposition

4.2.5.2.1 Ethane

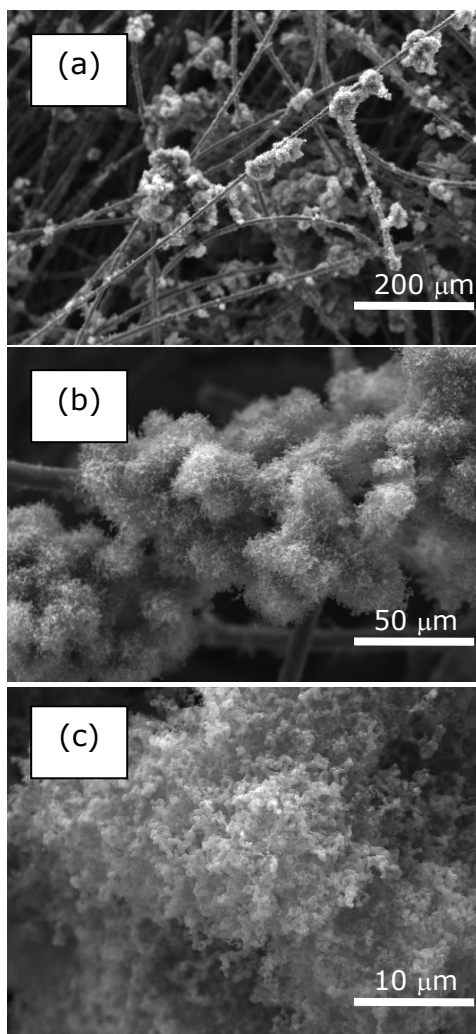


Figure 4.15: (a) – (c) SEM images of a carbon fibre mat, impregnated with nickel, after reaction in ethane at 650°C for 3 hours.

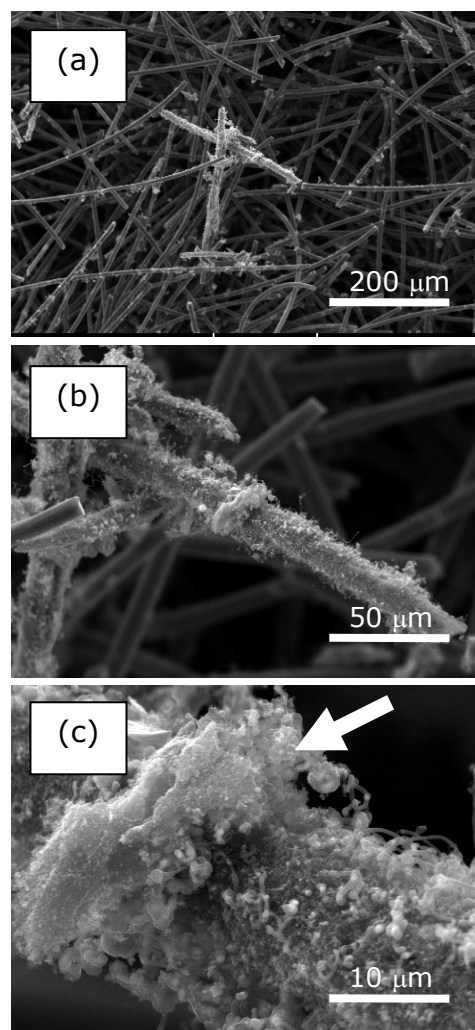


Figure 4.16: (a) – (c) SEM images of a carbon fibre mat, impregnated with nickel, after reaction in ethane at 700°C for 3 hours. A Large "crust" of deposited carbon is indicated by the arrow in (c).

The SEM images in Figure 4.15 show that, after reaction in ethane at 650°C, there was a coating of catalytically deposited carbon around the nickel catalyst particles, these carbon deposits were agglomerates of spherical "fluffy" deposits which mainly

consisted of nano-sized carbon filaments. The deposits grew along individual fibres and seemed to be in close contact with the fibres.

The SEM images in Figure 4.16 show that, after reaction in ethane at 700°C, the catalytically deposited carbon was dispersed along individual fibres. The deposits were in close contact with the individual fibres and the carbon deposited was made up of mainly nanosized filamentous carbon with some areas of encapsulation, as indicated by the arrow in Figure 4.16 (c).

The SEM images shown in Figure 4.17 are for a carbon fibre mat sample after reaction in ethane at 750°C. The carbon deposited appears to be mostly encapsulated catalyst particles in shells of graphitic carbon with only small amounts of filamentous carbon at the edges of the graphitic shells.

Figure 4.18 shows SEM images of a carbon fibre mat sample after reaction in ethane at 800°C. The main type of carbon deposited is encapsulation, consisting of small spherical particles which encapsulate the nickel catalyst particles. There are, however, some small filamentous deposits at the edges of the encapsulated catalyst particles.

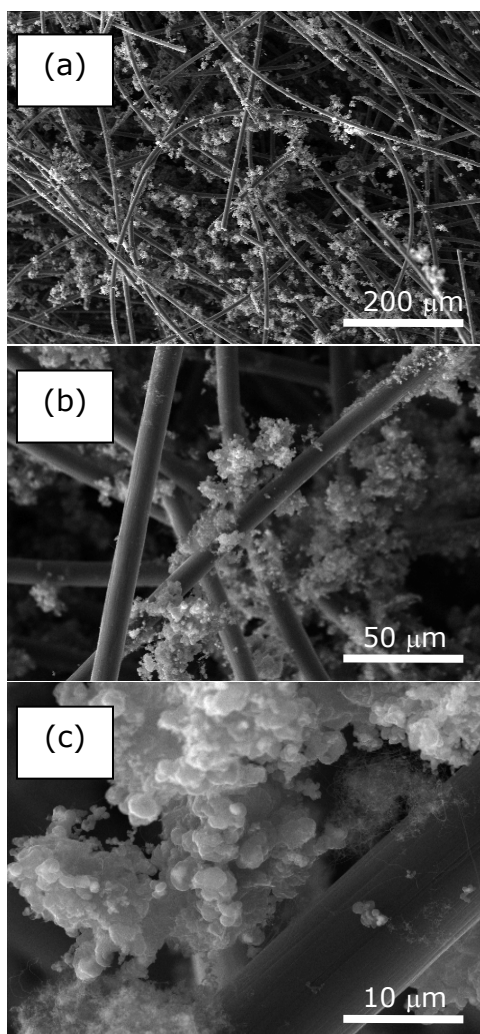


Figure 4.17: (a) – (c) SEM images of a carbon fibre mat, impregnated with nickel, after reaction in ethane at 750°C for 3 hours.

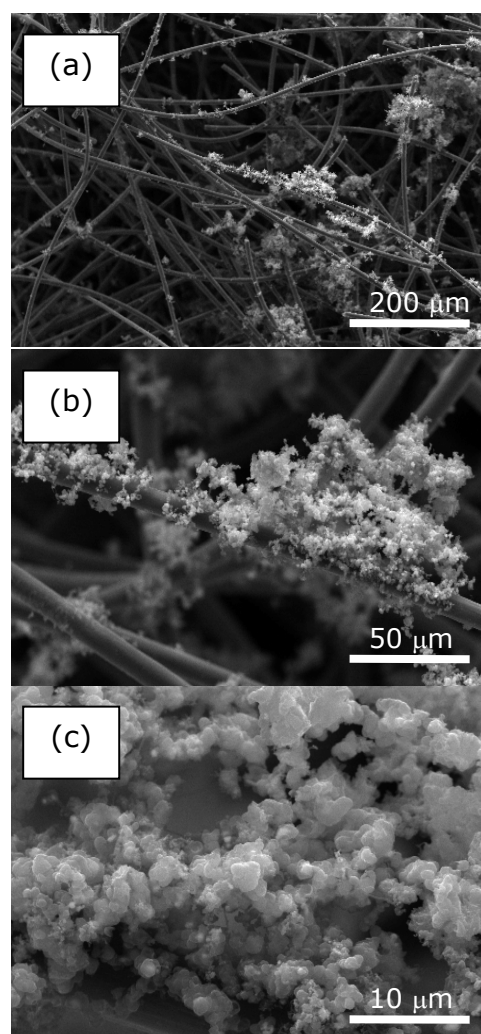


Figure 4.18: (a) – (c) SEM images of a carbon fibre mat, impregnated with nickel, after reaction in ethane at 800°C for 3 hours.

4.2.5.2.2 Synthetic Natural Gas

The SEM images shown Figure 4.19 are for a carbon fibre mat sample after reaction in synthetic natural gas at 650°C. The deposited carbon consists entirely of nanosized carbon filaments. These filaments are shown to be in close contact with the fibres from the mat and have formed “cobweb” like structures. These “cobweb” like structures appear to be relatively low in density.

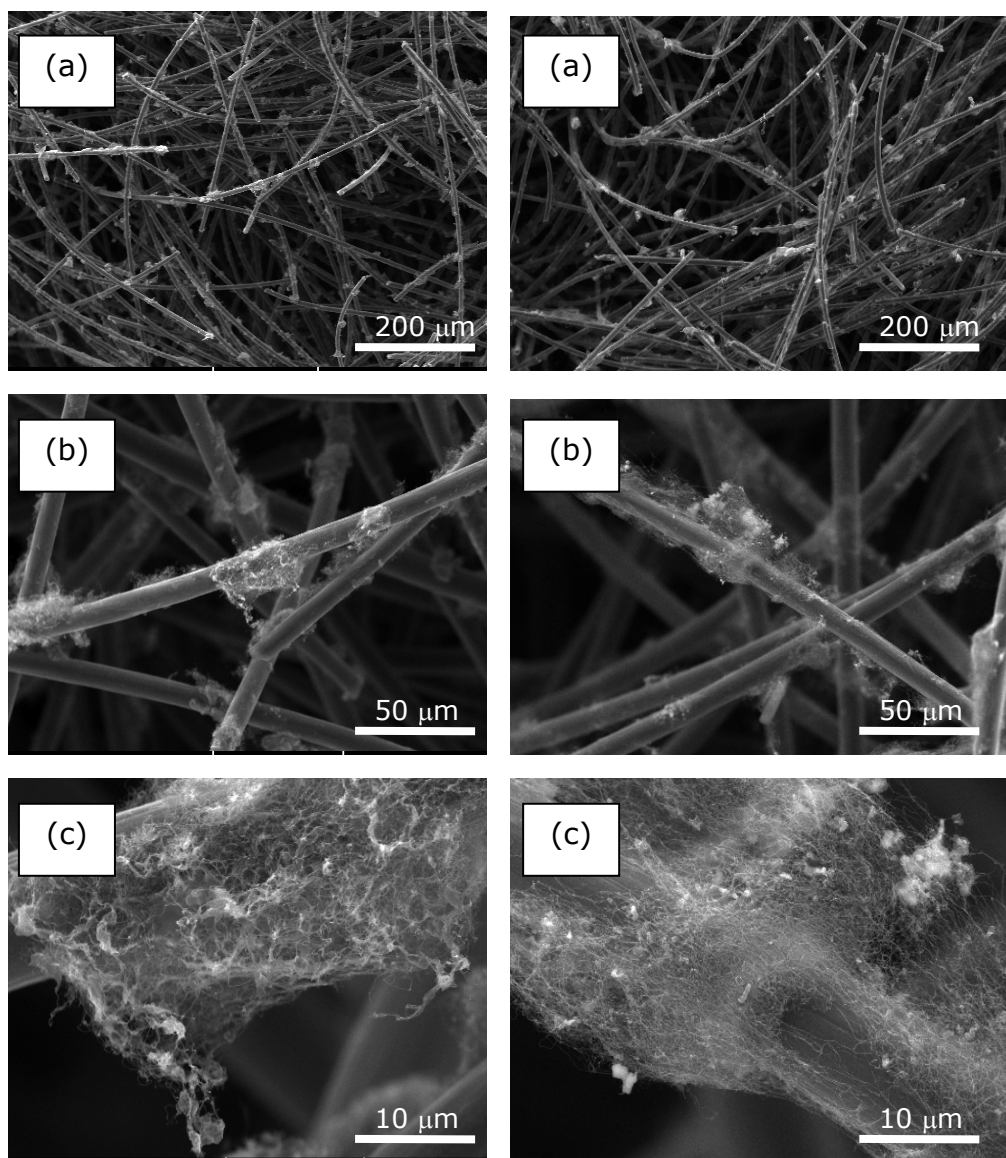


Figure 4.19: (a) – (c) SEM images of a carbon fibre mat, impregnated with nickel, after reaction in synthetic natural gas at 650°C for 3 hours.

Figure 4.20: (a) – (c) SEM images of a carbon fibre mat, impregnated with nickel, after reaction in synthetic natural gas at 700°C for 3 hours.

Figure 4.20 shows SEM images for a carbon mat sample after reaction in synthetic natural gas at 700°C. The type of carbon deposited is filamentous in nature and formed “cobweb” like structures which grew along and were in close contact with the individual carbon fibres.

The SEM images shown in Figure 4.21 are for a carbon fibre mat sample after reaction in synthetic natural gas at 750°C. The morphology of the catalytically deposited carbon was less filamentous in nature and the carbon deposits exhibited a more spherical morphology and seemed to accumulate in between crossing fibres, with less deposited carbon growing along individual carbon fibres.

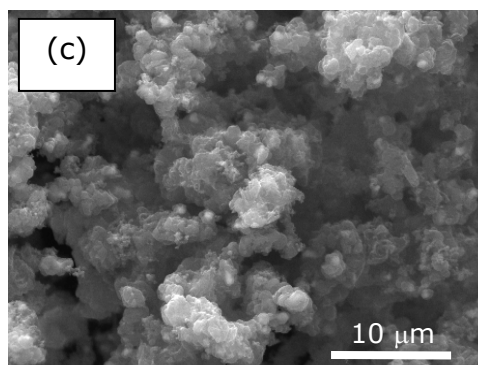
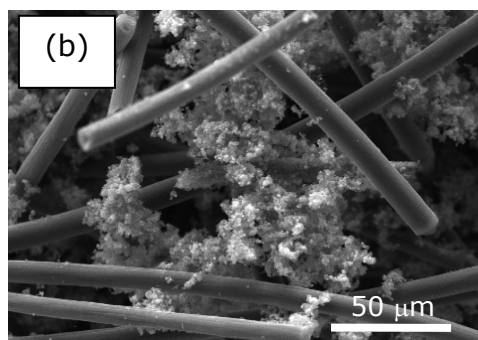
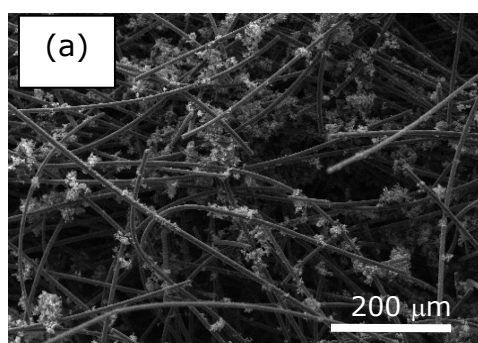


Figure 4.21: (a) – (c) SEM images of a carbon fibre mat, impregnated with nickel, after reaction in synthetic natural gas at 750°C for 3 hours.

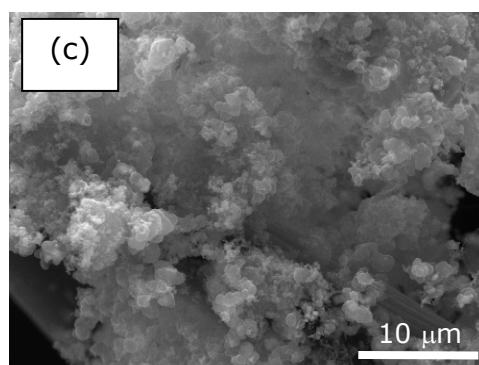
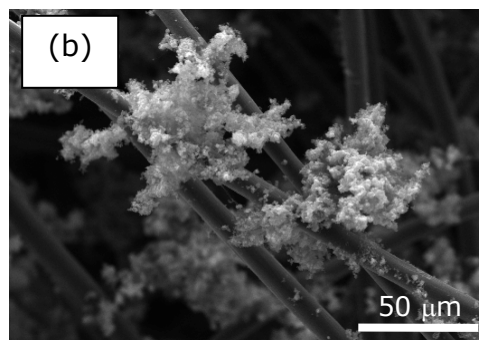
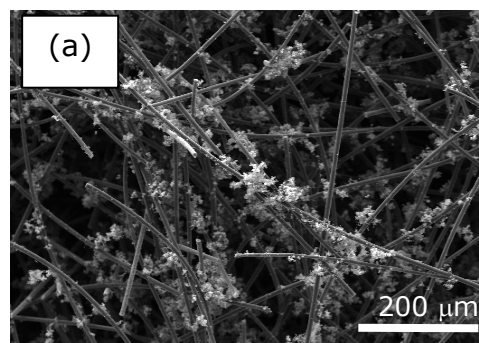


Figure 4.22: (a) – (c) SEM images of a carbon fibre mat, impregnated with nickel, after reaction in synthetic natural gas at 800°C for 3 hours.

The SEM images shown in Figure 4.22 are for a carbon fibre mat sample after reaction in synthetic natural gas at 800°C. For this reaction similar spherical deposits to those produced at 750°C were present and the dispersion across the surface of the mat was greater. The deposited carbon was also grown along individual fibres and seemed to be in close contact with the carbon fibres.

4.2.5.2.3 Ethane plus Hydrogen

The SEM images shown in Figure 4.23 are for a carbon fibre mat sample following reaction in ethane plus hydrogen at 650°C. The morphology of the catalytically deposited carbon shown here consists of spherical deposits of “fluffy” filamentous carbon which agglomerated together around and in between carbon fibres so that they bridged the individual carbon fibres of the mat.

Figure 4.24 shows SEM images for a carbon fibre mat sample following reaction in ethane plus hydrogen at 700°C. The deposited carbon was mainly filamentous in nature with some areas of encapsulation. The deposits also seemed to be in close contact with the fibres of the mat and were bridging gaps between individual fibres.

Figure 4.25 shows SEM images for a carbon fibre mat sample after reaction in ethane plus hydrogen at 750°C. The morphology of the catalytically deposited carbon became encapsulation with a reduction in the amount of filamentous carbon. However, the deposits seemed to grow well along individual fibres and the deposited carbon was in close contact with the fibres of the mat.

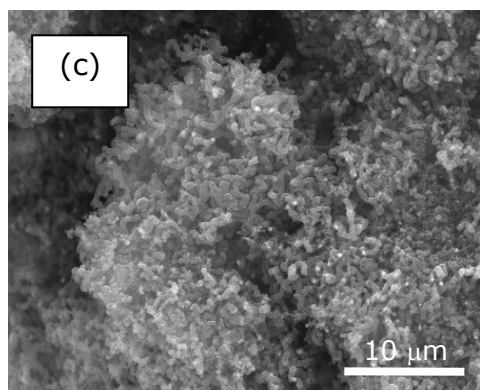
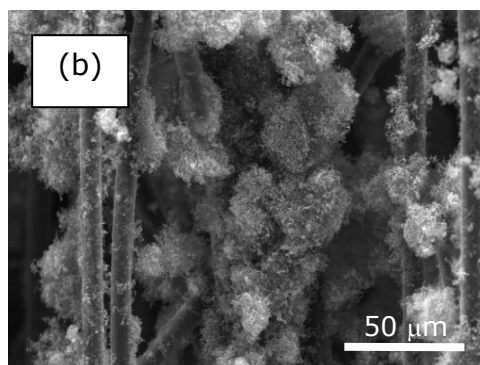
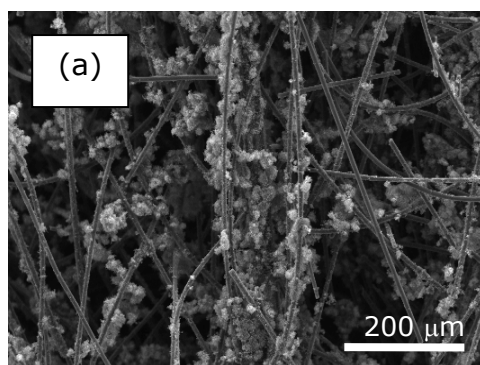


Figure 4.23: (a) – (c) SEM images of a carbon fibre mat, impregnated with nickel, after reaction in ethane plus hydrogen at 650°C for 3 hours.

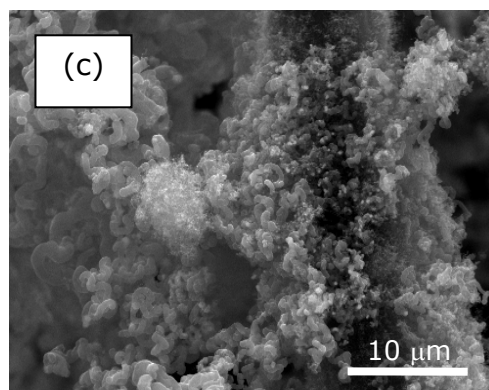
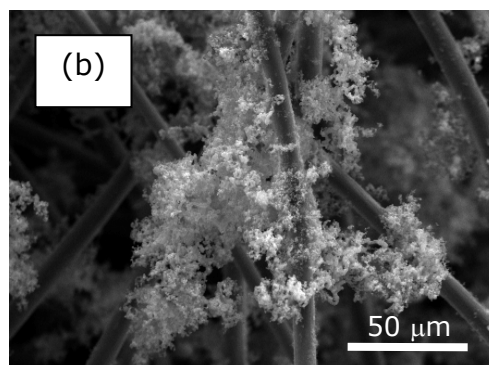
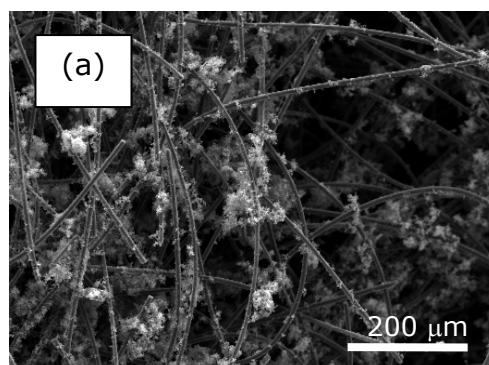


Figure 4.24: (a) – (c) SEM images of a carbon fibre mat, impregnated with nickel, after reaction in ethane plus hydrogen at 700°C for 3 hours.

The SEM images shown in Figure 4.26 are for a carbon fibre mat sample following reaction in ethane plus hydrogen at 800°C. The catalytically deposited carbon consisted of almost entirely encapsulation which was well dispersed over the surface of the mat and seemed to be in close contact with the individual fibres from the mat as well as being able to bridge individual fibres.

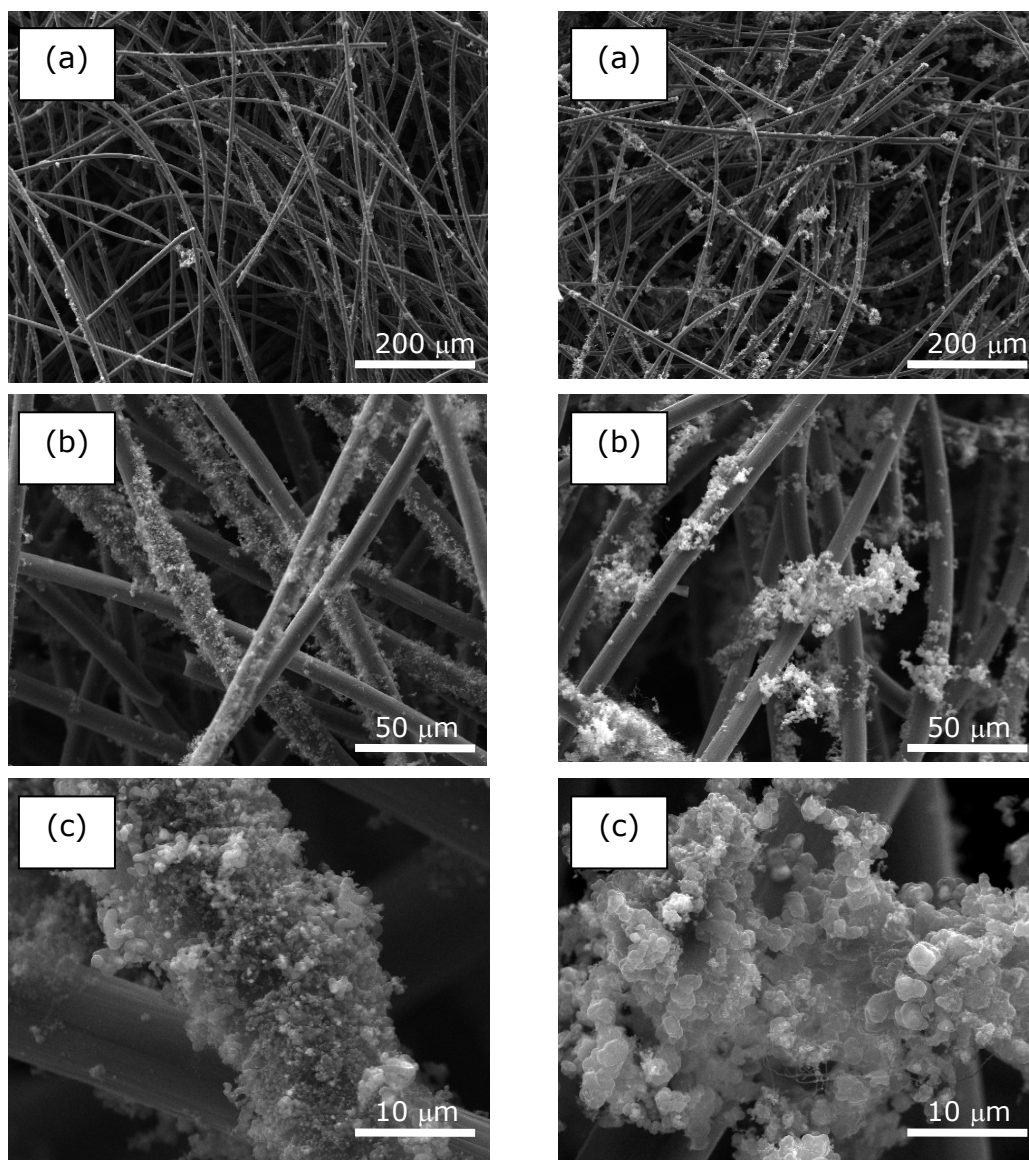


Figure 4.25: (a) – (c) SEM images of a carbon fibre mat, impregnated with nickel, after reaction in ethane plus hydrogen at 750°C for 3 hours.

Figure 4.26: (a) – (c) SEM images of a carbon fibre mat, impregnated with nickel, after reaction in ethane plus hydrogen at 800°C for 3 hours.

4.2.5.2.4 Synthetic Natural Gas plus Hydrogen

The SEM images shown Figure 4.27 are for a carbon fibre mat sample after reaction in synthetic natural gas plus hydrogen at 650°C. The deposited carbon was sparsely dispersed and consisted of thick carbon filaments which were in close contact with and bridged individual fibres of the mat.

Figure 4.28 shows SEM images for a carbon fibre mat sample after reaction in synthetic natural gas plus hydrogen at 700°C. The catalytically deposited carbon consisted of a mixture of filamentous carbon and encapsulation both of which were in close contact with the individual fibres of the mat.

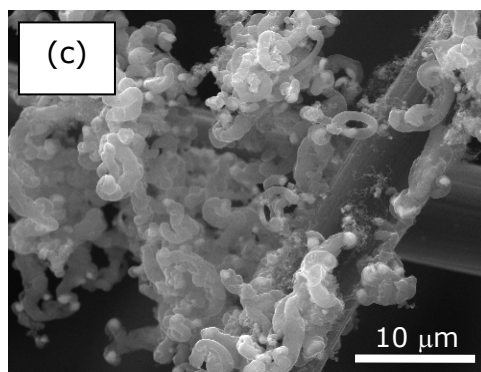
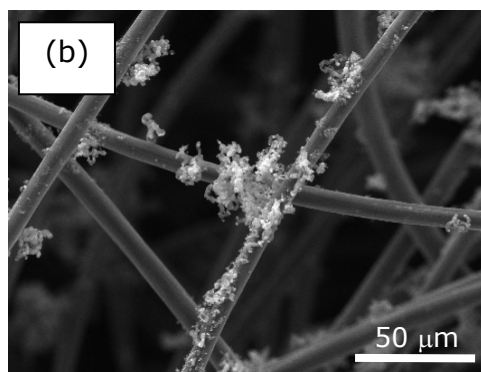
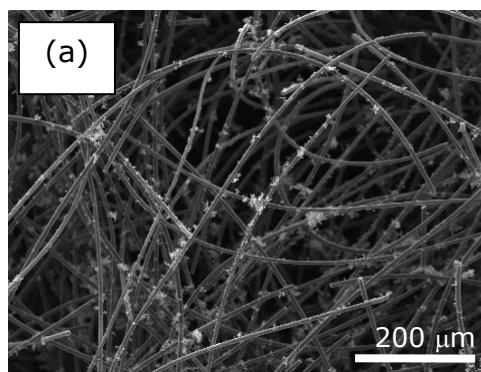


Figure 4.27: (a) – (c) SEM images of a carbon fibre mat, impregnated with nickel, after reaction in synthetic natural gas plus hydrogen at 650°C for 3 hours.

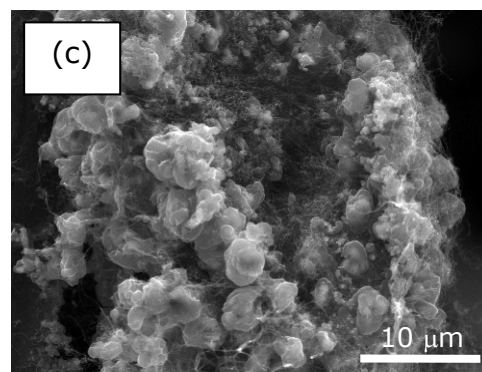
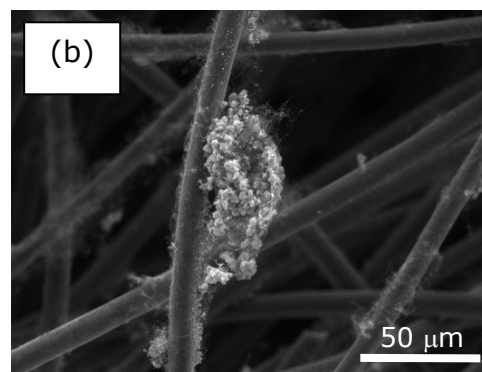
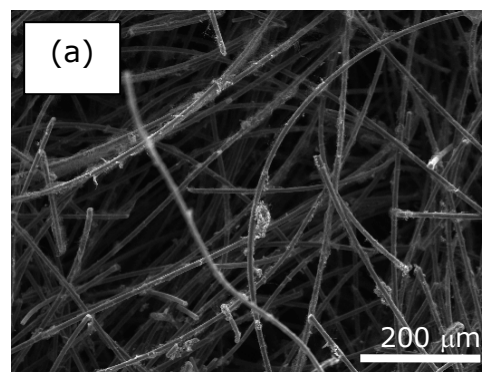


Figure 4.28: (a) – (c) SEM images of a carbon fibre mat, impregnated with nickel, after reaction in synthetic natural gas plus hydrogen at 700°C for 3 hours.

Figure 4.29 shows SEM images for a carbon fibre mat sample following reaction in synthetic natural gas plus hydrogen at 750°C. The deposited carbon had a spherical morphology indicative of encapsulation; however, there were some areas of filamentous carbon growth. The deposited carbon was also in close contact with and was capable of bridging gaps between individual fibres.

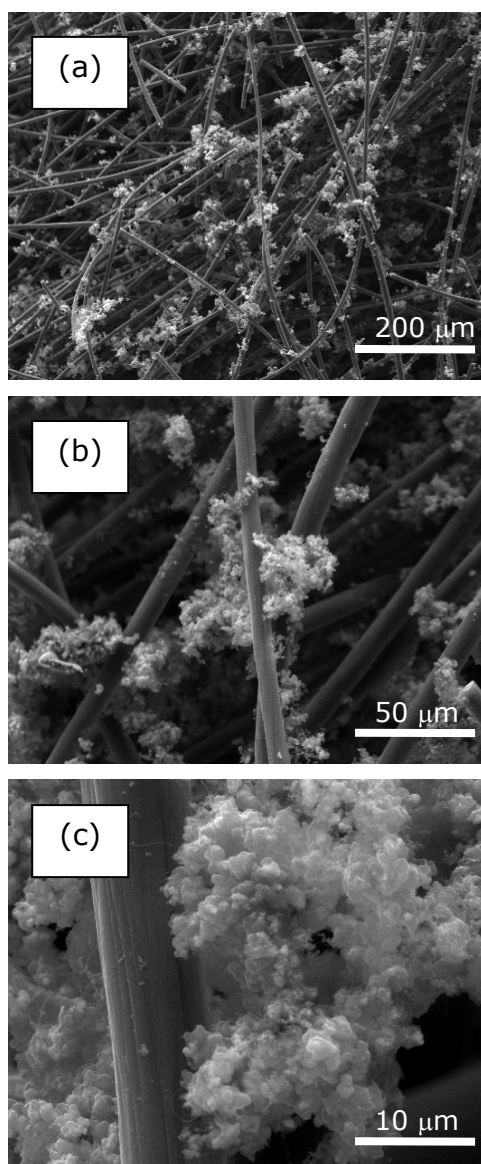


Figure 4.29: (a) – (c) SEM images of a carbon fibre mat, impregnated with nickel, after reaction in synthetic natural gas plus hydrogen at 750°C for 3 hours.

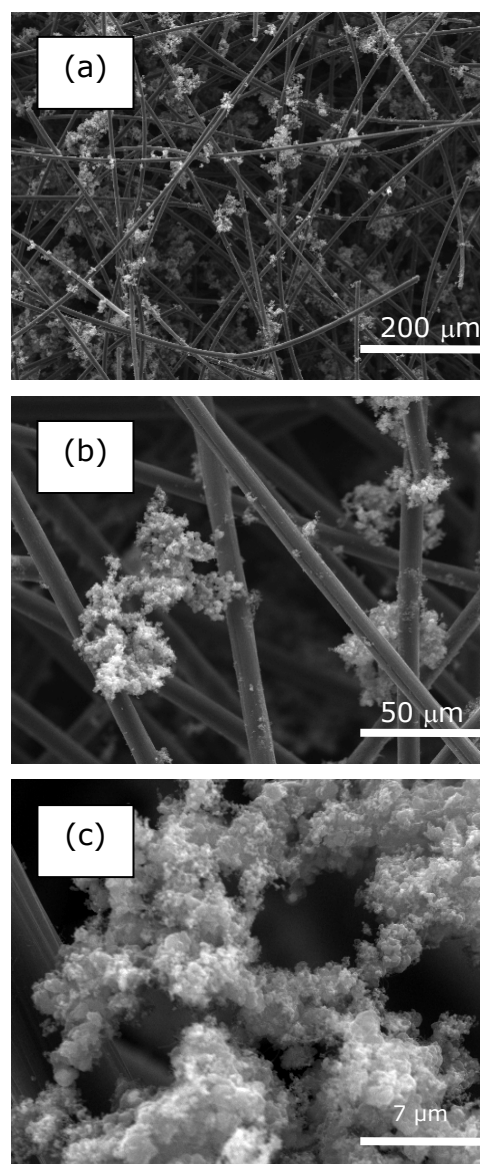


Figure 4.30: (a) – (c) SEM images of a carbon fibre mat, impregnated with nickel, after reaction in synthetic natural gas plus hydrogen at 800°C for 3 hours.

The SEM images shown in Figure 4.30 are for a carbon fibre mat sample after reaction in synthetic natural gas plus hydrogen at 800°C. The catalytically deposited carbon consisted mainly of encapsulation with areas of filamentous carbon both of which were in close contact with the fibres and together were capable of bridging large gaps between individual fibres.

A table summarising the findings from the SEM images presented in Figures 4.15 to 4.30, after catalytic carbon deposition, is shown in Table 4.4, in all cases the reaction time was 3 hours and 20 wt. % nickel was used as the catalyst.

<u>Deposition Conditions</u>		<u>Sample Attributes</u>			
		<u>Type Carbon Deposited</u>	<u>Fibre Bridging</u>	<u>Deposited Carbon Abundance</u>	<u>% PU/h</u>
650°C	Ethane	Filamentous	No	Low	5.54
	Syn NG	Filamentous	No	Very Low	-2.97
	Ethane + 20 vol. % H ₂	Filamentous	Yes	Very Low	2.17
	Syn NG + 20 vol. % H ₂	Filamentous	Yes	Very Low	0.26
700°C	Ethane	Mixture of Filamentous & Encapsulation	No	Low	8.04
	Syn NG	Filamentous	No	Very Low	-0.38
	Ethane + 20 vol. % H ₂	Mixture of Filamentous & Encapsulation	Yes	Low	12.21
	Syn NG + 20 vol. % H ₂	Mixture of Filamentous & Encapsulation	No	Very Low	2.46
750°C	Ethane	Mostly Encapsulation	Yes	Medium	35.94
	Syn NG	Mostly Encapsulation	Yes	Medium	31.35
	Ethane + 20 vol. % H ₂	Mixture of Filamentous & Encapsulation	No	Medium	32.13
	Syn NG + 20 vol. % H ₂	Mostly Encapsulation	Yes	Medium	30.59
800°C	Ethane	Mostly Encapsulation	No	High	55.97
	Syn NG	Mostly Encapsulation	Yes	Medium	33.65
	Ethane + 20 vol. % H ₂	Encapsulation	Yes	High	66.25
	Syn NG + 20 vol. % H ₂	Mostly Encapsulation	Yes	Medium	31.85

Table 4.4: Table summarising the SEM images and comparing the attributes of the deposited carbon as well as linking this to the mean percentage pick-up per hour obtained for each reaction condition. All reactions were carried out over 3 hours with a 20 wt. % Ni loading.

4.2.5.2.5 Effect of Increasing Hydrogen Concentration

This section shows SEM images of carbon fibre mat samples after catalytic carbon deposition in ethane or synthetic natural gas with varying concentration of hydrogen at 750°C. As SEM images for the pure ethane (Figure 4.17), pure synthetic natural gas (Figure 4.21), ethane plus 20 vol. % hydrogen (Figure 4.25) and synthetic natural gas plus 20 vol. % hydrogen (Figure 4.29) have been previously shown, this section will show the SEM images for both ethane and synthetic natural gas with 40, 60 and 80 vol. % hydrogen added.

The SEM images shown in Figure 4.31 are for a carbon fibre mat sample after reaction in ethane (60 vol. %) plus hydrogen (40 vol. %) at 750°C. The deposited carbon was mainly encapsulation with a small amount of filamentous carbon. The deposits were able to bridge fibres and were in close contact with them.

The SEM images shown in Figure 4.32 are for a carbon fibre mat sample following reaction in ethane (40 vol. %) plus hydrogen (60 vol. %) at 750°C. The deposited carbon was mostly filamentous in nature with some encapsulation. The filamentous carbon formed was in close contact with the fibres and grew along their length.

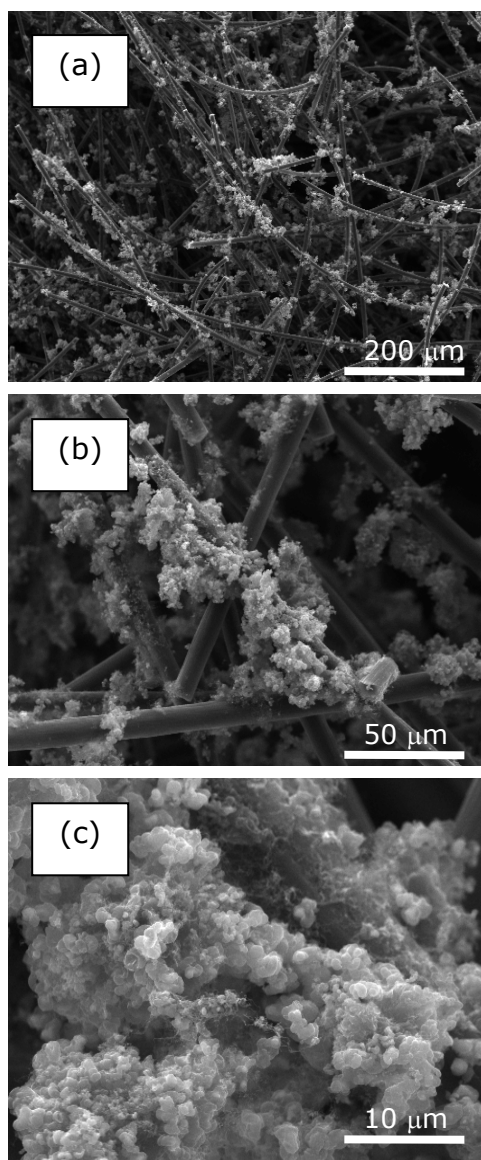


Figure 4.31: (a) – (c) SEM images of a carbon fibre mat, impregnated with nickel, after reaction in ethane plus 40 vol. % hydrogen at 750°C.

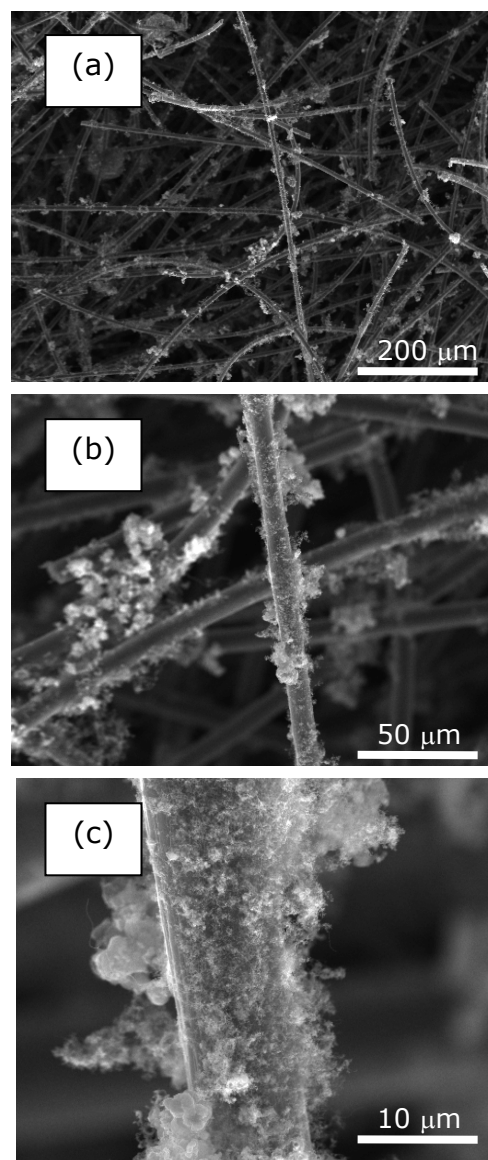


Figure 4.32: (a) – (c) SEM images of a carbon fibre mat, impregnated with nickel, after reaction in ethane plus 60 vol. % hydrogen at 750°C.

The SEM images shown Figure 4.33 are for a carbon fibre mat sample following reaction in ethane (20 vol. %) plus hydrogen (80 vol. %) at 750°C. The deposited carbon consisted of a mixture of encapsulation and filamentous carbon. The deposits were well dispersed over the surface of the mat and were in close contact with the fibres as well as bridging between individual fibres.

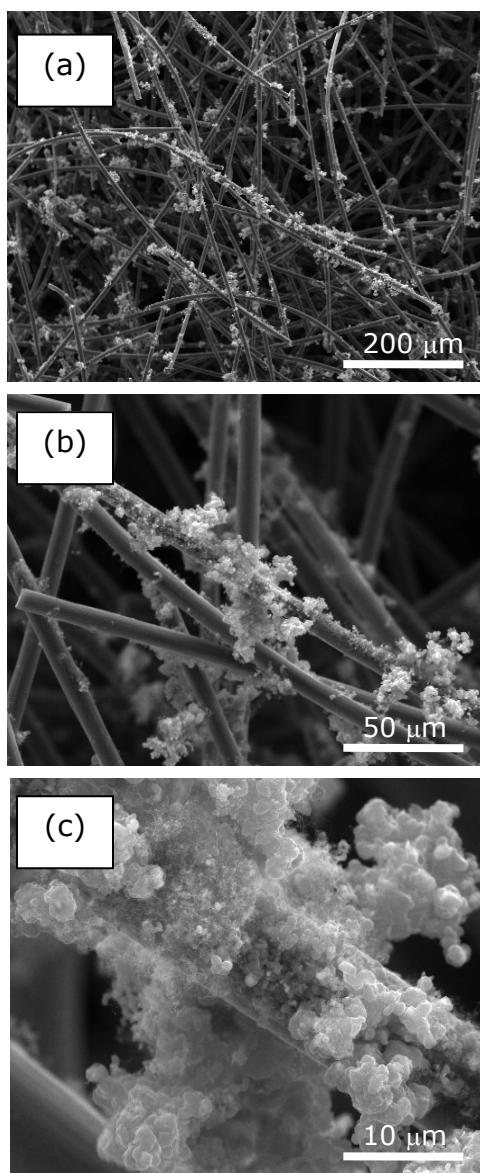


Figure 4.33: (a) – (c) SEM images of a carbon fibre mat, impregnated with nickel, after reaction in ethane plus 80 vol. % hydrogen at 750°C.

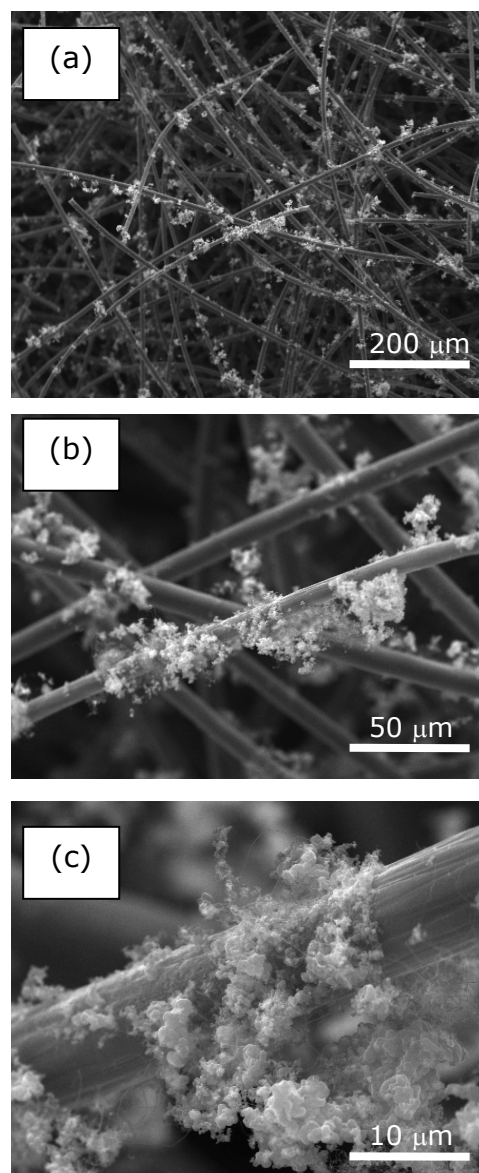


Figure 4.34: (a) – (c) SEM images of a carbon fibre mat, impregnated with nickel, after reaction in synthetic natural gas plus 40 vol. % hydrogen at 750°C.

The SEM images shown in Figure 4.34 are for a carbon fibre mat sample after reaction in synthetic natural gas (60 vol. %) plus hydrogen (40 vol. %) at 750°C. The deposited carbon was well dispersed across the surface of the mat and consisted of graphitic encapsulation and filamentous carbon which was in close contact with, growing along and bridging gaps between the fibres.

Figure 4.35 shows SEM images for a carbon fibre mat sample following reaction in synthetic natural gas (40 vol. %) plus hydrogen (60 vol. %) at 750°C. The deposited carbon consisted of a mixture of graphitic encapsulation and filamentous carbon which was well dispersed and in close contact with the fibres of the mat.

The SEM images shown in Figure 4.36 are for a carbon fibre mat sample after reaction in synthetic natural gas (20 vol. %) plus hydrogen (80 vol. %) at 750°C. The deposited carbon was almost entirely filamentous in nature and formed small “cobweb like” clusters around the fibres from the mat, these clusters were sparsely spread across the top surface of the carbon fibre mat. The clusters do, however, seem to be in close contact with the fibres.

A table summarising the findings from the SEM images presented in Figures 4.31 to 4.36, increasing the hydrogen concentration, is shown in Table 4.5, in all cases the reaction time was 3 hours, the temperature was 750°C and 20 wt. % nickel was used as the catalyst.

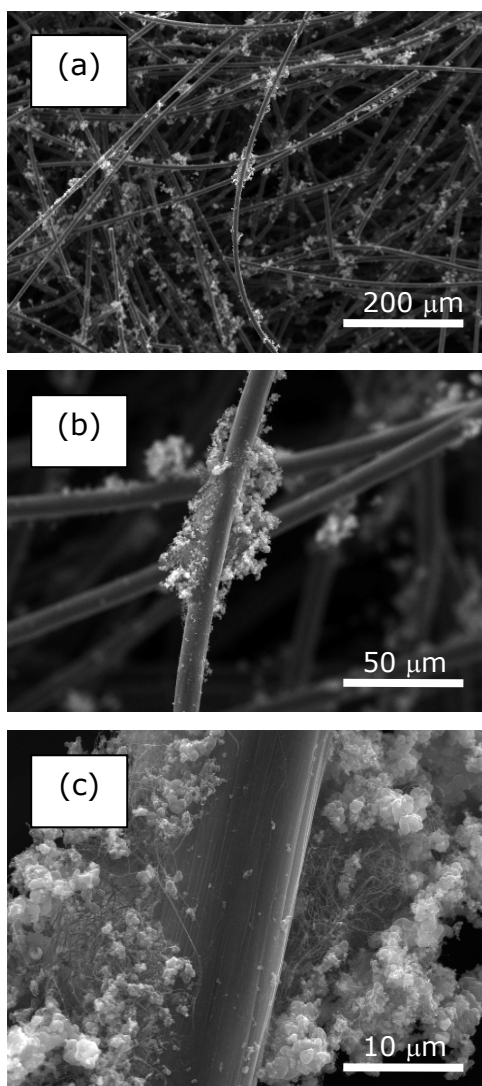


Figure 4.35: (a) – (c) SEM images of a carbon fibre mat, impregnated with nickel, after reaction in synthetic natural gas plus 60 vol. % hydrogen at 750°C.

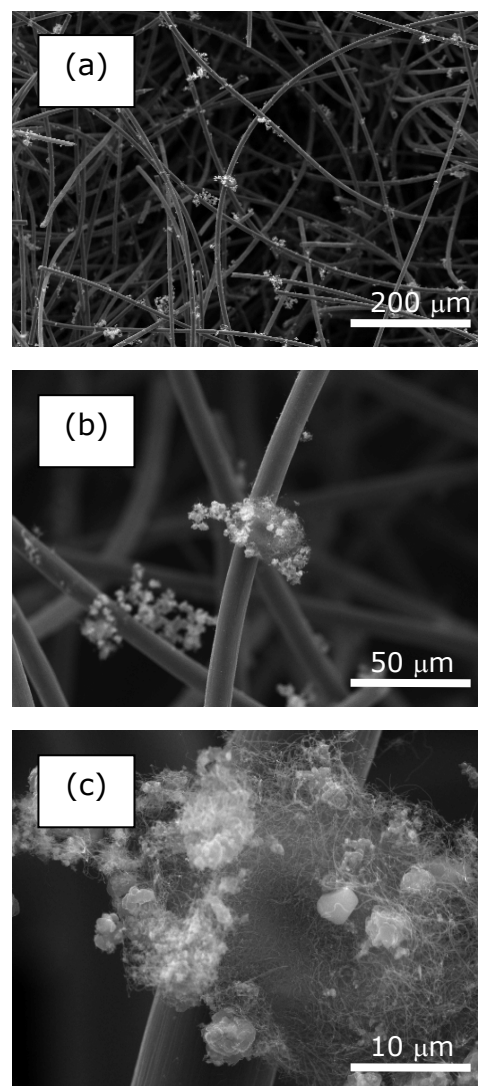


Figure 4.36: (a) – (c) SEM images of a carbon fibre mat, impregnated with nickel, after reaction in synthetic natural gas plus 80 vol. % hydrogen at 750°C.

<u>Deposition Gas Mixture</u>	<u>Sample Attributes</u>			
	<u>Type Carbon Deposited</u>	<u>Fibre Bridging</u>	<u>Deposited Carbon Abundance</u>	<u>% PU/h</u>
Ethane	Mostly Encapsulation	Yes	Medium	35.94
Ethane + 20 vol. % H ₂	Mixture of Filamentous & Encapsulation	No	Medium	32.13
Ethane + 40 vol. % H ₂	Mostly Encapsulation	Yes	Medium	33.73
Ethane + 60 vol. % H ₂	Mostly Filamentous	No	Medium / Low	29.65
Ethane + 80 vol. % H ₂	Mixture of Filamentous & Encapsulation	Yes	Medium / Low	26.85
Syn NG	Mostly Encapsulation	Yes	Medium	31.35
Syn NG + 20 vol. % H ₂	Mostly Encapsulation	Yes	Medium	30.59
Syn NG + 40 vol. % H ₂	Mixture of Filamentous & Encapsulation	Yes	Medium / Low	16.64
Syn NG + 60 vol. % H ₂	Mixture of Filamentous & Encapsulation	No	Low	8.45
Syn NG + 80 vol. % H ₂	Filamentous	No	Very Low	0.28

Table 4.5: Table summarising the SEM images and comparing the attributes of the deposited carbon as well as linking this to the mean percentage pick-up per hour obtained for each reaction condition. All reactions were carried out over 3 hours, at 750°C and with a 20 wt. % Ni loading.

4.2.5.2.6 Effect of Increasing Reaction Time

This section shows SEM images of carbon mat samples after catalytic carbon deposition reactions carried out in ethane and ethane plus hydrogen at reaction temperatures of 750°C and 800°C. The reactions were carried for a total of 12 hours processing (weighed at regular intervals: 2, 3 or 4 hours).

Figure 4.37 shows SEM images for a carbon fibre mat sample after reaction in ethane at 750°C for 12 hours. The fibre coverage of the deposited carbon on the top surface of the carbon fibre mat was relatively high with carbon deposits consisting filamentous carbon which formed at the intersections between fibres and which was capable of bridging gaps between the fibres.

The SEM images shown in Figure 4.38 are for a carbon fibre mat sample following reaction carried out in ethane plus hydrogen at 750°C for 12 hours. The deposited carbon formed from this reaction formed a crust of carbon across the top surface of the carbon fibre mat; this crust of deposited carbon consisted of a mixture of filamentous and graphitic encapsulation.

The SEM images shown in Figure 4.39 are for a carbon fibre mat sample after reaction in ethane at 800°C for 12 hours. The deposited carbon was well dispersed across the surface of the mat and was shown to bind together and bridge gaps between individual fibres. The morphology of the deposits was mainly encapsulation with some filamentous carbon.

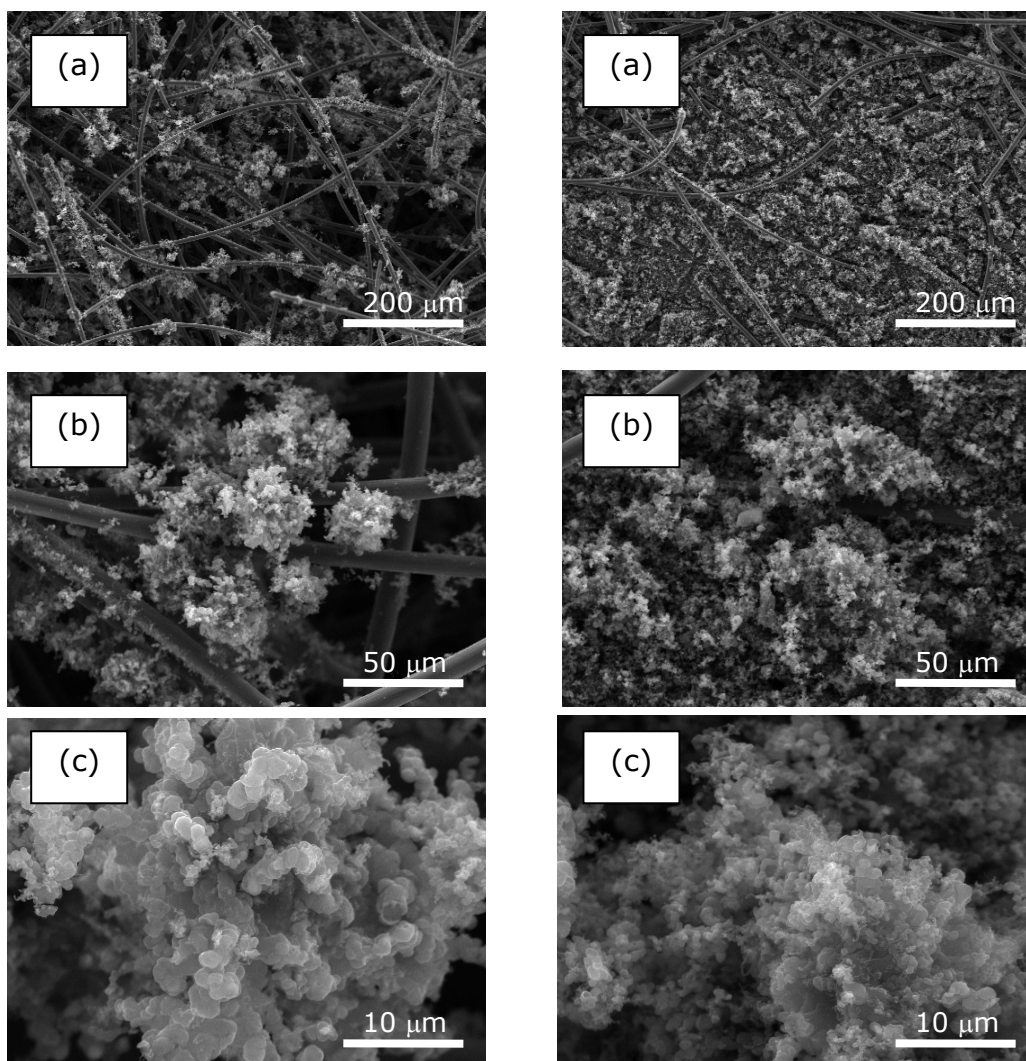


Figure 4.37: (a) – (c) SEM images of a carbon fibre mat, impregnated with nickel, after reaction in ethane at 750°C for 12 hours.

Figure 4.38: (a) – (c) SEM images of a carbon fibre mat, impregnated with nickel, after reaction in ethane plus hydrogen at 750°C for 12 hours.

The SEM images shown in Figure 4.40 are for a carbon fibre mat sample following reaction in ethane plus hydrogen at 800°C for 12 hours. The deposited carbon had formed a large crust that was supported by and was binding together a number of individual carbon fibres. The deposit was made up primarily of encapsulation.

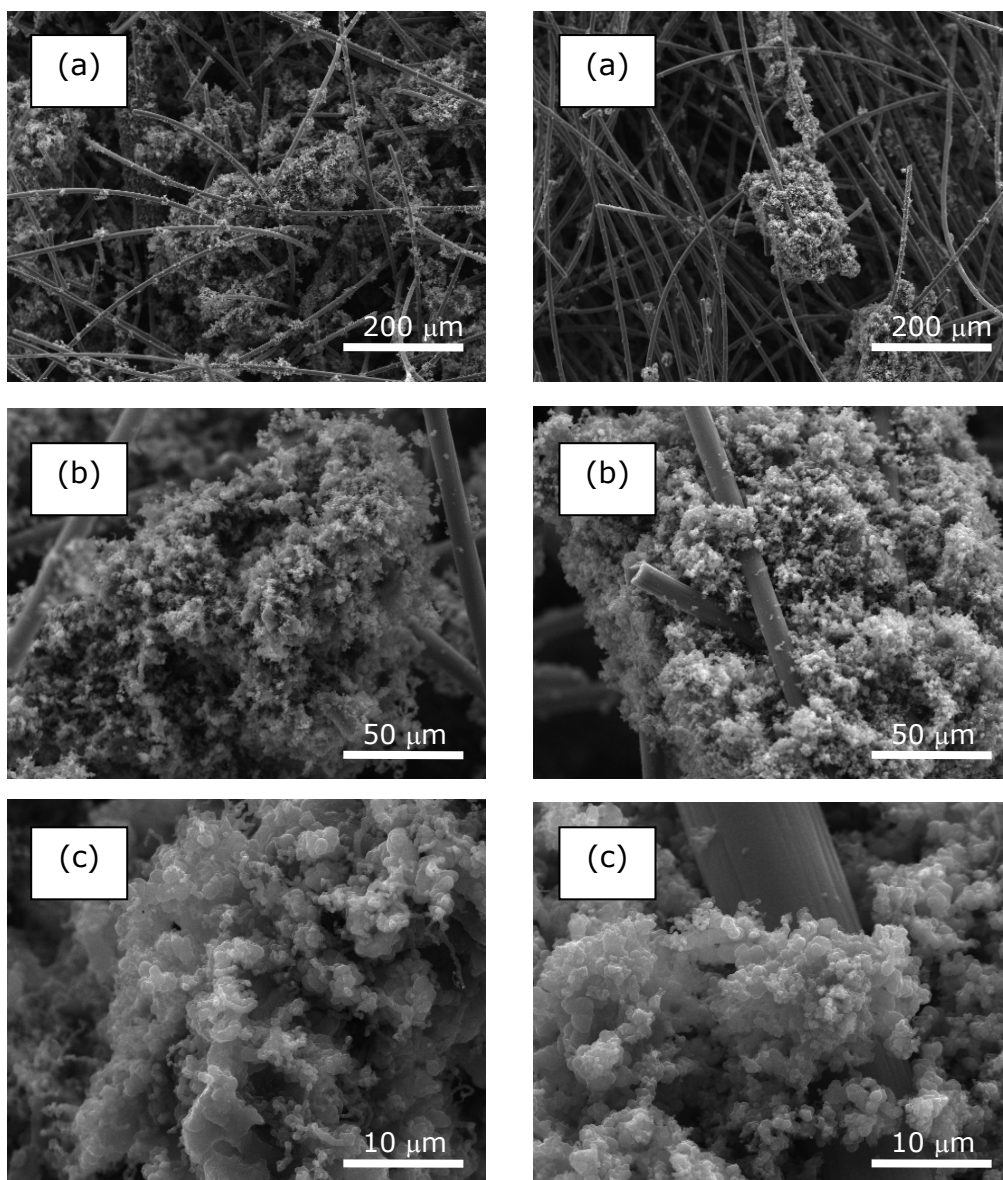


Figure 4.39: (a) – (c) SEM images of a carbon fibre mat, impregnated with nickel, after reaction in ethane at 800°C for 12 hours.

Figure 4.40: (a) – (c) SEM images of a carbon fibre mat, impregnated with nickel, after reaction in ethane plus hydrogen at 800°C for 12 hours.

A table summarising the findings from the SEM images presented in Figures 4.39 to 4.40, increasing the deposition time, is shown in Table 4.6, in all cases the total reaction time was 12 hours and 20 wt. % nickel was used as the catalyst. The percentage pick-up's per hour quoted are for an average taken over the entire 12 hour deposition time.

<u>Deposition Conditions</u>		<u>Sample Attributes</u>			
		<u>Type Carbon Deposited</u>	<u>Fibre Bridging</u>	<u>Deposited Carbon Abundance</u>	<u>% PU/h</u>
750°C	Ethane	Filamentous	Yes	High	23.63
	Ethane + H ₂	Mixture of Filamentous & Encapsulating	Yes	High	32.10
800°C	Ethane	Mostly Encapsulation	Yes	High	39.78
	Ethane + H ₂	Mostly Encapsulation	Yes	High	50.99

Table 4.6: Table summarising the SEM images and comparing the attributes of the deposited carbon as well as linking this to the mean percentage pick-up per hour obtained for each reaction condition. All reactions were carried out over 12 hours with a 20 wt. % Ni loading. The percentage pick-up's per hour quoted are averaged over the entire 12 hour deposition time.

4.2.6. TEM

TEM micrographs are presented to show the different types of carbon nanostructures deposited i.e. encapsulation and filamentous, from the reaction of nickel impregnated carbon fibre mats with ethane and ethane plus hydrogen at varying temperatures (650, 700, 750 and 800°C).

4.2.6.1. Ethane Gas Feedstock

Figure 4.41 shows a TEM micrograph of a carbon nanofilament with a diameter of ~ 60 nm, this nanofilament was produced from the reaction of an impregnated carbon fibre mat with ethane at 650°C, and is indicative of the filamentous carbon which made up the “fluffy” deposits shown in Figure 4.15. The SAED pattern (Figure 4.41) showed a diffuse ring joining more distinct spots, closest to the centre spot, this was indicative of amorphous or nanocrystalline graphite, in which the graphitic sheets were

randomly stacked, with the presence of crystallites of more ordered graphite.

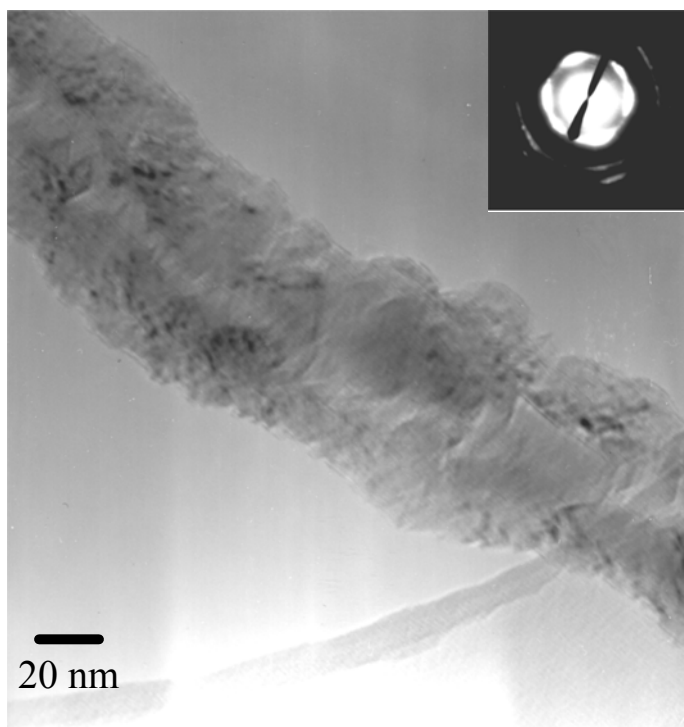


Figure 4.41: TEM micrograph with the corresponding selected area electron diffraction pattern of the catalytically deposited carbon on a carbon fibre mat after reaction with ethane at 650°C.

Figure 4.42 shows a TEM micrograph of the carbon nanotubes which made up the nanosized (10 – 20 nm) filamentous carbon, shown in Figure 4.16, produced from the reaction of an impregnated carbon fibre mat with ethane at 700°C.

The TEM micrograph shown in Figure 4.43 shows both the filamentous carbon and encapsulation which was observed in Figure 4.17 for the reaction of an impregnated carbon fibre mat with ethane at 750°C. The TEM micrograph shows that the encapsulated particles are in the form of a large ($\sim 5 \mu\text{m}$ in diameter) agglomerate and the carbon nanofilaments growing off from this

cluster are approximately 100 nm in diameter and several micrometers in length.

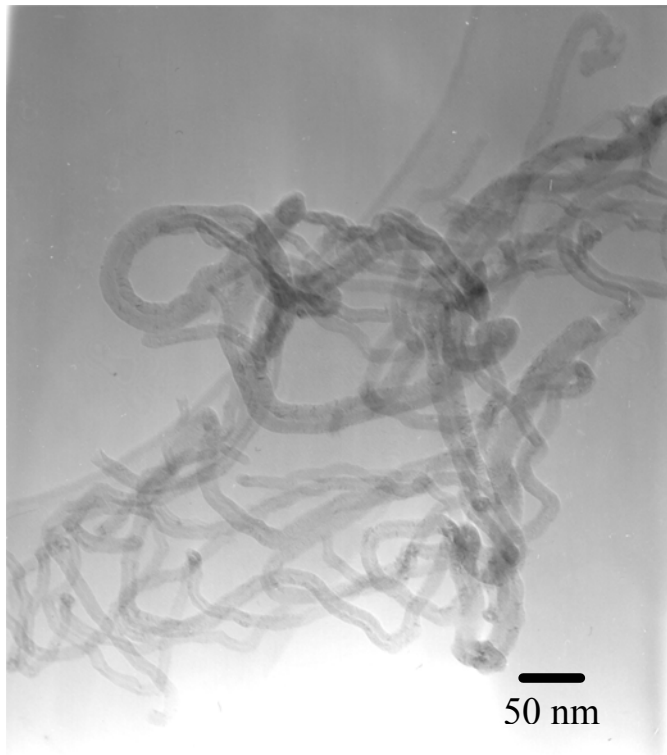


Figure 4.42: TEM micrograph of the catalytically deposited carbon on a carbon fibre mat after reaction with ethane at 700°C.

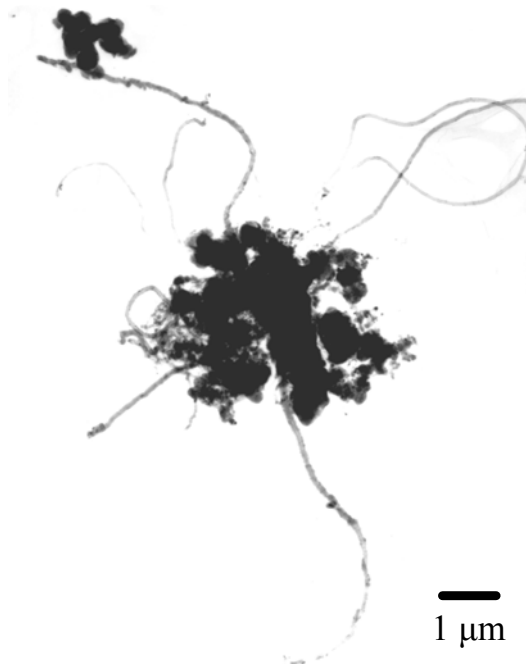


Figure 4.43: TEM micrograph for a typical carbon deposit produced from the reaction of the catalyst impregnated carbon fibre mat with ethane at 750°C.

Figure 4.44 shows TEM micrographs of carbon deposits produced from the reaction in ethane at 800°C. Figure 4.44 (a) shows deposited carbon consisting of a carbon nanofilament (≈ 70 nm in diameter) with nickel catalyst particles (dark areas) entrained and encapsulated within the nanofilament and Figure 4.44 (b) shows carbon encapsulated nickel catalyst particles.

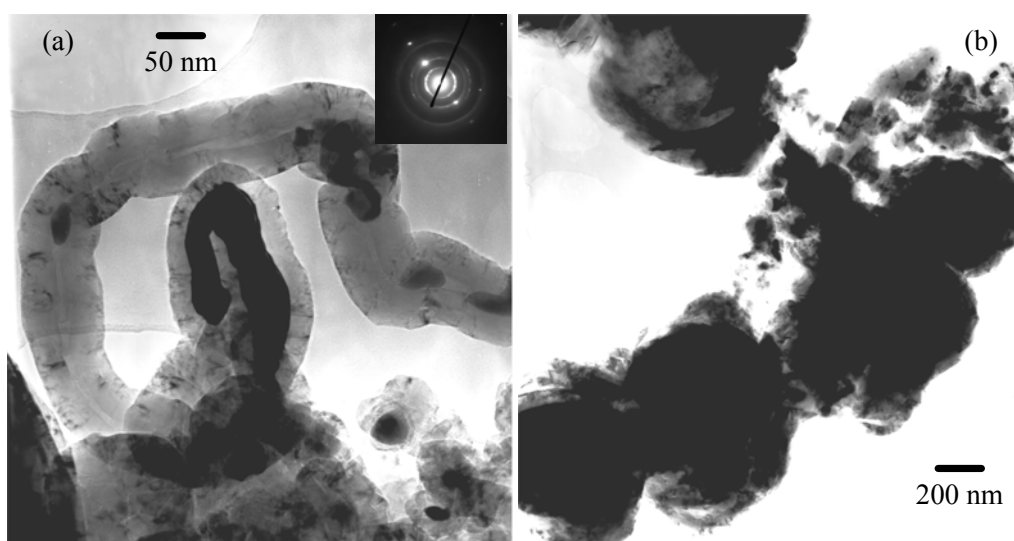


Figure 4.44: TEM micrograph of catalytic carbon produced from the reaction of the catalyst impregnated carbon fibre mat with ethane at 800°C. (a) with corresponding selected area diffraction pattern.

4.2.6.2. Ethane plus Hydrogen Gas Feedstock

Figure 4.45 shows TEM micrographs of two different carbon nanoforms produced from the reaction of an impregnated carbon fibre mat with ethane plus hydrogen at 650°C. The “fluffy” deposits shown in Figure 4.23 were made up from large diameter (ca. 250 nm) carbon nanofibres (Figure 4.45 (a)) and smaller diameter (ca. 10 – 20 nm) carbon nanotubes (Figure 4.45 (b)).

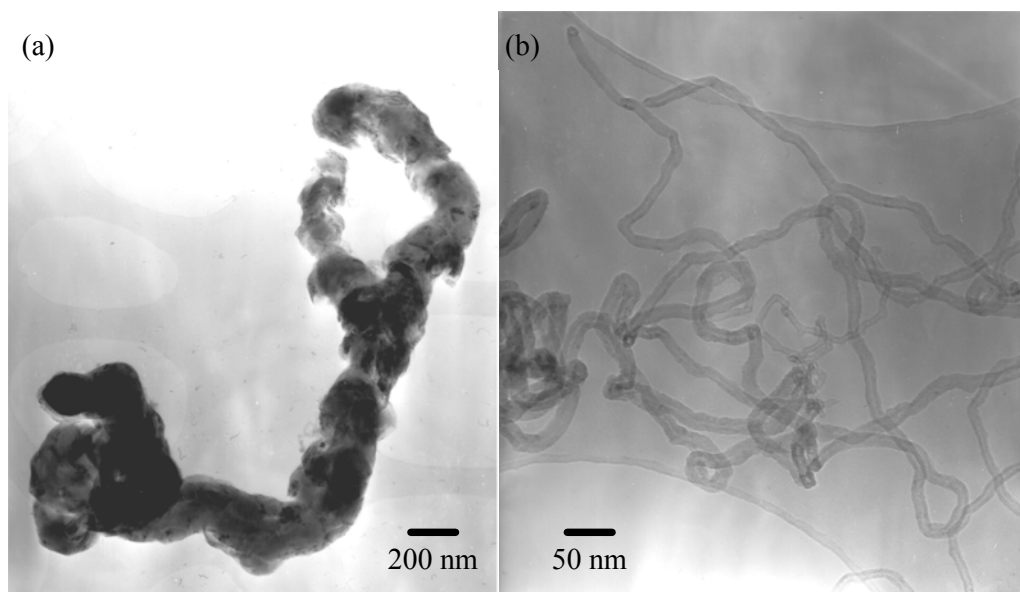


Figure 4.45: TEM micrographs of catalytic carbon produced from the reaction of an impregnated carbon fibre mat with ethane plus hydrogen at 650°C.

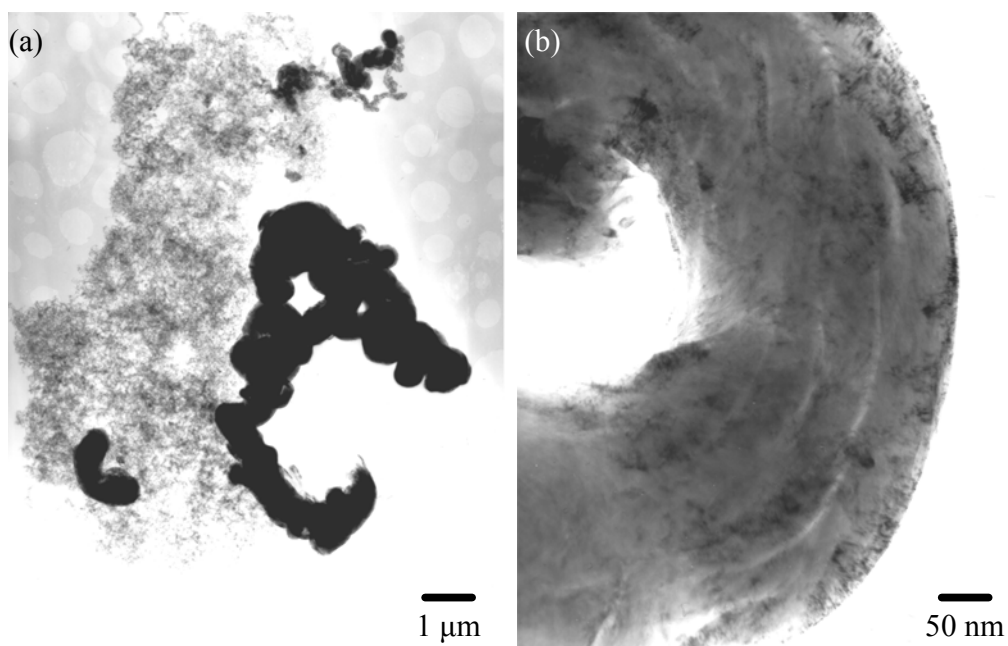


Figure 4.46: TEM micrographs of catalytic carbon produced from the reaction of an impregnated carbon fibre mat with ethane plus hydrogen at 700°C.

Figure 4.46 shows TEM micrographs of the carbon produced from the reaction of an impregnated carbon fibre mat in ethane plus hydrogen at 700°C, as for the reaction carried out at 650°C,

there were again two distinct forms of carbon deposited, carbon microcoils (ca. 1 μm in diameter) and carbon nanofibres (ca. 200 nm in diameter), see Figure 4.46 (a) and (b) respectively.

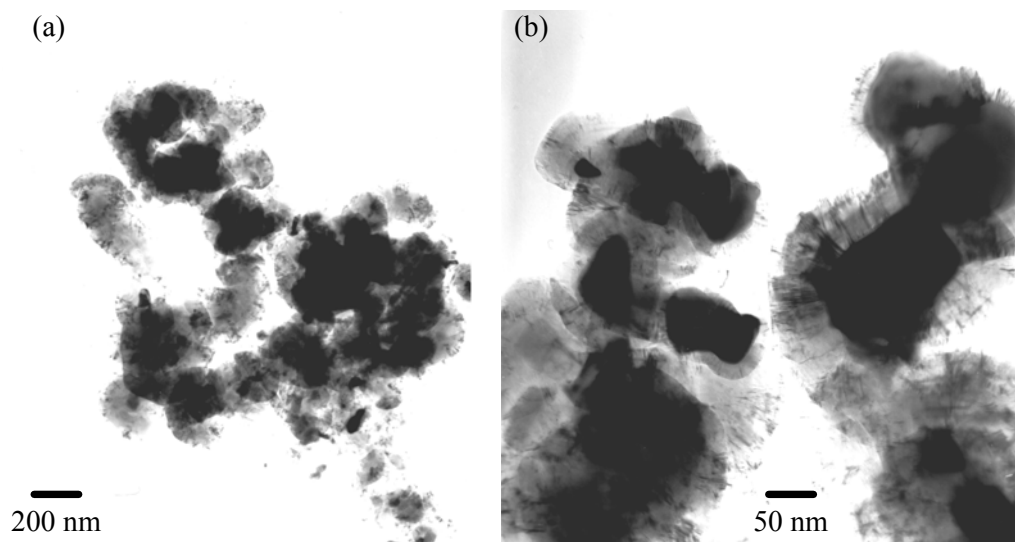


Figure 4.47: TEM micrographs of catalytic carbon produced from the reaction of the catalyst impregnated carbon fibre mat with ethane plus hydrogen at 750°C.

As was shown in Figure 4.25, the majority of the carbon produced from the interaction of an impregnated carbon fibre mat with ethane plus hydrogen at 750°C was encapsulation. The TEM micrographs shown in Figure 4.47 show encapsulated nickel catalyst particles (dark areas) in the form of a large cluster (ca. 1 μm in diameter) as shown in Figure 4.47 (a), within this cluster there were a number of nickel catalyst particles ranging from 50 – 200 nm in diameter, these nickel particles were encapsulated with a layer of carbon approximately 50 nm thick.

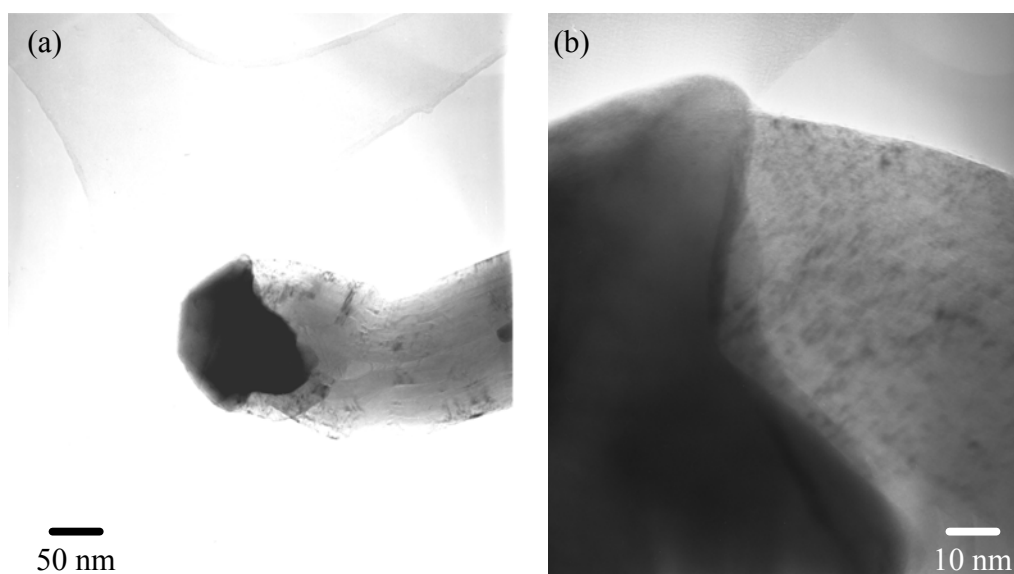


Figure 4.48: TEM micrographs of catalytic carbon produced from the reaction of the catalyst impregnated carbon fibre mat with ethane plus hydrogen at 800°C.

As for the reaction carried out in ethane plus hydrogen at 750°C, the reaction carried out in ethane plus hydrogen at 800°C also produced mainly encapsulation (as shown in Figure 4.47), however, there were some carbon nanofibres produced, TEM micrographs of one of these is shown in Figure 4.48, they show that the nickel catalyst particle (ca. 150 nm in diameter) was elongated and had growing off of it a carbon nanofibre, also 150 nm in diameter, see Figure 4.49 (a), the boundary between the catalyst particle and the resulting fibre is shown in Figure 4.48 (b).

4.3 Discussion

4.3.1. Original Screening

A set of initial reactions were carried out to determine the most suitable catalyst (iron, nickel or cobalt) for the deposition of carbon, a suitable catalyst loading and a suitable carbon deposition gas feedstock, in order to produce the highest rate of carbon deposition on carbon fibre mats, with a view to manufacturing carbon-carbon composites *via* catalytic means. Table 4.1 shows the results obtained from these initial reactions, from these results there were 3 main findings:

1. A 10 wt. % catalyst loading was insufficient to yield appreciable carbon deposition from methane at 700°C, whereas a 20 wt. % catalyst loading yielded appreciable carbon deposition from mains natural gas plus hydrogen at 600°C.
2. Mains natural gas plus hydrogen was a better carbon deposition gas feedstock than methane.
3. Nickel gave a higher rate of carbon deposition than iron or cobalt.

From these findings it was decided that 20 wt. % nickel should be used as the catalyst with natural gas as the carbon containing gas feedstock, however, as there are day-to-day variations in the composition of mains natural gas, a bottled synthetic natural gas was used, and as methane was found to be a poor carbon deposition gas feedstock, as supported by the literature [7, 57] which states that methane will not readily catalytically deposit

carbon at temperatures below 900°C, then the next logical step was to use ethane as a pure saturated hydrocarbon gas feedstock for comparison, due it being more reactive than methane, as illustrated by the thermodynamic data shown in Table 4.7, which shows that ΔG for the decomposition of methane becomes negative at 538°C and for ethane at 194°C [94], showing that the decomposition of ethane becomes thermodynamically feasible at a much lower temperature than methane, this trend also continues for propane which is more reactive than ethane and methane. In order to yield high carbon deposition rates whilst also maintaining a considerable temperature saving over industrially applied temperatures, which are currently in excess of 1000°C, a temperature range of 650-800°C was decided upon and a deposition time of 3 hours was chosen.

<u>Gas Decomposing</u>	<u>Temperature ΔG° becomes negative</u>
Methane	538°C
Ethane	194°C
Propane	82°C

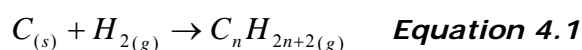
Table 4.7: Table showing the temperature at which ΔG becomes negative when plotted against temperature and standard pressure [94].

Prior to catalytic carbon deposition, experiments (TGA-MS and XRD) were carried out on the as received carbon fibre mat and nickel nitrate hexahydrate to determine their purity and thermal stability. Before this could be done a TGA-MS experiment was carried out with no sample present so that sample induced changes

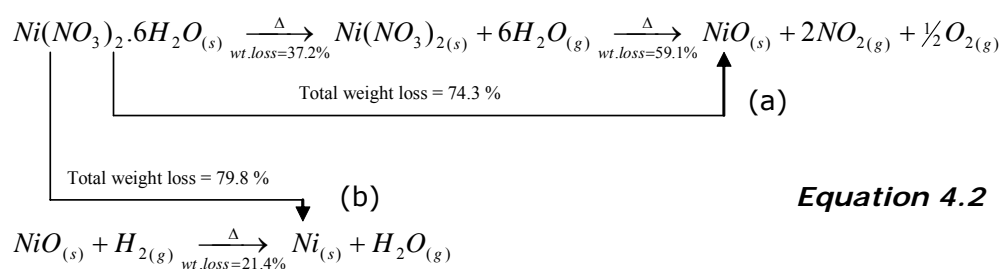
in weight and evolved gases could be assuredly determined when a sample was present.

The MS data for the blank run (Figure 4.5) showed that there was no increase in concentration of the monitored gases during heating from 50°C to 750°C in nitrogen, once the hydrogen was introduced at 750°C there was a marked increase in the water vapour concentration and a reduction in oxygen concentration, this was likely to be due to the reaction of trace gas phase oxygen with the introduced hydrogen to form water.

For the as received carbon fibre mat, consisting of clean, smooth carbon fibres each of which were free from contaminants and had a diameter of approximately 7 µm (Figure 4.12), the TGA data, Figure 4.6 (a), showed an 8.6 % total mass loss consisting of a 5.6 % weight loss by 250°C due to adsorbed water, Figure 4.6 and a 3.0 % weight loss upon the introduction of hydrogen at 750°C, which can be attributed to hydrogen reduction of the carbon fibres (see Equation 4.1), releasing hydrocarbons i.e. methane (n = 1), ethane (n = 2) and propane (n = 3), Figure 4.7 (b). Again there was an increase in the water vapour concentration which, as was shown from the blank run (Figure 4.5), was likely to be due to the gas phase reaction of trace oxygen with hydrogen. The XRD pattern (Figure 4.11 A) confirmed that there were no impurities on the as received carbon fibre mat, with the observed reflections being solely indicative of carbon.



For the as received nickel nitrate hexahydrate it can be seen from the TGA-MS data (Figure 4.7) that on heating from 100°C to 200°C the sample lost its six associated water molecules and started to thermally decompose, with an observed weight loss of 43.1 %, on further heating to 500°C there was a further weight loss of 30.5 % (total weight loss = 73.6 %), this total weight loss agreed well with the theoretical weight loss, of 74.3 %, for the drying and decomposition of nickel nitrate hexahydrate to nickel oxide, as illustrated in Equation 4.2 (a).



Once hydrogen was introduced to the gas feed at 750°C the nickel oxide reduced to nickel with the evolution of water, Figure 4.7 (b) and Equation 4.2 (b). Again there were gas phase reactions occurring as was seen for the blank run (Figure 4.5). The weight loss observed for the reduction of the nickel oxide to nickel was 6.2 %, Figure 4.7 (a), giving a total weight loss for the drying, decomposition and reduction of nickel nitrate hexahydrate to nickel of 79.2 %, which agreed well with the theoretical weight loss of 79.8 %.

4.3.2. Catalyst Formation

The catalyst was formed by impregnating a carbon fibre mat with a methanolic solution of nickel nitrate hexahydrate, the methanol was then evaporated off and the carbon fibre mat was left impregnated with particles of nickel nitrate hexahydrate which formed both large clusters at fibre intersections, which provide good nucleation sites, as well as smaller individual deposits along individual fibres, as shown in the SEM images in Figure 4.13.

Following impregnation the sample was heated to 500°C in nitrogen, as described in Chapter 3, this caused the nickel nitrate hexahydrate to thermally decompose to nickel oxide, as confirmed by the TGA-MS data shown in Figure 4.8, which, up to 500°C, followed the same pattern as that observed for the as received nickel nitrate discussed previously, the reaction taking place is outlined in Equation 4.2 (a).

However, upon further heating of the sample in nitrogen the TGA-MS data (Figure 4.8) showed there to be a sharp weight loss of 4.8 % observed at 600°C due to the production of carbon dioxide as the nickel oxide was reduced to nickel, as shown in Equation 4.3.



As the reduction of the nickel nitrate took place in an inert atmosphere and at a lower temperature, when the hydrogen was introduced the increase in gaseous products evolved was much reduced as was the observed weight loss, which was not as sharp

as previously observed (Figure 4.6). Here the gases evolved (hydrocarbons, water vapour, oxygen) were due to either gas phase reactions as for the blank run (Figure 4.5) or from the catalytic gasification of the carbon fibres by hydrogen, oxygen or water vapour interacting with the metallic nickel. The gases evolved correspond to a percentage weight loss of 25.6 % and the overall reaction percentage weight loss was 63.2 %.

Following the decomposition and reduction of the nickel nitrate hexahydrate to nickel the large clusters had reduced in size and they now formed small clusters of nickel particles, these clusters of metallic nickel particles varied in size and were randomly dispersed over the top surface of the mat, they also seemed to consist mainly of small spherical deposits which were clustered together, sometimes with a larger nickel agglomerate within the centre section of the cluster and with smaller particulate nickel around the edges of the cluster, as shown in Figure 4.14 (b), these deposits also appeared to be in close contact with the individual fibres of the carbon mat, see Figure 4.14.

The XRD pattern for the nickel nitrate hexahydrate impregnated carbon fibre mat, Figure 4.11 B, showed that the nickel nitrate hexahydrate was crystalline in nature. After the sample was heated to 700°C in nitrogen the XRD pattern (Figure 4.11 C) showed that the nickel nitrate hexahydrate had decomposed and reduced to metallic nickel, this confirmed that the presence of carbon from the carbon fibre mat caused the nickel oxide to be reduced to metallic nickel at temperatures in excess of 600°C, showing that if nickel

oxide catalysts or catalyst precursors are supported on carbon, then during or prior to (depending upon the deposition temperature) the catalytic deposition of carbon, the presence of nickel oxide could cause loss of the carbon support media used through reduction of the nickel oxide to nickel, as shown in Equation 4.3, however, there was no observed attack/pitting of the carbon fibres from the SEM images.

4.3.3. Carbon Deposition

This section will look at the effects of the different reaction variables investigated, these being the effect of changing the deposition gas feedstock and temperature, the effect of hydrogen addition to the deposition gas feedstock and the effect of deposition time.

4.3.3.1. Effect of Deposition Gas Mixture and Temperature

From Figure 4.1 it can be seen that, as expected, as the reaction temperature was increased, in all cases, the mean percentage pick-up per hour increased.

At 650°C for all of the gas mixtures studied (ethane and synthetic natural gas with or without hydrogen) the mean percentage pick up per hour was almost negligible ranging from - 2.97 % for synthetic natural gas to 5.54 % for ethane. This low rate of carbon deposition was mainly due to the low carbon deposition temperature of 650°C, however it can also be seen from Figures 4.15, 4.19, 4.23 and 4.27 that the type of carbon deposited for all of the samples reacted at 650°C was filamentous in nature.

These carbon nanofilaments were shown to consist of spherical deposits of masses of carbon nanofilaments both for the ethane and the ethane with hydrogen, with wisps of “cobweb-like” fine carbon nanofibres for the synthetic natural gas and clusters of relatively large diameter carbon filaments for the synthetic natural gas with hydrogen. It is therefore worth noting that at 650°C with all of the gas mixtures the type of carbon deposited was almost entirely filamentous in nature and Figure 4.41 shows a TEM micrograph of such a filamentous carbon deposit which was produced from the interaction of ethane with nickel at 650°C, this appears to be tubular in nature in that it seems to have a hollow core, and is approximately 55 nm in diameter. When hydrogen was added to the ethane gas feed, again the TEM micrographs showed that filamentous carbon was catalytically deposited, Figure 4.45 (a) showed a large diameter (> 200 nm) filamentous carbon deposit and (b) very narrow carbon nanotubes, approximately 10 nm in diameter.

When the temperature was increased to 700°C there was an increase in the rate of carbon deposition (mean percentage pick-up per hour) for all of the deposition gas compositions (Figure 4.1). A table showing the mean percentage pick-up per hour change from 650°C to 700°C is shown in Table 4.4.

From the data shown in Table 4.4 it can be seen that the mean percentage pick-up per hour increase from 650°C to 700°C is between 2 and 3 % for all of the gas mixtures except the ethane plus hydrogen where the observed increase in mean percentage

pick-up per hour is ca. 10 %. For all of the samples carried out at 700°C the main type of carbon deposited was, as was shown for the reactions at 650°C, filamentous in nature (Figures 4.16, 4.20, 4.24 and 4.28), although in the case of the ethane and synthetic natural gas plus hydrogen (Figures 4.16 and 4.28 respectively) it was evident that there were now some areas of encapsulation forming and it was this type of carbon that has been reported [8, 49] to be capable of encapsulating the nickel catalyst particles and preventing further carbon deposition. Figure 4.42 shows a TEM micrograph of carbon deposits that were formed from the interaction of ethane with nickel at 700°C, here there was a mixture of both narrow carbon nanotubes (shown) and large clusters of encapsulated nickel particles (not shown). For ethane plus hydrogen at 700°C (Figure 4.46) there were large diameter carbon deposits in excess of 1 µm in diameter growing alongside carbon nanofibres which were approximately 70 nm in diameter.

For the ethane and the ethane plus hydrogen the mean percentage pick-up per hour was shown (Figure 4.1) to increase almost linearly when the temperature was increased from 700°C through 750°C to 800°C, a table of the results obtained is shown in Table 4.4.

It can be seen from the SEM images in Figures 4.17, 4.18, 4.25 and 4.26 that as the temperature was increased to 750°C and 800°C the ratio of encapsulation to filamentous carbon increased. Figure 4.43 shows a catalytically deposited cluster which consists of encapsulated nickel particles with carbon nanofilaments growing off

from it, this was produced from the interaction of ethane with nickel at 750°C, with ethane plus hydrogen at 750°C the TEM micrographs shown in Figure 4.47 showed clusters of carbon encapsulated nickel particles. For ethane at 800°C the TEM micrographs shown in Figure 4.44 show large carbon encapsulated nickel particles (b) as well as large diameter carbon nanofibres which have entrained particles of nickel within their structure (a), at 800°C with ethane and hydrogen (Figure 4.48) the TEM micrographs showed a single carbon nanofibre growing off from a single nickel particle. Although this type of filamentous carbon was being formed, the majority of the carbon deposited was encapsulation.

This shift in the formation of filamentous carbon to encapsulation, as the temperature was increased, agrees with the literature [8, 49, 55]. The results discussed also showed that the addition of 20 vol. % hydrogen to the ethane gas mixture increased the mean percentage pick-up per hour, this could be due to the hydrogen causing the catalytic gasification of the deposited carbon at the metal carbon interface, this hypothesis is also stated in the literature [7, 45, 72], and it is well known that the catalytic gasification of carbon with hydrogen takes place in the presence of nickel at elevated temperatures [95, 96]. If this was the case then the hydrogen will in effect be keeping the surface of the nickel metal catalyst exposed to the gas feed and therefore enabling the continued catalytic deposition of carbon, whereas for the ethane without hydrogen the catalytically deposited carbon could start to form a crust of graphitic carbon around the nickel catalyst particle

and this would prevent the gas feed from coming into contact with the metallic nickel thus slowing and eventually preventing the continued deposition of carbon.

In order to try to determine the effect of hydrogen induced gasification of carbon TGA-MS experiments were carried out on two samples, one which had been densified in ethane plus hydrogen at 650°C for 3 hours to yield a low carbon deposition rate of 1.76 % PU/h (entitled “low carbon deposition” – Figure 4.9) and one which had been densified in ethane plus hydrogen at 800°C for 3 hours to yield a high carbon deposition rate of 75.22 % PU/h (entitled “high carbon deposition” – Figure 4.10).

The low carbon deposition sample showed, apart from the loss of adsorbed water, no significant weight loss on heating to 750°C in nitrogen. Once at 750°C and the hydrogen was introduced the TGA data showed that there was a relatively low percentage weight loss of 6.1 % giving a total percentage weight loss of 12.2 % over the entire reaction.

The MS data showed that there was a percentage weight loss due to an increase in the concentration of water vapour when the hydrogen was introduced. Again, as was shown in the blank run (Figure 4.5) this was likely to be due to a gas phase reaction of trace oxygen with hydrogen, although there could also be the loss of an oxide layer which could have formed on the nickel surface, as outlined in Equation 4.2 (b), however, the overall contribution from this reaction was likely to be a small. There was also a small increase in the concentration of CH_3^+ and ethane and propane

indicative ions, this was due to the catalytic gasification of the carbon by hydrogen (Equation 4.1) and the maximum rate of this gasification in grams of carbon lost per gram of catalyst per minute whilst at 750°C for 30 min was $0.012 \text{ g g}^{-1}_{\text{cat}} \text{ min}^{-1}$. The XRD pattern for the low carbon deposition carbon fibre mat shown in Figure 4.11 D, showed that there was only nickel and carbon present in the sample. It also showed that the carbon d_{002} peak at $26.6^\circ 2\theta$ had narrowed and shifted slightly to a higher 2θ ; this indicated that the catalytically deposited carbon was more graphitic than the relatively amorphous carbon of the carbon fibres from the carbon fibre mat.

The high carbon deposition sample also showed little percentage weight loss up to 750°C (6.4 %) and again this was due to the loss of adsorbed water, see Figure 4.10.

The weight loss under hydrogen was 53.6 % due to increases in the concentration of water vapour, oxygen and carbon dioxide, again through gas phase reactions and the loss of a possible oxide layer from the surface of the nickel. However, upon the introduction of hydrogen there was also a small increase in concentration of CH_3^+ and ethane indicative ions, this was due to the catalytic gasification of the carbon by the hydrogen (Equation 4.1), the maximum rate of this gasification in grams of carbon lost per gram of catalyst per minute whilst at 750°C for 30 min was $0.090 \text{ g g}^{-1}_{\text{cat}} \text{ min}^{-1}$. There is also a very small increase in the concentration of nitrogen dioxide; this was likely to be due to the reaction of oxygen atoms with nitrogen.

This increase in the rate of gasification from $0.012 \text{ g g}^{-1}_{\text{cat}} \text{ min}^{-1}$, for a sample with a low amount of carbon deposited on it, to $0.090 \text{ g g}^{-1}_{\text{cat}} \text{ min}^{-1}$, for a sample with a high amount of carbon deposited on it, indicates that the predominance of the gasification reaction over the competing deposition reaction increases as the reaction proceeds. This indicates that there is likely to be an optimum deposition time during which the carbon deposition reaction is dominant, and by determining this, reactions could be tailored to give the best rate of carbon deposition in the shortest time, thereby optimising the reaction parameters.

The XRD pattern for the high carbon deposition carbon fibre mat shown in Figure 4.11 E, showed that once again there was only nickel and carbon present in the sample. It also showed that the carbon d_{002} peak at $26.6^\circ 2\theta$ had narrowed and significantly increased in intensity when compared to the low carbon deposition sample, the peak had also shifted slightly to a higher 2θ ; this narrowing and shifting of the peak was due to the increase in catalytically deposited carbon on the sample and indicated that the catalytically deposited carbon was much more graphitic than the relatively amorphous carbon of the carbon fibres from the carbon fibre mat. This sharpening and shifting with an increase in intensity of the d_{002} peak was present in all the carbon fibre mat samples following deposition, with the sharpness and intensity increasing as the amount of catalytically deposited carbon increased.

Although the reactions carried out with ethane as the carbon source showed an almost linear increase in the mean percentage

pick-up per hour from 700 – 800°C, a totally different trend in the mean percentage pick-up per hour was observed for the reactions where synthetic natural gas was used as the carbon source.

For the synthetic natural gas reactions there was an almost negligible increase in the mean percentage pick-up per hour when the temperature was increased from 650°C to 700°C then when the temperature was increased further to 750°C there was a sharp increase in the mean percentage pick-up per hour followed by a levelling off once the temperature was further increased to 800°C, this gave the plots for these reactions a distinctive “s-shape” as can be seen in Figure 4.1. A summary of how the mean percentage pick-up per hour varied with temperature for the reactions carried out in synthetic natural gas with and without hydrogen is shown in Table 4.4.

The results also showed that, in the cases where synthetic natural gas was used as the carbon source, then the addition of hydrogen to the gas mixture had little effect on the rate of catalytic carbon deposition. The SEM images in Figures 4.21, 4.22, 4.29 and 4.30, show that at 750°C and 800°C when synthetic natural gas was used as the carbon source, the type of carbon catalytically deposited was almost all spherical and encapsulating in nature which would be expected due to the increase in the reaction temperature, however the addition of hydrogen to the synthetic natural gas did not have a positive effect upon the mean percentage pick-up per hour as was previously observed for the reactions carried out in ethane, indicating that when the catalytic

deposition of carbon takes place under an atmosphere where synthetic natural gas is used as the carbon source then, at temperatures in excess of 750°C, the nickel catalyst particles quickly become encapsulated and this would suggest that neither the deposition nor gasification of carbon can take place at the nickel surface, however, the rate of deposition is the same as that observed at 750°C therefore the reaction has not been entirely switched off, which could be due to one face of the catalyst particle being responsible for the adsorption of carbon into solution and another face being responsible for the deposition of carbon.

For all of the reactions carried out and discussed previously, there have been two main types of growth mechanism leading to the formation of filamentous carbon:

1. Tip-growth – indicating that the nickel has a low affinity for the carbon fibre support – see Figure 4.48 and
2. Elongation and fragmentation of the catalyst particle – see Figure 4.44.

Although there were areas where carbon filaments were growing off from encapsulated clusters of nickel particles, all of these had either catalyst particles at their tip or entrained catalyst fragments along their length, indicating that no or seldom fibres grew *via* a root growth mechanism.

The catalytic deposition of carbon, and in particular the growth of filamentous carbon, lead to the capability of catalytically deposited carbon to bridge individual fibres from the carbon fibre mat, as highlighted in Table 4.4. However, there was no apparent

trend to suggest whether or not the catalytically deposited carbon would be capable of bridging fibres. The presence of catalytically deposited carbon capable of bridging between fibres is due to the amount of catalytic carbon deposited with higher deposition rates leading to increased bridging, the type of carbon deposited with filamentous carbon being more capable of bridging than encapsulation and the vicinity of neighbouring carbon fibres to the deposited carbon.

The third type of commonly deposited carbon was encapsulation, whereby the nickel catalyst became encapsulated with a shell of carbon, there are two mechanisms for the production of this type of carbon, one whereby the catalyst particle changes shape but has a constant volume and the other whereby the catalyst spreads and decreases in volume and size, examples of encapsulated nickel catalyst particles are shown in Figures 4.43, 4.44 and 4.47.

4.3.3.2. Effect of Hydrogen Addition

The graph in Figure 4.2 shows two somewhat different trends for nickel impregnated carbon fibre mats which had been densified in either ethane with varying concentrations of hydrogen or synthetic natural gas with varying concentrations of hydrogen at 750°C for 3 hours. A tabular representation of the data shown in Figure 4.2 is shown in Table 4.5. From this it can be seen that if the volume percent hydrogen was increased from 0 vol. % to 80 vol. %, then, with the balance ethane, the mean percentage pick-up per hour remained virtually constant at 31 ± 5 %, whereas when the balance was synthetic natural gas then the mean percentage pick-

up per hour stayed almost constant with the addition of only 20 vol. % hydrogen then fell off sharply with further increases in the hydrogen concentration to a low mean percentage pick-up per hour of 0.28 % with 80 vol. % hydrogen.

For the reaction carried out with ethane as the carbon source then the almost constant mean percentage pick-up per hour seen with increasing hydrogen concentration was mirrored by the results shown in the SEM images in Figures 4.17, 4.25 and 4.31 – 4.33. These images showed that the type of carbon deposited varied little as the ratio of hydrogen to ethane was increased, in all cases there was a mixture of filamentous carbon and encapsulation, although as the volume percent of hydrogen was increased to 80 vol. % the trend in the graph showed that the mean percentage pick-up per hour may be starting to fall off, this was coupled with a slight increase in the amount of filamentous carbon present in the sample, Figure 4.33.

This showed that the effect of adding a significant amount of hydrogen to the ethane gas feed (80 vol. %) had little effect both upon the type of carbon formed or the rate of carbon deposition, and although it could be inferred from this data that the hydrogen was keeping the catalyst surface clean and allowing extended carbon deposition, this is not supported, as the highest mean percentage pick-up per hour was recorded when no hydrogen was added to the gas feed.

For the reaction carried out with synthetic natural gas as the carbon source there was a significant and marked decrease in the

mean percentage pick up per hour when the volume percent hydrogen was greater than 20 vol. %. This decrease in the mean percentage pick-up per hour was almost linear when the volume percent hydrogen was increased from 40 – 80 vol. %, this was likely to be due to a decrease in concentration of the hydrocarbon species in contact with the nickel metal catalyst particles through dilution with hydrogen of the synthetic natural gas (mainly methane) at the catalyst surface, this was not seen with the ethane, but this would be expected, as the ethane is more reactive than the synthetic natural gas, if ethane was used as opposed to synthetic natural gas then the dilution effect, by hydrogen, at the catalyst surface would have a smaller effect upon the rate of carbon deposition.

However, the carbon deposition for the synthetic natural gas feed was less than half that of the ethane gas feed, thus suggesting that the decrease in the mean percentage pick-up per hour was due to something other than the dilution of the hydrocarbon gas feed with hydrogen, one explanation for this could be the type of carbon being formed for the synthetic natural gas with increasing hydrogen concentrations in the gas feed (Figures 4.21, 4.29 and 4.34 – 4.36), it can be seen that as the amount of hydrogen was increased then the amount of filamentous carbon catalytically deposited also increased, whereas for the ethane the ratio of filamentous to encapsulation varied little with increasing hydrogen concentration.

This indicated that the highest mean percentage pick-up per hour rates were achieved when the majority of the catalytically

deposited carbon was either in the form of encapsulation or a mixture between encapsulation and filamentous, as opposed to filamentous carbon alone. This would oppose the theory that encapsulation deactivates the nickel catalyst, however for all of the reactions carried out so far the reaction time has only been 3 hours, therefore to investigate whether the catalyst becomes deactivated with longer catalytic carbon deposition times and the role that the addition of 20 vol. % hydrogen could play in the activation / deactivation of the catalyst, reactions were carried out over 12 hour periods with intermittent weighing of the samples, using ethane and ethane plus hydrogen as the gas feedstocks at 750°C and 800°C, the results obtained for these reactions are discussed in the following section.

4.3.3.3. Effect of Deposition Time

In order to try to show whether the addition of hydrogen to the gas feed could increase the activation time of the catalyst by causing gasification of the catalytically deposited carbon at the nickel metal surface, experiments were carried over 12 hours in ethane with and without hydrogen at 750°C and 800°C. The results obtained are shown graphically in Figures 4.3 and 4.4.

Figure 4.3 showed that, for the reaction carried out at 750°C, the addition of hydrogen (20 vol. %) initially (in the first 3 hours) increased the percentage pick-up per hour dramatically over ethane alone. However, as the reaction proceeded through 6, 9 and 12 hours then in both cases (with and without hydrogen) the percentage pick-up per hour decreased steadily from a value of

28.0 % from 0 – 3 hours to 4.6 % from 9 – 12 hours for the ethane and from 45.3 % to 3.0 % over the same time periods for the ethane plus hydrogen. The results obtained are outlined in Table 4.8, and the average percentage pick-up per hour rates for both gas mixtures over the 12 hour deposition are shown in Table 4.6.

<u>Deposition Time (h)</u>	<u>Percentage Pick-up per Hour (%)</u>	
	<u>Ethane</u>	<u>Ethane + Hydrogen</u>
3	28.00	45.27
6	14.17	16.66
9	7.16	6.66
12	4.61	2.97

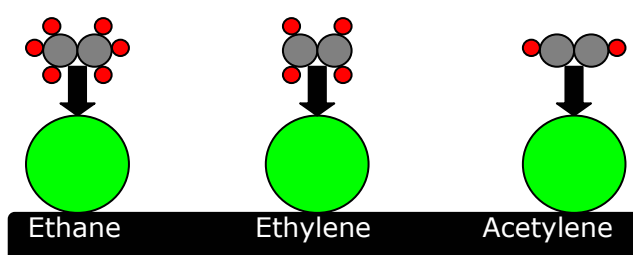
Table 4.8: Change in percentage pick-up per hour with increasing deposition time for ethane with and without hydrogen at 750°C over 12 hours.

The results showed that although the addition of hydrogen can initially increase the activity of the catalyst, over time the initial hydrogen induced increase in activity was lost and with or without hydrogen at 750°C the activity of the nickel catalyst was significantly reduced over a period of 12 hours, this loss in activity was likely due to the catalytically deposited carbon forming a shell around the nickel catalyst particles and preventing further catalytic carbon deposition, the observed loss in activity is contradictory to statements in the literature [7, 45, 72, 74] which states that the presence of hydrogen can induce carbon deposition and also extend catalyst lifetime.

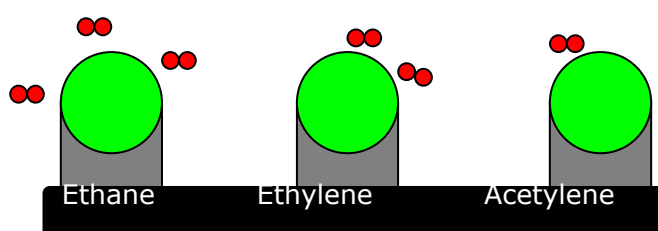
The reported work in the literature however, involves using unsaturated hydrocarbons (i.e. ethylene and acetylene) as the

carbon precursors, which when catalytically decomposed to form solid carbon and hydrogen are only capable of releasing low concentrations of hydrogen when compared to saturated hydrocarbons, therefore by using alkane gas feedstocks i.e. ethane, the concentration of hydrogen at the catalyst surface following the catalytic decomposition of the hydrocarbon will be greater when compared to using unsaturated hydrocarbons, as illustrated in Figure 4.49.

Key:  = Carbon atom;  = Hydrogen atom;
 = Hydrogen molecule;  = Nickel catalyst particle



(a) Adsorption of hydrocarbon on nickel surface



(b) Decomposition of hydrocarbon and deposition of carbon

Figure 4.49: Schematic illustration of the decomposition of ethane, ethylene and acetylene to form solid carbon and hydrogen over a nickel catalyst supported on a carbon fibre.

The SEM images in Figures 4.37 and 4.38 showed that the mass of catalytically deposited carbon after 12 hours of carbon deposition

at 750°C in ethane (Figure 4.37) and in ethane plus hydrogen (Figure 4.38) was much greater than over a 3 hour deposition. They also showed that, after 12 hours, in both cases the catalytically deposited carbon was forming large masses which seemed to be made up (at least on the surface) of large diameter (up to 1 μm) filamentous carbon which were now bridging several fibres over relatively large distances and, in particular for the ethane plus hydrogen (Figure 4.38 (a)), it could be seen that the catalytically deposited carbon had formed what appeared to be a solid layer of carbon over the top surface of the carbon fibre mat, this could reduce the rate of carbon deposition by blocking diffusion of the gas feedstock, however, this indicated that the use of a catalyst for the deposition of carbon could potentially be used for the formation of carbon-carbon composites.

For the reactions carried out at 800°C over 12 hours (Figure 4.4) the percentage pick-up per hour for both the ethane with and without hydrogen varied little as the reaction proceeded. In both cases there was an initial high percentage pick-up per hour after 2 hours followed by a sharp drop after 4 hours then a levelling off through 6 and 8 hours and up to 12 hours. The results obtained are shown in Table 4.9 and the average percentage pick-up per hour rates for both gas mixtures over the entire 12 hour deposition are shown in Table 4.6.

<u>Deposition Time (h)</u>	<u>Percentage Pick-up per Hour (%)</u>	
	<u>Ethane</u>	<u>Ethane + Hydrogen</u>
2	91.49	92.78
4	16.72	24.87
6	8.57	10.78
8	6.10	9.04
12	3.30	3.34

Table 4.9: Change in percentage pick-up per hour with increasing deposition time for ethane with and without hydrogen at 800°C over 12 hours.

These results showed that, as previously stated, the addition of hydrogen to the gas feed does not increase the activity of or extend the lifetime of the nickel catalyst to any significant extent over extended carbon deposition time periods of up to 12 hours, which again disagrees with the literature and can be described by the relatively high yield of hydrogen released at the catalyst surface when saturated hydrocarbons are used as the carbon precursor as opposed to unsaturated hydrocarbons (Figure 4.49).

Again, the SEM images (Figures 4.39 and 4.40) showed that the catalytically deposited carbon was capable of forming large deposits which could bridge and bind together several carbon fibres from the carbon fibre mat. In this case, however, the catalytically deposited carbon seemed to be more spherical and graphitic in nature than the previously filamentous deposits observed at 750°C, this was only to be expected, as it is known and has been shown previously, that as the temperature increases the amount of filamentous

carbon produced decreases. Yet again the formation of catalytically deposited carbon which is capable of bridging and binding fibres together indicated that the use of a nickel catalyst could possibly be employed in the formation of carbon-carbon composites.

4.4 Summary

The results presented and discussed in this chapter have shown that following impregnation of the carbon fibre mats with nickel nitrate the carbon fibres from the mat act as a reductant to reduce the nickel nitrate hexahydrate to nickel prior to the introduction of the deposition gas feedstock.

Following catalytic carbon deposition it was shown that increasing the reaction temperature increases the rate of reaction and that reactions carried out in ethane yield a higher mean percentage pick-up per hour than the reactions carried out in synthetic natural gas. This is due to the ethane gas being more reactive than the synthetic natural gas which mainly consists of methane.

It was also shown that increasing the hydrogen concentration in the gas feed from 20 vol. % to 80 vol. % had a significantly detrimental effect upon the rate of carbon deposition for the reactions where synthetic natural gas was the carbon source whereas the same increase in concentration had a much less marked effect upon the rate of carbon deposition for the samples in which ethane was the carbon source.

It was also found that by adding 20 vol. % hydrogen to the gas feed then the initial rate of carbon deposition could be increased, however, it was also discovered that the addition of the 20 vol. % of hydrogen was not capable of significantly extending the lifetime of the nickel catalyst.

The type of carbon deposited was also found to change as the reaction temperature was increased with a shift from the formation of filamentous carbon at lower temperatures (650°C) to the formations of graphitic encapsulating carbon at higher temperatures (800°C), and the addition of hydrogen to the gas mixture was also found to have a minor role in increasing the ratio of filamentous to encapsulating carbon, however, TEM showed that for the reactions carried out in ethane with or without hydrogen there was always a mixture in the type of carbon deposited at all of the reaction temperatures studied.

5 Carbon Deposition on Carbon Fibre Preforms

5.1 Introduction

This chapter presents results obtained using carbon fibre preforms which have been densified in an isothermal, isobaric induction furnace, using methane or synthetic natural gas at temperatures ranging from 650 – 1150°C for 12 and 24 total hour densification times either with or without a nickel catalyst present. The samples have been characterised using XRD, SEM, PLM, digital photography and from mass change results. The results are then discussed putting them into context with the published literature.

5.2 Results

5.2.1. Non-Catalytic Carbon Deposition

5.2.1.1. Temperature Profile

Prior to densification of the carbon fibre preforms (50 mm dia. x 30 mm thk.) using an isothermal isobaric induction furnace, a carbon fibre preform was placed into the furnace and heated to 1150°C under nitrogen with thermocouples placed at (1) the centre of the preform (this was used to control the temperature); (2) 1 cm from the outer edge of the preform and (3) approximately 1 cm to the side of the preform in the gas stream, the results obtained are shown in Figure 5.1. The graph showed that the temperature of the preform was constant across the diameter of the preform and that

the temperature of the gas stream also remained constant, although at a slightly lower temperature than the preform itself. The graph also showed that the preform took 10 minutes to reach the operating temperature specified (1150°C).

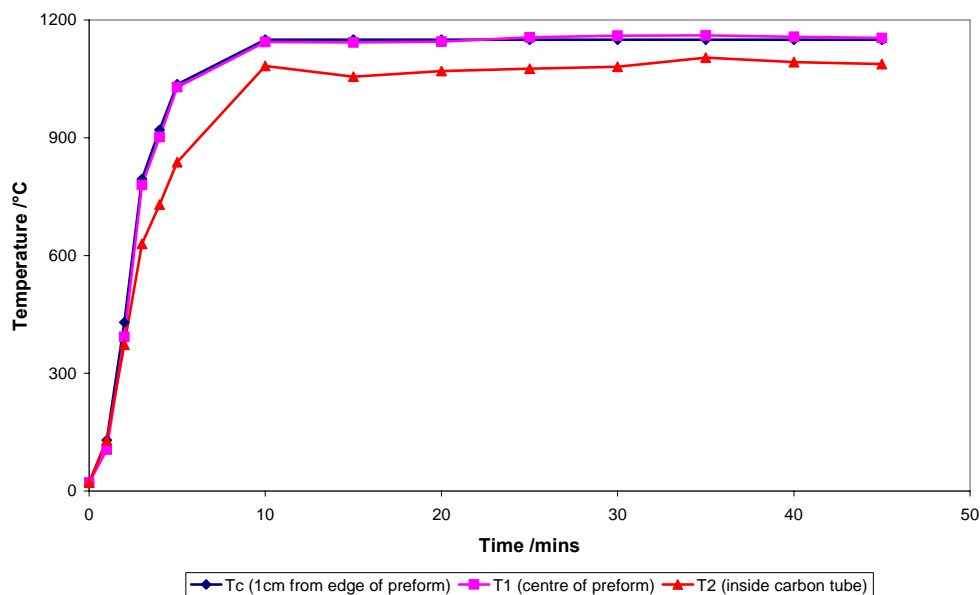


Figure 5.1: Temperature profile for isothermal induction heating of a carbon preform to 1150°C in nitrogen.

5.2.1.2. XRD

XRD of the as received carbon fibre preforms gave a very weak graphite pattern with peak positions corresponding to those observed for the as received carbon fibre mat, Figure 4.11 A.

5.2.1.3. Effects of Densification Time, Temperature and Gas Feedstock

The following graphs (Figure 5.2 and Figure 5.3) show the percentage pick-up per hour deposition rates for the densification of carbon fibre preforms in methane and synthetic natural gas over periods of 24 and 12 hours respectively. The reactions carried out in methane were only carried out once due to time constraints

whereas the reactions carried out in synthetic natural gas were repeated three times at each temperature to provide a more robust set of results which could be compared to the reactions carried out with a catalyst present in synthetic natural gas both with the carbon fibre preforms and the carbon fibre mats, however these were only carried out over a period of 12 hours, again due to time constraints.

Figure 5.2 shows the change in percentage pick-up per hour with time for carbon fibre preforms which have been densified in methane at 950, 1050 and 1150°C for 24 hours. A table of the data used to compile the graphs (Figures 5.2 and 5.3) is shown in Appendix 2

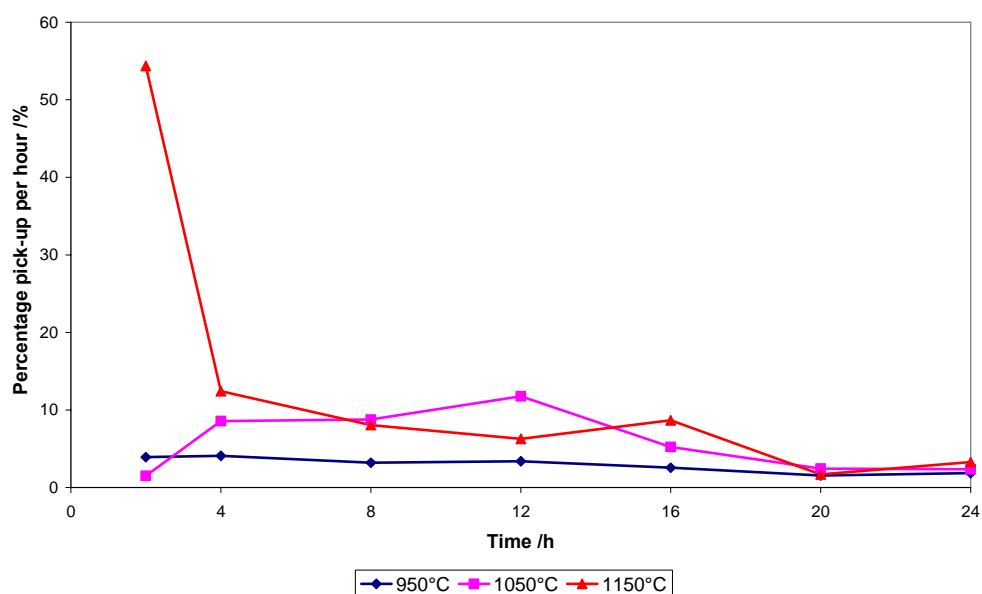


Figure 5.2: Percentage pick-up per hour rates for carbon fibre preforms densified in methane.

Figure 5.3 shows the change in mean percentage pick-up per hour with time for carbon fibre preforms which have been densified in synthetic natural gas at 950, 1050 and 1150°C for 12 hours.

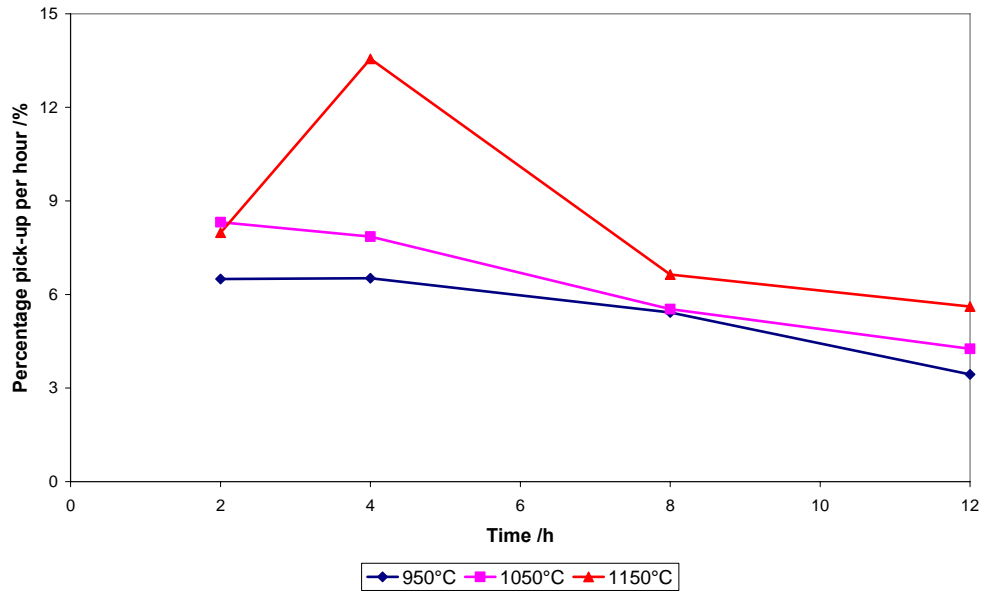


Figure 5.3: Percentage pick-up per hour rates for carbon fibre preforms densified in synthetic natural gas.

5.2.1.4. PLM

PLM was used to determine the microstructure of the deposited carbon. In order to do this the amount of carbon deposited needed to be great enough to be distinguishable under the microscope after grinding and polishing. For these reasons it was only possible to observe the samples that were densified for 24 hours under the optical microscope, the samples that were densified over 12 hour periods did not have appreciable amounts of carbon deposited on them and was not possible to determine the carbon deposited from the resin, this was also the case for the sample densified at 950°C over 24 hours.

Images showing the different microstructures observed (rough laminar, smooth laminar and isotropic) are shown in Figure 5.4.

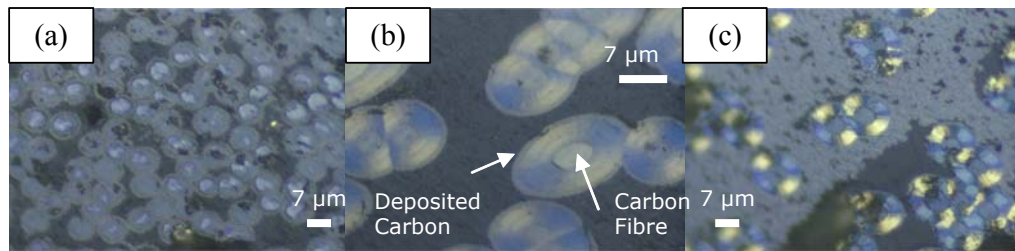


Figure 5.4: PLM images showing the three types of microstructure observed. (a) isotropic - from reaction with methane at 1150°C; (b) smooth laminar - from reaction with methane at 1150°C and (c) rough laminar - from reaction with methane at 1050°C. In all cases the diameter of the carbon fibre is 7 µm.

5.2.1.5. Digital Photography

Digital photographs of the carbon fibre preform following densification in methane at 1150°C for 24 hours are shown in Figure 5.5. These show how deposited carbon can build up on the outer surfaces of the preform and potentially block the internal pores of the preform to further carbon deposition, illustrating the need, during the manufacture of carbon-carbon composites, for the removal of these surface deposits.

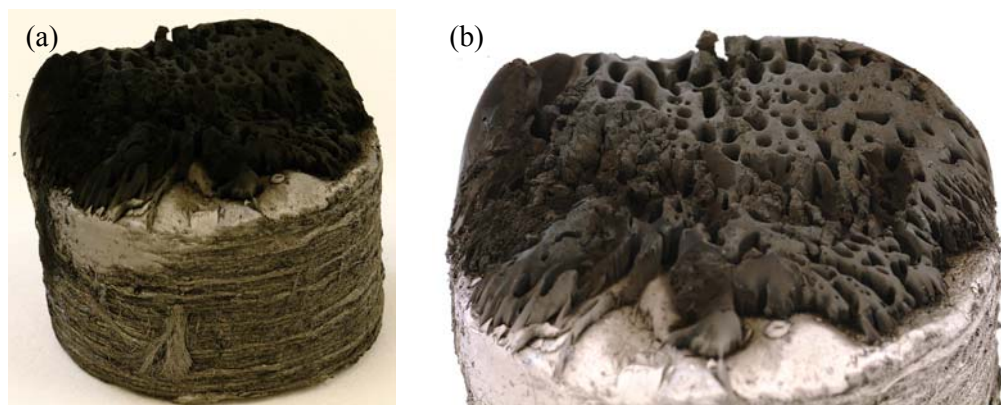


Figure 5.5: Digital photographs of a carbon fibre preform following densification in methane at 1150°C for 24 hours (preform dimensions are 50 mm in diameter and 30 mm in depth).

5.2.2. Catalytic Carbon Deposition

5.2.2.1. Effects of Densification Temperature and Gas Flow Rate

In order to introduce the catalyst into the carbon fibre preforms, a methanolic solution of nickel nitrate hexahydrate was injected into the centre section of the preforms to yield 1 wt. % nickel (detailed in Chapter 3). The samples were densified using the isobaric, isothermal induction furnace over 12 hour total densification times, at temperatures of 650, 700, 750 and 800°C, using synthetic natural gas as the feedstock. The results obtained are shown in Figure 5.6 (a table of data used to compile Figure 5.6 is given in Appendix 3).

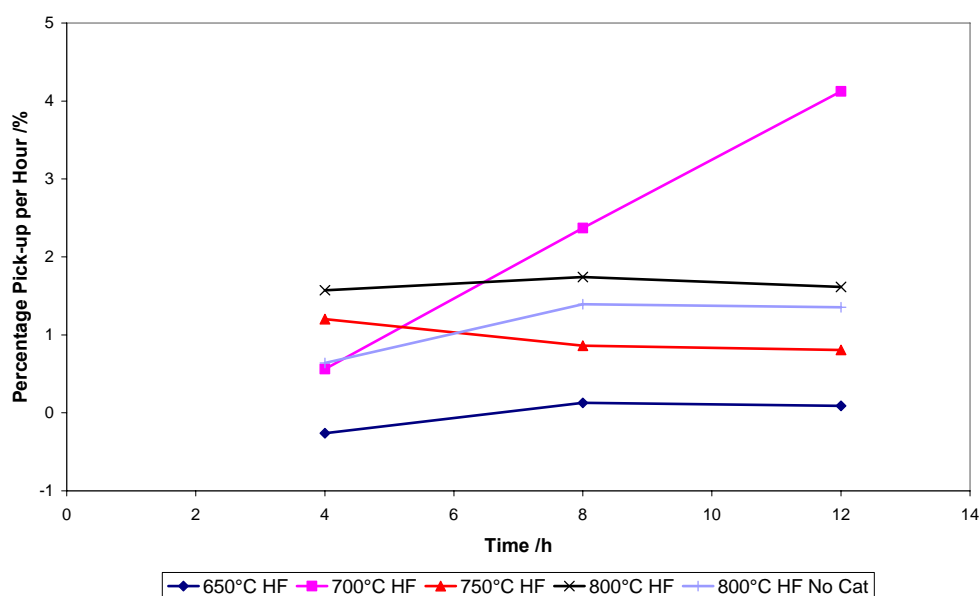


Figure 5.6: Percentage pick-up per hour rates for carbon preforms impregnated with nominally 1 wt. % nickel (except for 800°C HF No Cat. which was densified without a catalyst present) densified at different temperatures ($HF = 1.5 \text{ dm}^3 \text{ min}^{-1}$).

Figure 5.6 shows that when the temperature was increased from 650°C to 750°C and then to 800°C the rate of carbon

deposition increased as the temperature increased but did not vary significantly with reaction time, with only the reaction carried out at 800°C yielding a higher percentage pick-up per hour than the reaction carried out without a catalyst present. At 700°C the rate of carbon deposition was seen to increase linearly as the densification time increased, and after 12 hours the rate was nearly 3 times greater than that observed for the reaction carried out at 800°C.

5.2.2.2. SEM

Prior to SEM analysis the samples were sectioned by cutting out the central section of the preform, this section was then cut into four more sections (top, middle-top, middle-bottom and bottom) so that each section was of a suitable size to be imaged using the SEM, a schematic diagram illustrating which section originated from which part of the preform is shown in Figure 5.7. For all the densification conditions investigated, the SEM images showed the same trends, so, for ease of explanation, only the SEM images for one sample are shown, this sample was densified in synthetic natural gas at 800°C for 12 hours.

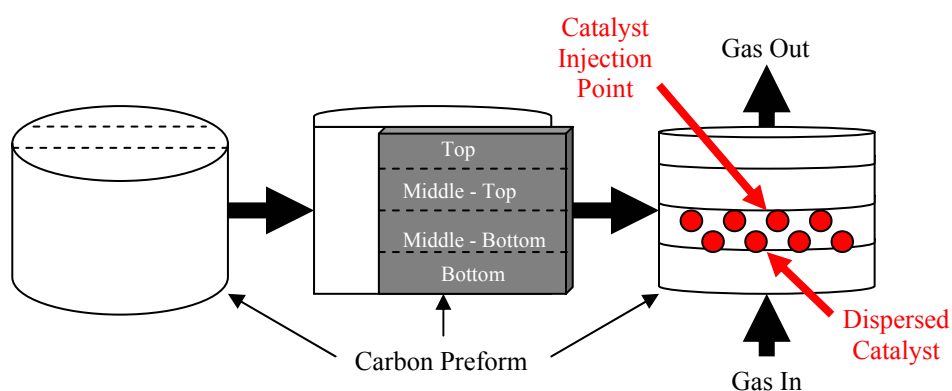


Figure 5.7: Schematic illustration detailing the sections of the preform used for SEM analysis.

The SEM images for each section of the carbon fibre preform densified in synthetic natural gas at 800°C with a 1wt. % nickel loading are shown in Figure 5.8.

Figure 5.8 (a) and (b) show images of the top section of the preform, these images show that in the upper quarter of the preform there were large deposits of carbon, these deposits were mainly filamentous in nature, and formed tight bundles and clusters in between fibres from the preform.

Figure 5.8 (c) and (d) show images of the upper middle section of the preform, these images show that in this section there was no carbon deposition and the fibre surfaces were clean and smooth.

Figure 5.8 (e) and (f) show images of the lower middle section of the preform, these images show deposits of carbon in and amongst the fibres from the preform, the deposits were still quite sparse but were also filamentous in nature.

Figure 5.8 (g) and (h) show images of the bottom section of the preform, here the images show wide spread dense deposits of carbon, which were globular in nature and consisted mainly of filamentous carbon deposits bundled together.

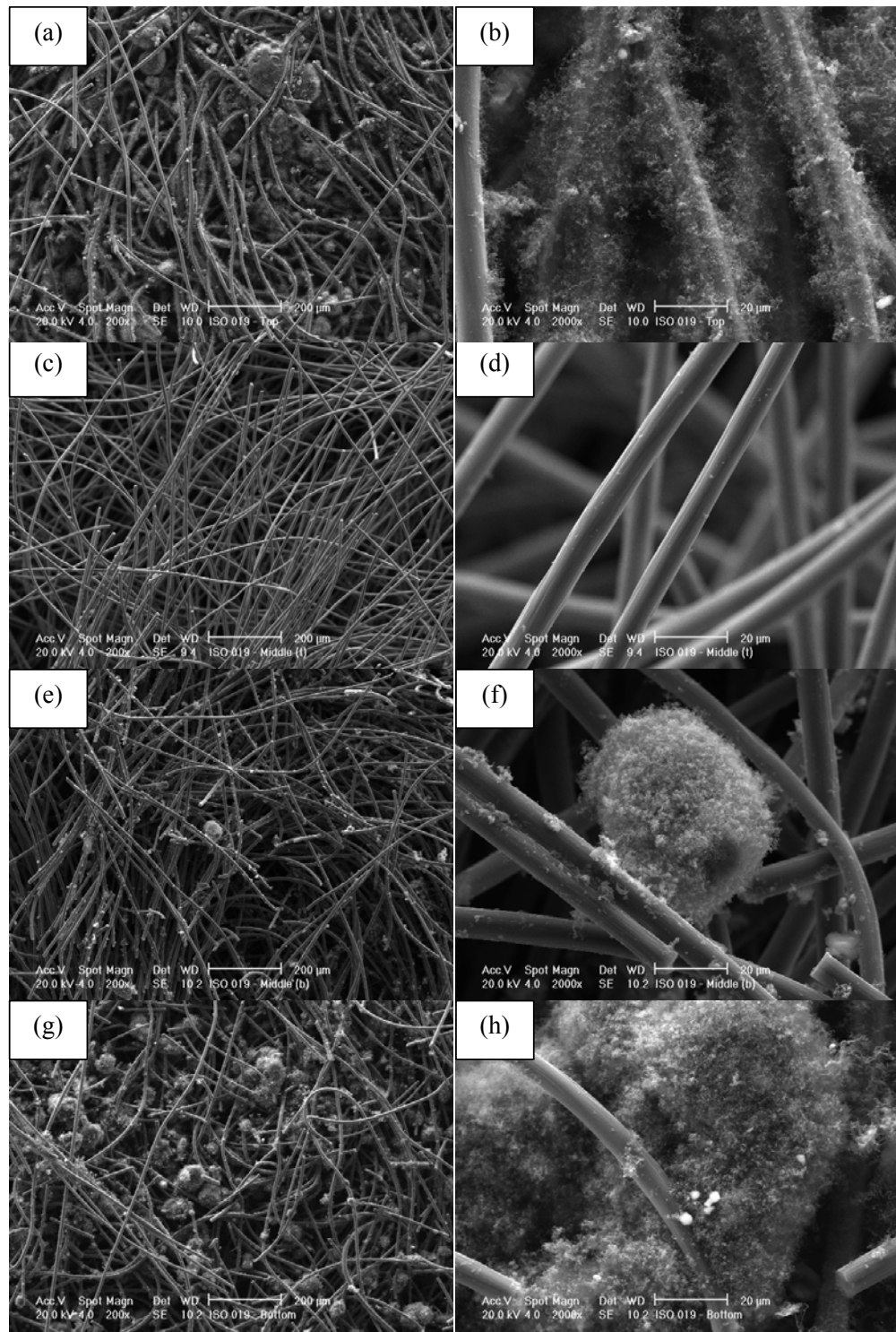


Figure 5.8: SEM Images for a carbon preform sample after densification in synthetic natural gas at 800°C for 12 hours with a 1 wt. % nickel loading. (a) and (b) top section; (c) and (d) middle-top section; (e) and (f) middle-bottom sections; (g) and (h) bottom section.

5.3 Discussion

5.3.1. Non-Catalytic Carbon Deposition

Prior to carbon deposition experiments it was confirmed that the preform was isothermally heated, Figure 5.1, and XRD showed that, as was the case with the carbon fibre mat, the carbon fibre preform was amorphous in nature but had a very weak graphite phase, as confirmed by the broadness of the graphite peaks at 26.6 and $44.7^\circ 2\theta$.

5.3.1.1. Effects of Densification Time, Temperature and Gas Feedstock

For the reactions carried out in methane over 24 hours (Figure 5.2) it can be seen that as the temperature was increased the rate of carbon deposition increased, although there were no significant distinctions between the rates of deposition between 4 and 24 hours for each of the temperatures investigated. However, after only 2 hours of deposition, whilst the rates were comparable for the reactions carried out at 950 and 1050°C , there was a high initial rate of carbon deposition for the experiment carried out at 1150°C .

For the experiments carried out over 12 hours with synthetic natural gas (Figure 5.3) it can be seen that for the reactions carried out at 950°C and 1050°C , there was a gradual decrease in the percentage pick-up per hour as the reaction time increased, whereas at 1150°C there was a small increase in the percentage pick-up per hour again followed by a gradual decrease as the reaction proceeded. As found for the reactions carried out in

methane as the temperature of reaction was increased the rate of carbon deposition increased.

At 950°C the deposition rate for the reaction with methane (Figure 5.2) does not decrease steadily with a rate of ca. 3.2 % being maintained from 8-12 hours, however, for the reaction carried out in synthetic natural gas (Figure 5.3), the deposition rate reduced much more rapidly, this could be due to the build up of surface deposits, similar to those shown in Figure 5.5, which would block the internal porosity of the preform to further deposition and therefore reduce the rate of deposition.

At 1050°C, for the reaction carried out in methane (Figure 5.2), the deposition rate increased from ca. 1.5 % to a maximum of ca. 12 %, after 12 hours of processing, the rate then reduced steadily with further processing to 2 % after 24 hours. For the reaction carried out in synthetic natural gas (Figure 5.3) the rate, as at 950°C, was shown to reduce steadily with increasing processing time.

At 1150°C, the reaction carried out in methane (Figure 5.2) showed the deposition rate to start high at 55 % after 2 hours before falling off rapidly after 4 hours to ca. 12 % followed by a steady decrease to ca. 4 % after 24 hours. For the reaction carried out in synthetic natural gas (Figure 5.3) the rate started low at 8 %, followed by an increase before steadily falling off, the rates of deposition for both the methane and the synthetic natural gas were comparable from 4 to 12 hours.

Although it might be expected that the rate of densification would be greater for the reactions carried out in synthetic natural gas as opposed to those carried out in methane due to the presence of the more reactive ethane and propane, this was not found to be the case throughout the entirety of the reactions investigated. For the reactions carried out at 950°C and 1050°C the initial rates of deposition were higher for the synthetic natural gas than the methane, however in both cases the rate of reaction declined much quicker for the synthetic natural gas than the methane as the processing time was increased. At 1150°C the initially higher rate observed for the methane as opposed to the synthetic natural gas fell off quickly and the rates for the two different gas feedstocks became and remained comparable.

There could be two explanations for the variations between the gas feedstocks, the first is that the synthetic natural gas was reacting *via* a mechanism which favoured the closure of pores (see Figure 5.9), this would reduce the volume and therefore the surface area of the preform leading to a reduction in the rate of carbon deposition. The second, which is in agreement with a series work carried out by Benzinger and Hüttinger [84-86, 97, 98], who concluded that the rate of carbon deposition was affected by the rate of infiltration and the rate of pore filling, is that as methane is a smaller molecule than ethane and propane (which are present in the synthetic natural gas) then methane can infiltrate more readily into the pores of the preform where it can react to deposit carbon. One mole of methane also produces half as many moles of

hydrogen per mole of ethane and a third of the number of moles of hydrogen per mole of propane; therefore, there will be a higher partial pressure of hydrocarbon in the pores of the preform if methane is used as the carbon precursor as opposed to ethane or propane, meaning that there will be a higher concentration of methane, to deposit carbon, within the internal porosity of the preform if methane is used as the gas feedstock.

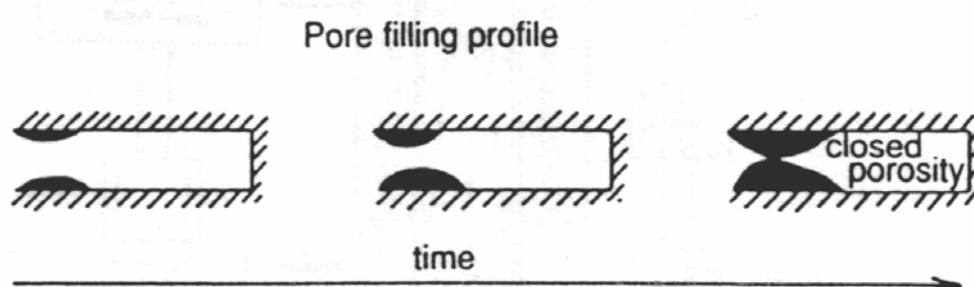


Figure 5.9: Schematic diagram of how the pores within the carbon preform can become closed to further densification.

5.3.1.2. PLM

For the samples densified in methane over 24 hours at 1050°C or 1150°C, sections were taken, mounted in resin and polished before being imaged using PLM. Figure 5.4 shows the different microstructures that were observed in the different samples. For the sample densified in methane at 1150°C over a period of 24 hours two main microstructures were present, the first of these was the isotropic microstructure shown in Figure 5.4 (a), which consisted of a concentric band of deposited carbon around each individual fibre, in this deposited carbon band the surfaces of the lamellar planes of the carbon are parallel or perpendicular to the polished surface and rotation of the sample does not change the

colour observed. The second was the smooth laminar microstructure (Figure 5.4 (b)) in which the yellows and blues observed are due to the exposed prismatic edges of the lamellae carbon planes [1] forming what is known as a “Maltese cross” formation, the rough laminar microstructure also exhibits the same yellow and blue colourations, also due to exposed prismatic edges and Figure 5.4 (c) shows the rough laminar microstructure observed from the reaction of the carbon fibre preform with methane at 1050°C over 24 hours. The presence of a dual microstructure consisting of smooth laminar and isotropic carbon observed following densification in methane at 1150°C is consistent with literature reporting the same observation of a mixture of smooth and isotropic carbon following reaction with propane at 1200°C [6].

5.3.1.3. Digital Photography

The digital photographs, shown in Figure 5.5, show how the deposited carbon can build up on the outer surfaces of the preforms, this can be due to the densification occurring through a closed pore mechanism, as described earlier and shown in Figure 5.9, which closes the internal surfaces of the preform to further densification and the carbon is forced to build up on the outer surfaces of the preform. As is shown the deposited carbon can form a porous structure of soot-like carbon on the outer surface of the preform, this carbon was relatively loose and powdery and was easily removed. However, there was also the formation of a silvery crust of carbon around the edges of the preform and it is this carbon

which was hard and adhered well to the structure of the carbon preform.

5.3.2. Catalytic Carbon Deposition

5.3.2.1. Effects of Densification Temperature and Gas Flow Rate

The plots shown in Figure 5.6 show that for the reactions carried out at 650, 750 and 800°C with a high gas flow rate, the deposition rates remained low and virtually linear over the reaction time of 12 hours. The deposition rate was also seen to increase as the temperature increased, as would be expected, but, as the reaction carried out with no catalyst present had a deposition rate which was comparable to the reactions carried out at 750 and 800°C and greater than the reaction carried out at 650°C, then it was difficult to determine whether the carbon being deposited was *via* a catalytic or pyrolytic reaction pathway.

So, from this it was possible to determine that the presence of 1 wt. % nickel on the preform had little or no effect upon the rate of carbon deposition at 650, 750 and 800°C over 12 hours with synthetic natural gas as the gas feedstock flowing at 1.5 dm³min⁻¹.

This was likely to be due to a poor contact time between the catalyst particles and the gas feed. As the catalyst was located only in the centre sections of the preform the densification gas had to infiltrate through to the inner pores of the preform in order to reach the nickel catalyst particles and as the flow rate was relatively high the gas would be swept away from the catalyst particles before it had time to react and therefore deposit an appreciable amount of

carbon. This was substantiated by the SEM images shown in Figure 5.8, these images showed that that the majority of the catalytically deposited carbon was being deposited on the top and bottom sections of the preform, even though the catalyst was injected into the central sections of the preform, indicating that the synthetic natural gas is incapable of infiltrating the centre sections of the preform, this is likely to be due to the presence of larger hydrocarbons (ethane and propane) which are incapable of infiltrating the pores of the preform and also to the high gas flow rate ($1.5 \text{ dm}^3\text{min}^{-1}$) which would sweep the synthetic natural gas around the outer surfaces of the preform before it had time to infiltrate the pores.

The anomalous result in Figure 5.6 for the reaction carried out at 700°C over 12 hours showed that the percentage pick-up per hour increased linearly as the reaction proceeded. This was different to the other results discussed previously and could be due to a number of different factors. The positioning of the preform and the thermocouple within the furnace was prone to error. It could also be that in this sample the catalyst was injected further into the preform meaning that it was nearer to the bottom of the preform and could more readily come into contact with the gas feedstock, however if these factors were responsible for the anomalous results then it would be expected that the initial percentage pick-up per hour after 4 hours of densification would be higher than for the reactions carried out at 650 , 750 and 800°C and that the linearity observed would not have been a result of poor reproducibility of the

preform and thermocouple placement in the furnace. The linear nature of the rate of deposition at 700°C could however be due to the reaction proceeding at maximum efficiency at this temperature, i.e. there was sufficient heat to allow a significant rate of carbon deposition (as opposed to 650°C) and the reaction was proceeding without pore closure, which would occur at higher temperatures (750 and 800°C).

In all cases the SEM images (Figure 5.8) showed that the type of carbon being catalytically deposited was mainly filamentous in nature, and was more prolific on the outer surfaces of the preform, as opposed to the central sections, with the majority of the carbon being catalytically deposited on the bottom section of the preform. This could be due to a combination of the gas feed coming into contact with the bottom section of the preform first, due to the design of the furnace, and also that the impregnated catalyst had travelled through to the bottom section of the preform after impregnation, through gravity. The lack of catalytic carbon deposits in the central sections of the preform are likely to be due to the lack of hydrocarbon gases within the central sections of the preform as discussed earlier, and the presence of deposits on the top section of the preform could be due to contact between catalyst particles, left there during impregnation or evaporation of the methanol, with the synthetic natural gas as it travels around the outer surfaces of the preform.

The experiments suggest that that the optimum temperature for catalytic densification of a preform, containing 1 wt. % nickel, is

700°C. At 650°C there was almost no catalytic carbon deposition due to the low temperature whereas at 750 and 800°C the rate of carbon deposition was too great which led to the catalytically deposited carbon filling the pores in which the nickel catalyst particles were located therefore preventing further contact between the catalyst and the gas feed, causing the catalytic deposition of carbon to cease.

In all cases the percentage pick-up per hour rates observed for the catalytic reactions carried out with a nickel catalyst present (Figure 5.6) were relatively low and were lower than the observed percentage pick-up per hour rates observed for the reactions carried out in synthetic natural gas without a catalyst present at minimum investigated temperature of 950°C (Figures 5.2 and 5.3). However, if you consider that in the case of the catalyst impregnated preforms the catalyst is only, at best, occupying 40 % of the volume of the preform, therefore if only 40 % of the volume of the preform is contributing to the overall percentage pick-up per hour then, from the results shown in Figure 5.6, the maximum percentage pick-up per hour obtainable, if the whole preform were to contribute to the percentage pick-up per hour, could be over 10 % after 12 hours, which would be achieved using 2.5 wt. % nickel catalyst at 700°C with a flow rate of 1.5 dm³min⁻¹. This is comparable to the results seen for the synthetic natural gas (1.5 dm³min⁻¹) at 1150°C without a catalyst present after 8 hours (Figure 5.3).

This would indicate that the use of a catalyst can improve the rate of carbon deposition for the formation of carbon-carbon composites and may also help eliminate the current industrial manufacturing problems, whereby the preforms need to be systematically removed from the furnace and mechanically ground to remove surface carbon deposits, if the right catalyst loading and temperature is determined. However, in order to make the use of a catalyst in an industrial environment there would need to be a more rigorous and reproducible way of introducing the catalyst into the preform and tests would need to be performed on an industrial scale where the intricacies in charging the furnace are eliminated.

5.4 Summary

This chapter has shown that pyrolytic deposition of carbon can be carried out using an isothermal induction furnace at temperatures of 950, 1050 and 1150°C with methane and synthetic natural gas over periods of 24 and 12 hours respectively, and that the reactivity of the densification gas is not the only factor to influence the rate of carbon deposition, the infiltration rate and pore filling rate also have a significant effect [84-86, 97, 98].

The work has shown that a nickel catalyst can be incorporated into the manufacturing process of carbon-carbon composites and was capable of increasing the rate of carbon deposition and lowering the temperature of deposition, when compared to that currently used in industrial manufacturing processes (> 1000°C), however, there is little work in the literature concerning the use of

catalysts for the catalytic deposition of carbon for the manufacture of carbon-carbon composites [12, 13, 15, 53], and what work there is focuses mainly upon using reactive unsaturated hydrocarbons [12, 13, 15], which would not be a feasible solution on an industrial scale due to costs involved in using expensive reactive gases and rates of infiltration associated with larger hydrocarbon molecules. It has also been stated that the addition of carbon nanotubes to carbon-carbon composites can increase the wear resistance of the composites [99].

6 Conclusions

In conclusion the work presented in this thesis has shown that it was possible to impregnate 3D carbon fibre supports with a methanolic solution of nickel nitrate hexahydrate which then decomposed and reduced to metallic nickel during heating in nitrogen to the predetermined reaction temperature of 650 – 800°C.

Once impregnated with nickel it was shown that it was then possible to catalytically deposit carbon onto and within the internal structure of 3D carbon fibre supports using short straight chain alkanes (synthetic natural gas or ethane) as the gaseous carbon source at temperatures of 650 - 800°C, therefore increasing the mass and density of the support through the addition of carbon, with higher rates of carbon deposition observed as the temperature was increased and also with ethane as the gas feedstock when compared to synthetic natural gas. It has also been shown that the catalytically deposited carbon was capable of bridging carbon fibres of the support, thus forming a composite structure.

The type of carbon deposited varied with reaction temperature and gas mixture, with filamentous carbon (nanofibres and nanotubes) forming at lower temperatures (650 and 700°C) and with the addition of 20 vol. % hydrogen, whilst encapsulation ("shell-like" carbon) was prevalent at higher temperatures (750 and 800°C) and in the absence of added hydrogen.

The addition of hydrogen, from 0 – 80 vol. %, to an ethane gas feedstock at 750°C was shown to have little or no significant affect

upon the rate of carbon deposition, whereas the same addition of hydrogen to a synthetic natural gas feedstock at 750°C significantly reduced the rate of carbon deposition. Using 20 vol. % hydrogen with the balance being ethane at 750 and 800°C showed that the addition of hydrogen to the gas feed did not increase the active lifetime of the catalyst with respect to the catalytic deposition of carbon.

It has also been shown that, by injecting a methanolic solution of nickel nitrate hexahydrate into the centre of a carbon fibre preform support to yield a 1 wt. % nickel loading on the preform, carbon can be catalytically deposited within the preform using synthetic natural gas at 650 - 800°C.

These conclusion show that under the predetermined reaction conditions (20 wt. % nickel catalyst loading and 650 - 800°C) the optimum conditions are a temperature of 800°C, using ethane as the carbon containing gas feedstock with 20 vol. % of added hydrogen with a low total gas flow rate ($0.25 \text{ dm}^3\text{min}^{-1}$), these conditions will yield the highest rate of carbon deposition with almost all of that deposition taking place in the first three hours of deposition.

7 Future Work

Although this thesis has shown how different experimental parameters can affect the rate and type of carbon deposited over nickel, using 3D carbon fibre supports, further work in the area could involve the implementation of different catalysts i.e. iron, cobalt and alloys of these. It would also be interesting to determine the amount of catalyst (wt. %) required to yield a specified carbon deposition rate.

This thesis has also focussed upon using alkane gas feedstocks, as these would be more attractive from an industrial perspective, as industry currently use piped mains natural gas which mainly consists of methane, however an investigation into the affects of using different unsaturated hydrocarbons e.g. ethylene, acetylene, propylene, as well as some aromatic and polyaromatic carbon precursors i.e. benzene and naphthalene, with and without the addition of hydrogen, upon the rate and type of carbon deposited within 3D carbon fibre supports would be interesting, as would an optimisation of the gas flow rate, although this thesis has shown that a low gas flow rate is preferred to a high gas flow rate in order to increase the contact time between the catalyst and the gas, in order to determine an optimum flow rate more work would have to be carried out using different gas flow rates.

One of the main aspects arising from the work carried out in this thesis would be to determine a practical and industrially viable way of introducing a catalyst into large carbon fibre preforms.

Although a solution injection method could potentially be utilised for this purpose there are other methods which could possibly be more industrially attractive. For example there are now commercially available nickel plated carbon fibres which could potentially be incorporated in the lay-up process of the carbon preforms.

Another potential method would be to introduce the catalyst into the gas stream either as a vapour or as gaseously suspended nanoparticles which would then be carried into the pores of the preforms by the gas feed, however to incorporate this method into industrially sized furnaces and produce a uniform distribution over a number of differently sized preforms would probably not be feasible.

However, with these considerations in mind I believe that catalysts could be used to improve the current manufacturing process for the production of carbon-carbon composites; however, more research would have to be carried out in order to determine optimum conditions for carbon deposition as well as determining a practical way of utilising a catalyst on an industrial scale before catalyst utilisation is incorporated into current carbon-carbon composite manufacturing methods.

8 References

1. Savage, G., *Carbon-Carbon Composites*. 1st ed. 1993, London: Chapman and Hall. 389.
2. Windhorst, T. and G. Blount, *Carbon-carbon composites: a summary of recent developments and applications*. *Materials & Design*, 1997. **18**(1): p. 11-15.
3. Capel-Davies, J., Materials Literature Project. School of Mechanical, Materials, Manufacturing Engineering and Management. 1999-2000. University of Nottingham, Nottingham.
4. Golecki, I., *Rapid vapor-phase densification of refractory composites*. *Materials Science & Engineering R-Reports*, 1997. **20**(2): p. 37-124.
5. Reznik, B., M. Guellali, D. Gerthsen, R. Oberacker, and W. Hoffmann, *Microstructure and mechanical properties of carbon-carbon composites with multilayered pyrocarbon matrix*. *Materials Letters*, 2002. **52**(1-2): p. 14-19.
6. Reznik, B., D. Gerthsen, and K.J. Huttinger, *Micro- and nanostructure of the carbon matrix of infiltrated carbon fiber felts*. *Carbon*, 2001. **39**(2): p. 215-229.
7. Kim, M.S., N.M. Rodriguez, and R.T.K. Baker, *The Interaction of Hydrocarbons with Copper Nickel and Nickel in the Formation of Carbon Filaments*. *Journal of Catalysis*, 1991. **131**(1): p. 60-73.
8. Rostrup-Nielsen, J. and D.L. Trimm, *Mechanisms of Carbon Formation on Nickel-Containing Catalysts*. *Journal of Catalysis*, 1977. **48**: p. 155-165.
9. Baker, R.T.K., M.S. Kim, A. Chambers, C. Park, and N.M. Rodriguez, *The relationship between metal particle morphology and the structural characteristics of carbon deposits*, in *Catalyst Deactivation 1997*. 1997, Elsevier Science Publ B V: Amsterdam. p. 99-109.
10. Rodriguez, N.M., A. Chambers, and R.T.K. Baker, *Catalytic Engineering of Carbon Nanostructures*. *Langmuir*, 1995. **11**(10): p. 3862-3866.
11. Zielinski, R.E. and D.T. Grow, *An Iron Catalyst for Cvd of Methane on Carbon-Fibers*. *Carbon*, 1992. **30**(2): p. 295-299.
12. Downs, W.B. and R.T.K. Baker, *Novel Carbon Fiber-Carbon Filament Structures*. *Carbon*, 1991. **29**(8): p. 1173-1179.
13. McAllister, P. and E.E. Wolf, *Ni-Catalyzed Carbon Infiltration of Carbon-Fiber Substrates*. *Carbon*, 1992. **30**(2): p. 189-200.
14. Zielinski, R.E., *The Use of Magnetite as a Catalyst for the Chemical Vapor Deposition of Carbon on Carbon Fibers*. *Chemical Engineering*. 1991. University of North Dakota, Grand Forks, North Dakota. 58

15. Wolf, E.E. and P. McAllister, Nickel Catalyzed Carbon Infiltration of Carbon Fiber Substrates. 1994. University of Notre Dame du Lac, Notre Dame, Ind., United States. 5,312,679
16. McMurry, J. and R.C. Fay, *Chemistry*. Second ed. 1998: Prentice-Hall Inc.
17. Kroto, H.W., J.R. Heath, S.C. Obrien, R.F. Curl, and R.E. Smalley, *C-60 - Buckminsterfullerene*. *Nature*, 1985. **318**(6042): p. 162-163.
18. Iijima, S., *Helical Microtubules of Graphitic Carbon*. *Nature*, 1991. **354**(6348): p. 56-58.
19. Iijima, S. and T. Ichihashi, *Single-Shell Carbon Nanotubes of 1-Nm Diameter*. *Nature*, 1993. **363**(6430): p. 603-605.
20. Bethune, D.S., C.H. Kiang, M.S. Devries, G. Gorman, R. Savoy, J. Vazquez, and R. Beyers, *Cobalt-Catalyzed Growth of Carbon Nanotubes with Single-Atomic- Layerwalls*. *Nature*, 1993. **363**(6430): p. 605-607.
21. Rodriguez, N.M., M.S. Kim, R.T.K. Baker, F. Fortin, and I. Mochida, *Carbon Deposition on Nickel-Iron Alloys*. Abstracts of Papers of the American Chemical Society, 1995. **210**: p. 96.
22. Greenwood, N.N. and A. Earnshaw, *Chemistry of the Elements*. 2nd ed. 1997, Oxford: Reed Educational and Professional Publishing Ltd.
23. Popov, V.N., *Carbon nanotubes: properties and application*. Materials Science & Engineering R-Reports, 2004. **43**: p. 61-102.
24. Chen, J., Y. Li, Y. Ma, Y. Qin, and L. Chang, *Formation of bamboo-shaped carbon filaments and dependence of their morphology on catalyst composition and reaction conditions*. *Carbon*, 2001. **39**: p. 1467-1475.
25. Jang, J.W., C.E. Lee, T.J. Lee, C.J. Lee, and S.J. Noh, *Atomic force microscopy of bamboo-shaped multiwalled carbon nanotube structures*. *Solid State Communications*, 2003. **127**: p. 29-32.
26. Lu, Y., Z. Zhu, D. Su, D. Wang, Z. Liu, and R. Schloegl, *Formation of bamboo-shape carbon nanotubes by controlled rapid decomposition of picric acid*. *Carbon*, 2004. **42**: p. 3199-3207.
27. Gan, B., J. Ahn, Q. Zhang, Rusli, S.F. Yoon, J. Yu, Q.F. Huang, K. Chew, V.A. Ligatchev, X.B. Zhang, and W.Z. Li, *Y-junction carbon nanotubes grown by in situ evaporated copper catalyst*. *Chemical Physics Letters*, 2001. **333**(1-2): p. 23-28.
28. Motojima, S., S. Asakura, T. Kasemura, S. Takeuchi, and H. Iwanaga, *Catalytic effects of metal carbides, oxides and Ni single crystal on the vapor growth of micro-coiled carbon fibers*. *Carbon*, 1996. **34**(3): p. 289-296.
29. Qin, Y., Z.K. Zhang, and Z.L. Cui, *Helical carbon nanofibers with a symmetric growth mode*. *Carbon*, 2004. **42**(10): p. 1917-1922.

30. Wen, Y. and Z. Shen, *Synthesis of regular coiled carbon nanotubes by Ni-catalyzed pyrolysis of acetylene and a growth mechanism analysis*. Carbon, 2001. **39**(15): p. 2369-2374.
31. Hughes, T.V. and C.R. Chambers, *Manufacture of Carbon Filaments*. 1889. United States. 405,480
32. Baker, R.T.K., M.A. Barber, R.J. Waite, P.S. Harris, and F.S. Feates, *Nucleation and Growth of Carbon Deposits from Nickel Catalyzed Decomposition of Acetylene*. Journal of Catalysis, 1972. **26**(1): p. 51.
33. Baker, R.T.K., P.S. Harris, R.B. Thomas, and R.J. Waite, *Formation of Filamentous Carbon from Iron, Cobalt and Chromium Catalyzed Decomposition of Acetylene*. Journal of Catalysis, 1973. **30**(1): p. 86-95.
34. Harris, P.S., R.T.K. Baker, and R.A. Birch, *Formation of Carbon Deposits from Decomposition of Acetone over Nickel*. Carbon, 1973. **11**(5): p. 531.
35. Baker, R.T.K., P.S. Harris, and S. Terry, *Unique Form of Filamentous Carbon*. Nature, 1975. **253**(5486): p. 37-39.
36. Baker, R.T.K., G.R. Gadsby, R.B. Thomas, and R.J. Waite, *Production and Properties of Filamentous Carbon*. Carbon, 1975. **13**(3): p. 211-214.
37. Baker, R.T.K., G.R. Gadsby, and S. Terry, *Formation of Carbon Filaments from Catalyzed Decomposition of Hydrocarbons*. Carbon, 1975. **13**(3): p. 245-246.
38. Baker, R.T.K. and R.J. Waite, *Formation of Carbonaceous Deposits from Platinum-Iron Catalyzed Decomposition of Acetylene*. Journal of Catalysis, 1975. **37**(1): p. 101-105.
39. Baker, R.T.K., P.S. Harris, J. Henderson, and R.B. Thomas, *Formation of Carbonaceous Deposits from Reaction of Methane over Nickel*. Carbon, 1975. **13**(1): p. 17-22.
40. Keep, C.W., R.T.K. Baker, and J.A. France, *Origin of Filamentous Carbon Formation from Reaction of Propane over Nickel*. Journal of Catalysis, 1977. **47**(2): p. 232-238.
41. Hettige, C., K.R.R. Mahanama, and D.P. Dissanayake, *Cyclohexane oxidation and carbon deposition over metal oxide catalysts*. Chemosphere, 2001. **43**(8): p. 1079-1083.
42. Vajtai, R., K. Kordas, B.Q. Wei, J. Bekesi, S. Leppavuori, T.F. George, and P.M. Ajayan, *Carbon nanotube network growth on palladium seeds*. Materials Science and Engineering: C, 2002. **19**(1-2): p. 271-274.
43. Hullmann, D., G. Wendt, U. Singliar, and G. Ziegenbalg, *Propane dehydrogenation over supported platinum silicon nitride catalysts*. Applied Catalysis A: General, 2002. **225**(1-2): p. 261-270.
44. Lin, L.W., T. Zhang, J.L. Zang, and Z.S. Xu, *Dynamic Process of Carbon Deposition on Pt and Pt-Sn Catalysts for Alkane Dehydrogenation*. Applied Catalysis, 1990. **67**(1): p. 11-23.
45. Park, C. and R.T.K. Baker, *Carbon deposition on iron-nickel during interaction with ethylene-hydrogen mixtures*. Journal of Catalysis, 1998. **179**(2): p. 361-374.

-
46. Park, C. and R.T.K. Baker, *Carbon deposition on iron-nickel during interaction with ethylene-carbon monoxide-hydrogen mixtures*. Journal of Catalysis, 2000. **190**(1): p. 104-117.
 47. Geurts, F., R.G. Cnossen, A. Sacco, and R.R. Biederman, *Carbon Deposition over Transition-Metal Alloys .2. Kinetics of Deposition over (Feni) and (Feco) Alloy Foils*. Carbon, 1994. **32**(6): p. 1151-1169.
 48. Kichambare, P.D., D. Qian, E.C. Dickey, and C.A. Grimes, *Thin film metallic catalyst coatings for the growth of multiwalled carbon nanotubes by pyrolysis of xylene*. Carbon, 2002. **40**(11): p. 1903-1909.
 49. Rodriguez, N.M., M.S. Kim, F. Fortin, I. Mochida, and R.T.K. Baker, *Carbon deposition on iron-nickel alloy particles*. Applied Catalysis a-General, 1997. **148**(2): p. 265-282.
 50. Tanaka, A., S.H. Yoon, and I. Mochida, *Formation of fine Fe-Ni particles for the non-supported catalytic synthesis of uniform carbon nanofibers*. Carbon, 2004. **42**(7): p. 1291-1298.
 51. Fenelonov, V.B., A.Y. Derevyankin, L.G. Okkel, L.B. Avdeeva, V.I. Zaikovskii, E.M. Moroz, A.N. Salanov, N.A. Rudina, V.A. Likholobov, and S.K. Shaikhutdinov, *Structure and texture of filamentous carbons produced by methane decomposition on Ni and Ni-Cu catalysts*. Carbon, 1997. **35**(8): p. 1129-1140.
 52. Tekunova, T.V. and P.A. Tesner, *Kinetics of the Formation of Pyrocarbon from Methane on Nickel, Molybdenum and a Tungsten-Rhenium Alloy*. Khimiya Tverdogo Topliva, 1977. **11**(5): p. 151-153.
 53. Grow, D.T., *Catalytic Carbon-Carbon Deposition Process*. 1997. Sioux manufacturing Corporation, United States. 5,690,997
 54. Sacco, A., P. Thacker, T.N. Chang, and A.T.S. Chiang, *The Initiation and Growth of Filamentous Carbon from Alpha-Iron in H-2, CH4, H2O, CO2, and CO Gas-Mixtures*. Journal of Catalysis, 1984. **85**(1): p. 224-236.
 55. Tsai, S.H., C.W. Chao, C.L. Lee, X.W. Liu, I.N. Lin, and H.C. Shih, *Formation and field-emission of carbon nanofiber films on metallic nanowire arrays*. Electrochemical and Solid State Letters, 1999. **2**(5): p. 247-250.
 56. Soneda, Y., L. Duclaux, and F. Beguin, *Synthesis of high quality multi-walled carbon nanotubes from the decomposition of acetylene on iron-group metal catalysts supported on MgO*. Carbon, 2002. **40**(6): p. 965-969.
 57. Kong, J., A.M. Cassell, and H.J. Dai, *Chemical vapor deposition of methane for single-walled carbon nanotubes*. Chemical Physics Letters, 1998. **292**(4-6): p. 567-574.
 58. Liao, K.H. and J.M. Ting, *Effects of Ni-catalyst characteristics on the growth of carbon nanowires*. Carbon, 2004. **42**(3): p. 509-514.
 59. Figueiredo, J.L., C.A. Bernardo, J.J. Chludzinski, and R.T.K. Baker, *The Reversibility of Filamentous Carbon Growth and Gasification*. Journal of Catalysis, 1988. **110**(1): p. 127-138.
-

-
60. Yokomichi, H., F. Sakai, M. Ichihara, and N. Kishimoto, *Carbon nanotubes and a-C films simultaneously fabricated by thermal CVD*. *Journal of Non-Crystalline Solids*, 2002. **299**: p. 868-873.
 61. Baker, R.T.K. and J.J. Chludzinski, *Filamentous Carbon Growth on Nickel-Iron Surfaces - the Effect of Various Oxide Additives*. *Journal of Catalysis*, 1980. **64**(2): p. 464-478.
 62. Kim, M.S., N.M. Rodriguez, and R.T.K. Baker, *The Role of Interfacial Phenomena in the Structure of Carbon Deposits*. *Journal of Catalysis*, 1992. **134**(1): p. 253-268.
 63. Rodriguez, N.M., M.S. Kim, and R.T.K. Baker, *Deactivation of Copper Nickel-Catalysts Due to Changes in Surface-Composition*. *Journal of Catalysis*, 1993. **140**(1): p. 16-29.
 64. Park, C., N.M. Rodriguez, and R.T.K. Baker, *Carbon deposition on iron-nickel during interaction with carbon monoxide hydrogen mixtures*. *Journal of Catalysis*, 1997. **169**(1): p. 212-227.
 65. Park, C. and R.T.K. Baker, *Modifications in the catalytic properties of nickel supported on different dielectric oxides*. *Chemistry of Materials*, 2002. **14**(1): p. 273-280.
 66. Baker, R.T.K., J.R. Alonzo, J.A. Dumesic, and D.J.C. Yates, *Effect of the Surface-State of Iron on Filamentous Carbon Formation*. *Journal of Catalysis*, 1982. **77**(1): p. 74-84.
 67. Baker, R.T.K., J.J. Chludzinski, and C.R.F. Lund, *Further-Studies of the Formation of Filamentous Carbon from the Interaction of Supported Iron Particles with Acetylene*. *Carbon*, 1987. **25**(2): p. 295-303.
 68. Owens, W.T., N.M. Rodriguez, and R.T.K. Baker, *Carbon-Filament Growth on Platinum Catalysts*. *Journal of Physical Chemistry*, 1992. **96**(12): p. 5048-5053.
 69. Baker, R.T.K., J.J. Chludzinski, N.S. Dudash, and A.J. Simoens, *The Formation of Filamentous Carbon from Decomposition of Acetylene over Vanadium and Molybdenum*. *Carbon*, 1983. **21**(5): p. 463-468.
 70. Rodriguez, N.M., M.S. Kim, and R.T.K. Baker, *Promotional Effect of Carbon-Monoxide on the Decomposition of Ethylene over an Iron Catalyst*. *Journal of Catalysis*, 1993. **144**(1): p. 93-108.
 71. Carneiro, O.C., M.S. Kim, J.B. Yim, N.M. Rodriguez, and R.T.K. Baker, *Growth of graphite nanofibers from the iron-copper catalyzed decomposition of CO/H₂ mixtures*. *Journal of Physical Chemistry B*, 2003. **107**(18): p. 4237-4244.
 72. Chambers, A., N.M. Rodriguez, and R.T.K. Baker, *Modification of the Catalytic Behavior of Cobalt by the Addition of Copper*. *Journal of Physical Chemistry*, 1995. **99**(26): p. 10581-10589.
 73. Lim, S., A. Shimizu, S.H. Yoon, Y. Korai, and I. Mochida, *High yield preparation of tubular carbon nanofibers over supported Co-Mo catalysts*. *Carbon*, 2004. **42**: p. 1276-1277.
 74. Ting, J.M. and N.Z. Huang, *Thickening of chemical vapor deposited carbon fiber*. *Carbon*, 2001. **39**(6): p. 835-839.
-

-
75. Wilson, J.I.B., N. Scheerbaum, S. Karim, N. Polwart, P. John, Y. Fan, and A.G. Fitzgerald, *Low temperature plasma chemical vapour deposition of carbon nanotubes*. *Diamond and Related Materials*, 2002. **11**(3-6): p. 918-921.
 76. Carneiro, O.C., P.E. Anderson, N.M. Rodriguez, and R.T.K. Baker, *Decomposition of CO-H₂ over graphite nanofiber-supported iron and iron-copper catalysts*. *Journal of Physical Chemistry B*, 2004. **108**(35): p. 13307-13314.
 77. Baker, R.T.K., *Catalytic Growth of Carbon Filaments*. *Carbon*, 1989. **27**(3): p. 315-323.
 78. Chambers, A., C. Park, R.T.K. Baker, and N.M. Rodriguez, *Hydrogen storage in graphite nanofibers*. *Journal of Physical Chemistry B*, 1998. **102**(22): p. 4253-4256.
 79. Lueking, A.D., R.T. Yang, N.M. Rodriguez, and R.T.K. Baker, *Hydrogen storage in graphite nanofibers: Effect of synthesis catalyst and pretreatment conditions*. *Langmuir*, 2004. **20**(3): p. 714-721.
 80. Bourrat, X. *Characterisation of Carbon Structure*. in *Design and Control of Structure of Advanced Carbon Materials for Enhanced Performance*.
 81. Hou, X.H., H.J. Li, J. Shen, C. Wang, and Z.G. Zhu, *Effects of microstructure on the internal friction of carbon-carbon composites*. *Materials Science and Engineering a-Structural Materials Properties Microstructure and Processing*, 2000. **286**(2): p. 250-256.
 82. Guellali, M., R. Oberacker, and M.J. Hoffmann, *Influence of the matrix microstructure on the mechanical properties of CVI-infiltrated carbon fiber felts*. *Carbon*, 2005. **43**: p. 1954-1960.
 83. Park, H.S., W.C. Choi, and K.S. Kim, *Process - Microstructure Relationships of Carbon-Carbon Composites Fabricated by Isothermal Chemical-Vapor Infiltration*. *Journal of Advanced Materials*, 1995. **26**(4): p. 34-40.
 84. Benzinger, W. and K.J. Huttinger, *Chemical vapor infiltration of pyrocarbon - II. The influence of increasing methane partial pressure at constant total pressure on infiltration rate and degree of pore filling*. *Carbon*, 1998. **36**(7-8): p. 1033-1042.
 85. Benzinger, W. and K.J. Huttinger, *Chemical vapor infiltration of pyrocarbon - III: the influence of increasing methane partial pressure at increasing total pressure on infiltration rate and degree of pore filling*. *Carbon*, 1999. **37**(2): p. 181-193.
 86. Benzinger, W. and K.J. Huttinger, *Chemistry and kinetics of chemical vapor infiltration of pyrocarbon-IV. Investigation of methane hydrogen mixtures*. *Carbon*, 1999. **37**(6): p. 931-940.
 87. Golecki, I., R.C. Morris, and D. Narasimhan, *Method of Rapidly Densifying a Porous Structure*. 1994. AlliedSignal Inc., United States. 5,348,774
-

-
88. Williams, D.H. and I. Fleming, *Spectroscopic methods in organic chemistry*. 5th ed. 1995, Maidenhead: McGraw-Hill Publishing Company.
 89. Cullity, B.D. and S.R. Stock, *Elements of X-ray diffraction*. 3rd ed. 2001, Upper Saddle River, N.J.: Prentice Hall.
 90. Laidler, K.J. and J.H. Meiser, *Physical Chemistry*. 2nd ed. 1995, Boston: Houghton Mifflin Company.
 91. Skoog, D.A., D.M. West, and F.J. Holler, *Analytical Chemistry - An Introduction*. 6th ed. 1993, Orlando: Harcourt Brace College Publishers.
 92. Watt, I.M., *The Principles and Practice of Electron Microscopy*. 2nd ed. 1997, Cambridge: Cambridge University Press.
 93. MicroscopyU, Introduction to Polarized Light Microscopy. Nikon. <http://www.microscopyu.com/articles/polarized/polarizedintro.html>
 94. Lide, D.R., *CRC Handbook of Chemistry and Physics*. 85th ed, ed. D.R. Lide. 2004, Boca Raton: CRC Press.
 95. Baker, R.T.K., J.R. Alonzo, and D.J.C. Yates, *Effect of the Surface-State of Iron on Filamentous Carbon Formation*. Abstracts of Papers of the American Chemical Society, 1981. **182**(AUG): p. 48.
 96. Matsumoto, S., *Catalyzed Hydrogasification of Yallourn Char in the Presence of Supported Hydrogenation Nickel-Catalyst*. Energy & Fuels, 1991. **5**(1): p. 60-63.
 97. Benzinger, W. and K.J. Huttinger, *Chemical vapour infiltration of pyrocarbon .1. Some kinetic considerations*. Carbon, 1996. **34**(12): p. 1465-1471.
 98. Benzinger, W. and K.J. Huttinger, *Chemistry and kinetics of chemical vapor infiltration of pyrocarbon-V. Infiltration of carbon fiber felt*. Carbon, 1999. **37**(6): p. 941-946.
 99. Lim, D.S., J.W. An, and H.J. Lee, *Effect of carbon nanotube addition on the tribological behavior of carbon/carbon composites*. Wear, 2002. **252**(5-6): p. 512-517.

Appendix 1

<u>Ethane</u>				<u>Ethane + H2</u>			
<u>Temp</u>	<u>% Pick-up</u>	<u>Mean</u>	<u>SD</u>	<u>Temp</u>	<u>% Pick-up</u>	<u>Mean</u>	<u>SD</u>
650	15.31	5.54	8.44	650	1.76	2.17	0.90
650	12.24			650	1.72		
650	-0.58			650	1.47		
650	-4.82			650	3.72		
700	14.11	8.04	4.48	700	9.09	12.21	3.89
700	6.63			700	10.90		
700	1.80			700	10.01		
700	9.62			700	18.85		
750	29.90	35.94	4.96	750	34.83	32.13	3.67
750	38.91			750	35.60		
750	32.56			750	31.82		
750	42.40			750	26.26		
800	60.86	55.97	4.42	800	71.52	66.25	7.52
800	49.78			800	61.97		
800	59.37			800	56.28		
800	53.87			800	75.22		

<u>Syn NG</u>				<u>Syn NG + H2</u>			
<u>Temp</u>	<u>% Pick-up</u>	<u>Mean</u>	<u>SD</u>	<u>Temp</u>	<u>% Pick-up</u>	<u>Mean</u>	<u>SD</u>
650	0.25	-2.97	1.94	650	8.95	0.26	5.10
650	-3.28			650	-1.15		
650	-4.07			650	-3.55		
650	-4.80			650	-3.20		
700	2.00	-0.38	3.19	700	6.39	2.46	2.93
700	0.23			700	-0.13		
700	-5.76			700	-0.58		
700	2.00			700	4.15		
750	28.31	31.35	3.03	750	28.34	30.59	1.37
750	28.83			750	31.80		
750	35.82			750	30.63		
750	32.43			750	31.60		
800	32.20	33.65	3.07	800	34.18	31.85	10.85
800	32.16			800	48.5		
800	31.32			800	20.28		
800	38.93			800	24.45		

Table of data used to compile Figure 4.1, showing carbon deposition rates for samples reacted in ethane or synthetic natural gas with and without the addition of 20 vol. % hydrogen at 650, 700, 750 and 800°C with 20 wt. % nickel catalyst for 3 hours.

<u>Ethane + H2 - 750°C</u>					<u>Syn. NG + H2 - 750°C</u>				
<u>% Ethane</u>	<u>% H2</u>	<u>% Pick-up</u>	<u>Mean</u>	<u>SD</u>	<u>% Syn. NG</u>	<u>% H2</u>	<u>% Pick-up</u>	<u>Mean</u>	<u>SD</u>
100	0	42.40	35.94	4.96	100	0	28.31	31.35	3.03
100	0	29.90			100	0	28.83		
100	0	38.91			100	0	35.82		
100	0	32.56			100	0	32.43		
80	20	34.83	32.13	3.67	80	20	28.34	30.59	1.37
80	20	35.60			80	20	31.80		
80	20	31.82			80	20	30.63		
80	20	26.26			80	20	31.60		
60	40	37.00	33.73	2.41	60	40	16.96	16.64	3.55
60	40	31.95			60	40	20.82		
60	40	35.03			60	40	12.14		
60	40	30.95			40	60	12.81	8.45	3.84
40	60	30.11	29.65	3.65	40	60	4.67		
40	60	34.79			40	60	4.58		
40	60	29.19			40	60	11.73		
40	60	24.51			20	80	-0.7	0.28	0.78
20	80	25.38	26.85	3.21	20	80	0.31		
20	80	23.86			20	80	1.22		
20	80	31.30							

Table of the data used to compile Figure 4.2, showing carbon deposition rates for samples reacted in ethane or synthetic natural gas with and without the addition of 20, 40, 60 or 80 vol. % hydrogen at 750°C with 20 wt. % nickel catalyst for 3 hours.

Ethane @ 750°C for 12 hours		
Total Densification Time (h)	Section Time (h)	% Pick-up/hr
3	3	28.00
6	3	14.17
9	3	7.16
12	3	4.61
	Average	23.63
Ethane plus Hydrogen @ 750°C for 12 hours		
Total Densification Time (h)	Section Time (h)	% Pick-up/hr
3	3	45.27
6	3	16.66
9	3	6.66
12	3	2.97
	Average	32.10
Ethane @ 800°C for 12 hours		
Total Densification Time (h)	Section Time (h)	% Pick-up/hr
2	2	91.49
4	2	16.72
6	2	8.57
8	2	6.10
12	4	3.30
	Average	39.78
Ethane plus Hydrogen @ 800°C for 12 hours		
Total Densification Time (h)	Section Time (h)	% Pick-up/hr
2	2	92.78
4	2	24.87
6	2	10.78
8	2	9.04
12	4	3.34
	Average	50.99
Ethane @ 800°C for 8 hours - no catalyst		
Total Densification Time (h)	Section Time (h)	% Pick-up/hr
4	4	-0.66
8	4	1.44
12	4	-0.25
	Average	0.16

Table of the data used to compile Figures 4.3 and 4.4, showing carbon deposition rates for samples reacted in ethane or synthetic natural gas with and without the addition of 20 vol. % hydrogen at 750 and 800°C with 20 wt. % nickel catalyst for 12 hours.

Appendix 2

950°C

<u>Methane</u>		<u>Syn NG</u>	
<u>Total Dens. (hours)</u>	<u>% Pick Up/hr</u>	<u>Total Dens. (hours)</u>	<u>% Pick Up/hr</u>
2	3.92	2	6.50
4	4.09	4	6.52
8	3.19	8	5.42
12	3.38	12	3.44
16	2.56		
20	1.54		
24	1.85		

1050°C

<u>Methane</u>		<u>Syn NG</u>	
<u>Total Dens. (hours)</u>	<u>% Pick Up/hr</u>	<u>Total Dens. (hours)</u>	<u>% Pick Up/hr</u>
2	1.51	2	8.32
4	8.58	4	7.86
8	8.77	8	5.53
12	11.77	12	4.26
16	5.22		
20	2.44		
24	2.37		

1150°C

<u>Methane</u>		<u>Syn NG</u>	
<u>Total Dens. (hours)</u>	<u>% Pick Up/hr</u>	<u>Total Dens. (hours)</u>	<u>% Pick Up/hr</u>
2	54.37	2	7.98
4	12.43	4	13.56
8	8.07	8	6.64
12	6.28	12	5.61
16	8.67		
20	1.70		
24	3.27		

Table of the data used to compile Figures 5.2 and 5.3, showing carbon deposition rates for samples reacted in methane or synthetic natural gas at 950, 1050 and 1150°C without a catalyst, for 12 and 24 hours.

Appendix 3

650°C Syn NG (1.5)

<u>Total Dens. (hours)</u>	<u>% Pick Up/hr</u>
4	-0.26
8	0.13
12	0.09

700°C Syn NG (1.5)

<u>Total Dens. (hours)</u>	<u>% Pick Up/hr</u>
4	0.56
8	2.37
12	4.12

750°C Syn NG (1.5)

<u>Total Dens. (hours)</u>	<u>% Pick Up/hr</u>
4	1.20
8	0.86
12	0.81

800°C Syn NG (1.5)

<u>Total Dens. (hours)</u>	<u>% Pick Up/hr</u>
4	1.57
8	1.74
12	1.62

800°C Syn NG (1.5) - No Cat.

<u>Total Dens. (hours)</u>	<u>% Pick Up/hr</u>
4	0.64
8	1.39
12	1.36

Table of the data used to compile Figure 5.6, showing carbon deposition rates for samples reacted in synthetic natural gas at 650, 700, 750 and 800°C with either 20 wt. % nickel catalyst or without a catalyst for 12 hours.